UNIVERSIDADE DE LISBOA
FACULDADE DE CIÊNCIAS
DEPARTAMENTO DE FÍSICA

Atmospheric Dynamics of Venus using Space based observations and cloud tracking techniques

Daniela Cortes Espadinha

Mestrado em Física
Especialização em Astrofísica e Cosmologia

Dissertação orientada por:
Doutor Pedro Machado

2019

Acknowledgments

Astronomy and Astrophysics were a passion and a dream since I first got a book on the Solar System when I was at the very young age of three. My first memories of space came from that little book, which I requested my parents to read to me over and over again. For five years now, and especially since I began my Master's degree on Astrophysics and Cosmology, that dream of working on what I loved the most progressively became a reality. The support of many people along the way was a crucial factor for my success and for all the work that I have done throughout this time.

Firstly, I would like to thank my parents, Clarinda Margarida Morais Cortes and José João Mendes Espadinha. They always supported my decision of following my dreams, even if we some time did not see eye to eye, but I know they always had my best interest in mind. In fact, they were the ones that opened many doors in my way and that made continuous efforts to raise and teach me the basics of a fulfilling life. They were the ones who still offered me all the support I needed when I left my small town's home and travelled to the capital of Lisbon to study. I only hope I can make them proud.

I also want to thank my sister Adelaide, for her endless support and for coming with me to the bustling Lisbon. I never felt alone in my endeavours and surely I had someone always by my side whom I could trust and who was a shoulder to cry on if needed. And when those moments when all we think is giving up and that continuing is impossible, I want to thank my boyfriend, Joseph Wilkinson, for making me realise that I should keep giving my dream a chance and rely more on myself and my decisions.

I will always thank my friends Ana Carvalho and Inês Costa, for all their support, the way they helped me grow and all they taught me. Because of them I am a much better person today and I just hope that I also contributed somehow to their lives so that our relationship can last.

I cannot leave unsaid a special thanks to the team working with me at IA (Institute of Astrophysics and Space Sciences) for welcoming me with open arms, and for all the advice and help given since I started my career.

And last but not the least, I am grateful to my supervisor Pedro Mota Machado, he was not only a teacher but also a guide and a friend. I could never imagine to have such a generous and helpful person so early in my career. He trusted in my abilities and competence, gave me opportunities to start fulfilling my research and, most important of all, taught me the beauty of being a scientist and the value of teamwork.

Resumo

O planeta mais próximo da Terra e o segundo objecto mais brilhante no céu nocturno é Vénus. Nomeado em honra da deusa romana do amor e da beleza, o nosso vizinho e planeta "irmão" partilha muitas características semelhantes às da Terra, nomeadamente a massa, a densidade e o tamanho. No entanto, Vénus e a Terra não podiam ser planetas mais diferentes. As condições propícias à vida, como esta é conhecida na Terra, contrastam fortemente com as condições hostis que Vénus apresenta. Exemplos destas características incluem a temperatura superficial: no nosso planeta a temperatura ronda os 15 °C mas em Vénus chega aos 460 $^{\circ}C$, uma temperatura capaz de derreter chumbo na superfície Venusiana. Em Vénus, a pressão atmosférica chega a ser aproximadamente 90 bar, ou seja, a pressão correspondente à verificada a 1 km de profundidade nos oceanos terrestres e a sua massa atmosférica é cerca de 92 vezes a massa da atmosfera terrestre. O efeito de estufa descontrolado existente em Vénus é outra característica que distingue os dois planetas. Este fenómeno é causado principalmente devido à quantidade de CO_2 que, em Vénus, representa 96% da totalidade da atmosfera ao invés de que, na Terra, esta quantidade não ultrapassa os 0.034%. Estas características são consequências directas das diferentes composições químicas, massas atmosféricas e moléculas condensáveis. Todo este cenário contrasta com a hipótese de que ambos os planetas se formaram na mesma altura de evolução do sistema solar, com as mesmas condições iniciais, e a partir da mesma nuvem proto-estelar mas, como é possível concluir, seguiram evoluções diferentes entre si. Além das condições superficiais e atmosféricas já referidas, existem ainda outras características que tornam a Terra e Vénus tão diferentes. Vénus é um planeta com rotação retrógada cujo período é de 243 dias terrestres o que, leva a que um dia solar em Vénus seja de 117 dias terrestres. Seria de esperar que a atmosfera Venusiana acompanhasse este períodos de rotação, o que não se verifica.

A atmosfera de Vénus está num estado denominado de super-rotação. Isto advém do facto de que esta apresenta um período de rotação de cerca de 4.4 dias terrestres, onde o seu movimento acompanha o movimento de rotação retrógado do planeta. Na região equatorial, os ventos podem alcançar velocidades superiores a 100 m/s, ou seja, velocidades superiores a 360 km/h. A caracterização completa e pormenorizada deste fenómeno torna-se então um factor de alta importância na compreensão dos mecanismos que criam e regem as atmosferas planetárias.

A densa camada de nuvens que envolve a atmosfera Venusiana é composta na sua maior parte por gotículas de ácido sulfúrico e um composto ainda por identificar mas que absorve fortemente a radiação ultravioleta no topo da mesma. Os contrastes resultantes da interacção da radiação solar e estes constituintes criam padrões nas nuvens, tornando-se marcadores ideais para seguir o movimento das camadas atmosféricas. Através da observação e análise de imagens sucessivas destes padrões é possível, utilizando uma técnica de seguimento de nuvens ("cloud tracking") abordada neste trabalho, determinar as velocidades dos ventos na atmosfera de Vénus

e, posteriormente, construir perfis latitudinais do vento zonal (vento com direcção paralela ao equador). Com observações obtidas pelo instrumento VMC e VIRTIS da missão Venus Express da Agência Espacial Europeia, foi possível observar o topo e a base da camada de nuvens que envolve Vénus, nos comprimentos de onda situados no Ultravioleta e no Infravermelho respectivamente. Os resultados destes instrumentos permitiram ainda detectar e caracterizar, embora de uma forma preliminar, ondas atmosféricas de gravidade. Estas ondas são observadas geralmente na estratosfera e tratam-se de perturbações periódicas cuja força de restauro é a impulsão. Estas são responsáveis pelo transporte de energia, momento e espécies químicas na atmosfera possuindo um papel importante na dinâmica atmosférica de um planeta uma vez que estas ondas apenas se propagam em zonas onde o equilíbrio estático da atmosfera é positivo.

Nesta dissertação foram também analisadas imagens provenientes do instrumento UVI a bordo da Akatsuki, ou Venus Climate Orbiter (VCO), pertencente à JAXA, com dois filtros centrados em dois comprimentos de onda do ultravioleta (365 nm e 283 nm). Estes comprimentos de onda são considerados relevantes pois são bandas de absorção do dióxido de enxofre e do composto desconhecido. Esta imagens permitiram determinar velocidades de vento zonal e meridional no topo da camada de nuvens seguindo os trabalhos de Peralta et al. (2008) e Horinouchi et al. (2018) para construir os perfis de velocidade de vento em função da latitude onde se pode comparar os dois filtros.

As imagens de Vénus captadas pelo instrumento VIRTIS e seleccionadas neste trabalho foram obtidas directamente através dos arquivos públicos PSA (Planetary Science Archive) pertencentes à ESA da missão Venus Express. As restantes imagens usadas foram sempre fornecidas pelo orientador Doutor Pedro Machado.

Para realizar seguimento de nuvens, todas as imagens seleccionadas foram sujeitas a um processo de tratamento de imagem com a ajuda de dois softwares distintos: PLIA (Planetary Laboratory for Image Analysis) foi utilizado para processar imagens do instrumento VIRTIS e foi fornecido pela equipa de ciências planetárias de Bilbau enquanto que o software ACT (Automatic Cloud Tracking) foi utilizado para processar as imagens da sonda japonesa Akatsuki tendo sido fornecido pelo Javier Peralta da JAXA. Este tratamento foi necessário de modo a fazer sobressair os padrões existentes nas nuvens para posteriormente se aplicar o método de seguimento de nuvens.

No caso das imagens dos VIRTIS e VMC, o método de seguimento de nuvens foi empregue utilizando uma ferramenta auxiliar do PLIA denominada PICV2 (Planetary Image Correlation Velocimetry) que faz uso de um algoritmo de correlação de imagem que identifica os padrões de nuvens contrastantes e semelhantes entre duas imagens, espaçadas por um intervalo de tempo conhecido. Com esta identificação realizada, o programa calcula o desfasamento, em pixéis, de cada padrão. Para tal, é imperativo que as imagens em utilização estejam correctamente navegadas. Assim é possível calcular a velocidade de cada padrão de nuvens e obter vectores de ventos para os perfis latitudinais de vento zonal. Para as imagens dos dois filtros da Akatsuki o processo foi semelhante, mas inteiramente realizado com o software ACT. Entre os dois softwares, PICV2 e ACT, a mais relevante diferença está no nível de automação do método de seguimento de nuvens. No caso do PICV2 o método é aplicado de forma semi-automática onde o utilizador apenas aceita ou rejeita os vectores determinados enquanto que, no caso do ACT, todo o método é realizado de forma manual, desde a seleção dos padrões nas nuvens à decisão de manter ou não os vectores e tracers calculados.

Como resultados deste trabalho, destaco os resultados obtidos pela análise dos perfis gerados

através dos vectores obtidos das imagens Akatsuki. Ao comparar os perfis de vento nos dois filtros é possível verificar que o filtro de 283 nm (com uma velocidade média de vento zonal de 110 m/s na zonas de baixa e média latitude) apresenta velocidades de vento zonal superiores às do filtro de 365 nm (com uma velocidade média de vento zonal de 102 m/s na zonas de baixa e média latitude), no entanto, o mesmo não se verifica nos perfis de vento meriodional. Utilizando alguns argumentos dinâmicos foi possível colocar como hipótese que estes filtros penetram a atmosfera até chegar a altitudes distintas estudando camadas com cerca de 2 a 3 km de diferença em altitude.

Palavras-chave: Vénus, Atmosfera, Seguimento de Nuvens, Ondas Atmosféricas de Gravidade , Vento Zonal

Abstract

General circulation models for planetary atmospheres are one of the most important bases and tools of atmosphere dynamics in planetary sciences. Such models are often the result of the analysis of great amounts of observations, so they can be accurate enough to properly describe atmospheric circulation on our target planets. In addition, there is also the interesting and promising possibility of application of these models to other celestial bodies outside of our own solar system.

Essential to this understanding of planetary atmospheres, the cloud-tracking is without doubt a key element. This method makes use of image sequences of the atmosphere of a planet to infer and measure wind characteristics as, for example, velocity. This method yields important results that can be crucial for better understanding the cloud circulation on Venus and, consequently, one of its most fascinating characteristics: the superrotation of its atmosphere.

To achieve the ambitious goals set for planetary sciences, there is no doubt that space missions also play an important role paving the road to knowledge. Highlighting the first discoveries by Mariner 2, followed by Venera, Pioneer and Venus Express as well as the more recent Akatsuki or Venus Climate Orbiter (VCO), we could be spectators of new revolutionary discoveries that could change our perception of the hostile world that Venus is.

The fundamental aim of this thesis is to use this cloud tracking method to explore Venus Express observations in VIRTIS and VMC and Akatsuki's UVI instruments. One of the goals was to build wind profiles in different wavelengths which allow us to analyse several layers of the Venusian atmosphere. This work makes use of specialised software (Hueso et al., 2010) to follow the works of Sánchez-Lavega et al. (2008), Hueso et al. (2013) and Horinouchi et al. (2018).

Complementary work on atmospheric gravity waves was also carried out, characterisation and detection of these waves was done as part of an effort to understand these features of the Venusian atmosphere.

Keywords: Venus, Atmosphere, Cloud Tracking Atmospheric Gravity Waves, Zonal Wind

Contents

List of Figures

List of Tables

Chapter 1

Introduction

1.1 Motivation

Venus is the closest planet to Earth and, as described in the following chapter, is the most Earth-like planet we know so far. Both planets share similar size, mass and density, they both were formed around the same time and place and from the same list of ingredients. Even so, Venus has ended up with an extreme climate, making the possibility of sheltering life as we know it very unlikely. It is clear that the evolution path that Venus followed at some point of its evolution became very distinct from Earth's own path. However, it is because of the paradoxical differences and similarities that exist between Venus and Earth that Venus becomes a key element in understanding Earth's evolution. Two similar planets with similar births had different evolution paths and destinies. If we fail to fully understand the conditions that led to this, it is possible that we can never fully understand how life appeared on Earth, or be able to tell if an exoplanet is more Venus-like or Earth-like. There are a few major key aspects/reasons for studying Venus and, particularly, its atmosphere. Firstly, the study of Venus runaway greenhouse effect should improve the understanding of Earth's present climate change process that is currently taking place. Secondly, understanding Venus' climatology can help constraining the concept of Habitable Zone (HZ) which will surely be of extreme importance to the exoplanet community. Finally, by comparing Venus and Earth's atmospheric physics and dynamics, one can understand the differences that led to such distinct planetary evolution histories and also predict their long-term atmospheric transformations.

1.2 Venus - Earth's "Twin" Sister

Shining visibly in the night sky, the second planet from the sun is a key piece to understand so many mysteries and answering the numerous questions that the universe can offer us. Also known as Earth's twin, Venus (Fig. 1.1) is similar to our planet in radius, mass, density and overall bulk composition (Table 1.1) (Svedhem et al., 2007) . Both planets evolved from the same proto-solar nebula, and were formed (cooled down) at nearly the same time.

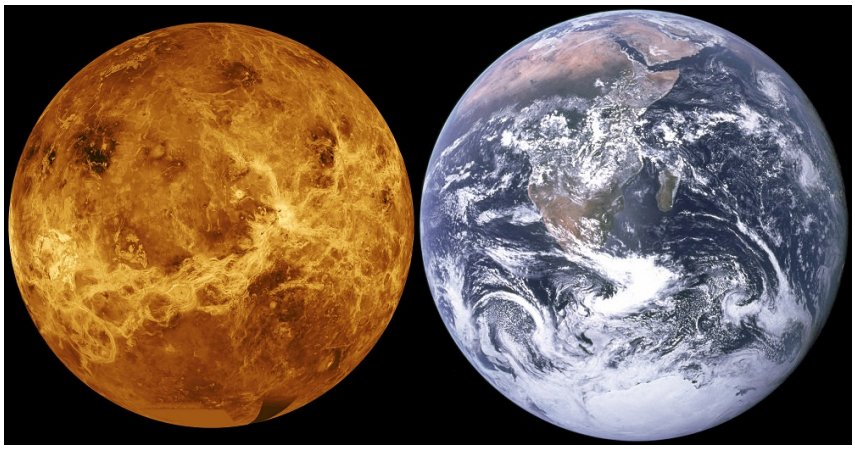

Figure 1.1: Venus and Earth sizes compared. Credit: NASA/JPL/Magellan

	Earth	Venus
Mass (kg)	5.98×10^{24}	4.87×10^{24}
Radius (km)	6378	6051
Density (g/cm^3)	5.5	5.3
Distance to Sun (UA)	1	0.72
Sidereal Year (Earth days)	365	226 (0.26 year)
Rotacional Period (Earth days)	1	243 (retrograde)
Obliquity (°)	23.5	177
Solar Constant	1380	2610
Albedo	0.3	0.75
Equilibrium Temperature (°C)	-15	15
Surface Tempearture (°C)	15	460
Surface Pressure (atm)	1	92
Atmospheric Composition	78.1% N_2 20.9% O_2 0.034% CO_2	96% CO_2 3% N_2
Atmospheric Condensables	H_2O	H_2SO_4

Table 1.1: Venus' and Earth's physical and atmospheric properties. Credit: Gonçalves (2016)

However, if a closer look is taken at these "twins", one can uncover the proof of the striking present contrasts between them. In spite of the existing solar system's formation arguments that support the similar initial atmospheric conditions for both Venus and Earth, the two planets developed in fundamentally different ways. (Ringwood and Anderson, 1977) In the end, Venus presents us with conditions so different from Earth that we are left wondering how two planets could reach such contrasting states.

The motion of this planet is certainly one of the best examples of its peculiarities. Venus is the only terrestrial planet with a retrograde rotation in the whole Solar System. In addition, its obliquity, or axis tilt, is of 177 °, which means that Venus' rotational axis is almost perpendicular to the ecliptic. Because of this, both of the planet's hemispheres receive approximately the same amount of radiation throughout the year making seasonal variations negligible. (Bougher et al., 1997)

It is also worth mentioning that Venus is the slowest rotating planet of the Solar System. It takes about 243 Earth days (de Pater and Lissauer, 2007) to spin around (one day in Venus, 243 Earth days, is actually longer than a venusian year which is approximately 226 Earth days). If its retrograde rotation is considered, a solar day (the time it takes for Venus to rotate about its axis so that the Sun appears in the same position in the sky) is about 117 Earth days in total. (Grinspoon, 1997) It should also be expected that Venus' atmosphere to keep up with this rotation speed, however the rotation of the solid planet contrasts dramatically with the much faster clouds' rotation, which can circle Venus in only 4.4 days at 70 km of altitude and about 6 days at 48 km. This phenomena is widely known as superrotation and its driving mechanisms still lack a proper description and understanding. (Machado, 2013)

The surface conditions are also worthy of attention. For example, the extremely high pressure on the surface of Venus amounts to 90 times the atmospheric pressure on Earth's surface, which is very close to 1 km depth at a terrestrial ocean. Furthermore, the 460° C (730K) temperatures caused by the high CO_2 concentration in the atmosphere and consequent runaway greenhouse effect mean that lead can melt on Venus' surface. These aggressive conditions turn Venus' surface into a hostile environment with a visual horizon that does not extend beyond 400 meters in a yellowish desolated world (probably due to sulphur compounds). (Grinspoon and Bullock, 2007) For Venus, thermodynamically speaking, the pressure and temperature at surface lead the atmospheric properties to be much closer to the liquid phase than a gaseous one.

1.2.1 Magnetic Field and Magnetosphere

Most planets and comets explored to date are encased in a strong magnetic field or magnetosphere. These magnetic fields protect a planet from the charged particles streaming out from the Sun in the form of the solar wind that flows radially outward from the Sun at supersonic speeds, acting as a protective shield around the planet.

Venus is a rarity among planets. It is a world that does not internally generate a magnetic field. In part because of its slow rotation and its predicted lack of internal thermal convection, any liquid metallic portion of its core could not be rotating fast enough to generate a measurable global magnetic field (Russell, 2001).

This absence of an internal magnetic field and of a relevant magnetosphere leads to a direct interaction of the solar wind with the upper atmosphere, affecting the distribution of plasma particles and atoms in the excited state. Although, the evidence of a weak magnetic field around the planet suggests the hypothesis of a magnetosphere generated, not by a dynamo effect, as on Earth, but rather by the interaction of solar wind with the charged particles of the ionosphere (Goody and Walker, 1975). This is known as induced magnetic field or magnetosphere. Venus, Mars and Titan are examples of induced magnetospheres (Russell, 2001). Venus' magnetosphere is far weaker than Earth's and closer to the planet (Fig. 1.2).

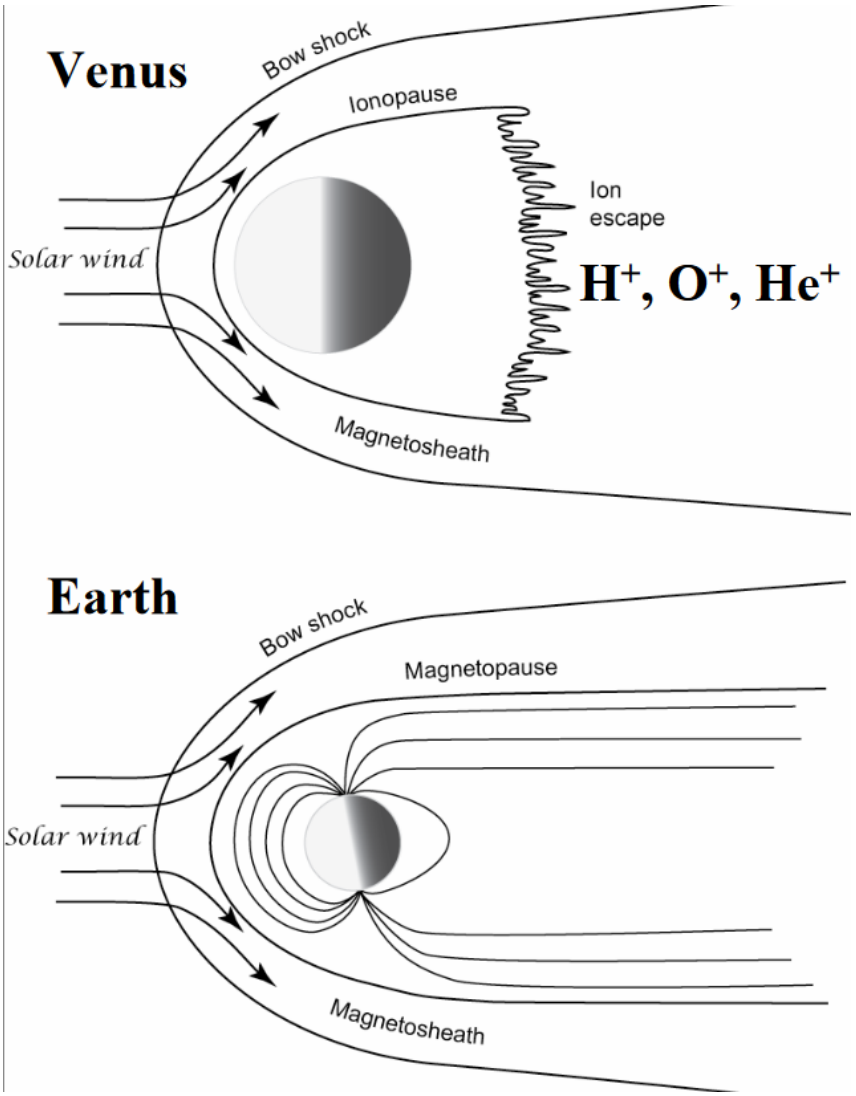

Figure 1.2: Bow shock of the interaction between the plasma particles of solar wind and the induced Venus' magnetosphere (upper part) and Earth's intrinsic magnetosphere (lower part). Credit: Titov, D., in "Planetary Atmospheres"

1.2.2 Geological Structure and Vulcanism

The fact that the density of Venus and Earth is so similar suggests that both these planets had a similar thermal history controlled by core differentiation. Since the two are approximately the same size and formed from similar primordial materials it is assumed that, in the beginning of planetary history (about 4.5 billion years), they had equal amounts of radioactive materials and consequently, produced roughly equal amounts of internal heat (Machado, 2013). Most thermal models suggest that Venus was initially mostly composed by chondritic (non-metallic) material. Its core might have accumulated most of it radioactive reservoir leading to a gradual rise of the planet's temperature over time. Some of this internal heat escapes through molten crust rocks at *hot spots*. (Phillips and Malin, 1983) On Venus, these *hot spots* are not randomly scattered but rather concentrated in defined areas which are believed to be mantle plumes (Smrekar et al., 2010).

Venus' internal structure is very much alike Earth's and is composed by a thin silicate crust, a thick mantle and a heavy metallic core (nickel and iron). The major difference is that Venus'

core shows evidence of being solid and much colder than Earth's. (Lewis, 2004) Although Venus does not show sign of active tectonic plates as on Earth, there are evident remains of deep gorges and canyons which can lead to a possibility of significant tectonic activity in the past (Machado, 2013). In Earth's case, the plate tectonics mechanism is closely linked to the carbon dioxide cycle, burying large amounts of it at subduction zones, stabilising in this way the atmospheric amount of CO_2. Such process could not occur in the single plate Venus' crust.

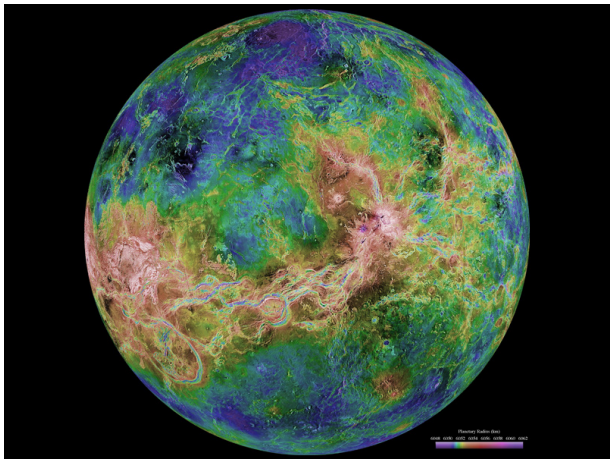

Figure 1.3: The hemispheric view of Venus, as revealed by more than a decade of radar investigations culminating in the 1990-1994 Magellan mission, is centered at 180 degrees east longitude. Credit: NASA/JPL/USGS

Venus' surface is coated with volcanoes, lava flows and signs of impact craters. The low density of impact craters randomly scattered and almost pristine condition of the surface point to an age of 600-1100 million years (Schaber et al., 1992) and strongly suggests that an older surface was swept away and submerged by a large scale resurfacing process. A cataclysmic event capable of this would entirely disrupt the crust and consequently release a large amount of volatile components into the atmosphere. These impact craters found on Venus' surface are generally quite large, since the thick atmosphere protects the planet against most impacts of smaller objects.

Regarding vulcanism, Venus does not have a thermal escape valve working in continuous mode as it happens on Earth, and consequently, the energy is accumulated and warms up the entire surface until lava erupts through thousands of volcanoes of all sizes. Periodically (on a scale of billions of years) the planet endures successive eras of intense vulcanism across the surface, erasing old craters and transfiguring the planet's surface in enormous resurface processes. The past massive vulcanism and resurfacing episodes led to vulcanic outgassing of sulphur dioxide and water which was responsible for the formation of extensive sulphuric acid and water clouds, and the increasing albedo contributed to a cooling of the surface. Afterwards, a cloud differentiation process might have happened, which sank the heavier sulphuric acid droplets. The remaining thin high water vapour cloud layer endured photolysis under the upper atmosphere intense solar radiation, which caused the loss of atmospheric water. (Machado, 2013)

1.2.3 Runaway Greenhouse Effect

Despite having a solar constant of almost twice the Earth constant, Venus absorbs much less sunlight than our planet mainly due to the highly reflective cloud layer which completely envelops it, leading to an extremely high albedo of roughly 75%. This is one of the reasons that

Venus shines so brightly in the sky (reaching the apparent magnitude of -4.6), the brightest after the Sun and the Moon.

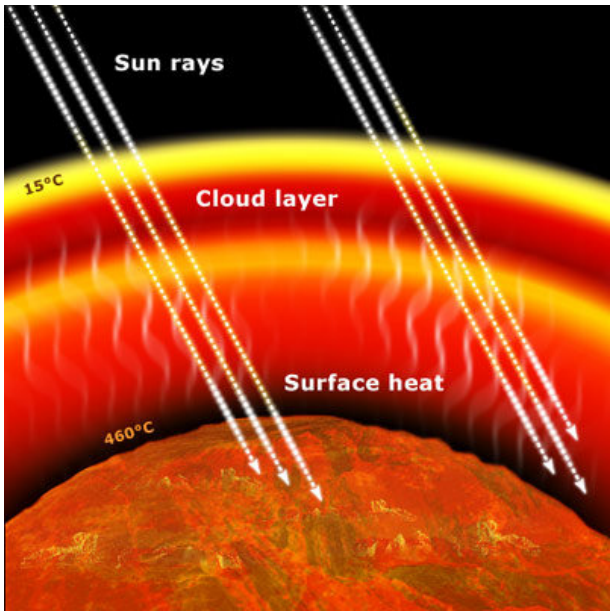

Figure 1.4: Schematic of Venus' Runaway Greenhouse Effect. Credit: ESA website

If we consider Venus as a black body and also take into account its albedo, Venus would be cooler than Earth. So it appears that the major contribution for the high surface temperature in Venus is its atmosphere. By Wien's displacement law (Eq. 1.1) the maximum of the wavelength radiation emitted (approximating Venus to a blackbody) is in the infrared range. The high concentration of CO_2 traps this planet's infrared radiation causing it to be reabsorbed which leads to an uncontrolled greenhouse effect (Fig. 1.4), causing Venus to have the highest surface temperature among the planets of the solar system.

$$\lambda_{max} T = 2.898 \times 10^{-3} mK \tag{1.1}$$

It is still unknown if the surface temperature has ever been low enough to allow condensation of water, even in possibly reduced solar illumination conditions in the early solar system which is a crucial question to answer regarding the complex evolution of the planet. (Chassefière et al., 2012)

1.2.4 Venus' Atmosphere

Origin

It was during the formation of the solar system that planetesimals, orbiting in primitive orbit paths, swept through space collecting debris, dust and later gas, in a process denominated accretion. During this process there was a gravitational energy release, which added to the energy that comes from unstable radioactive isotopes. After this, because of the protoplanet rotation, which acts as a huge centrifuge, the planet suffers an internal differentiation process in layers (mantle and crust) depending on its constituents density. (Turcotte, 1995) It is during this phase that volatiles start to migrate to the surface where they can remain in liquid form

(like the oceans on Earth) or in gaseous form, which provides the planet with its own gaseous layer called atmosphere. There are other processes that can contribute to the formation of the atmosphere or its alteration (Fig. 1.5) but in short, the genesis of Venus' atmosphere was, most likely, a process of accretion followed by a continuous degassing of volatiles from an intense mantle outgassing, as well, amplified by the overheating due to core differentiation processes. (Bullock and Grinspoon, 2001)

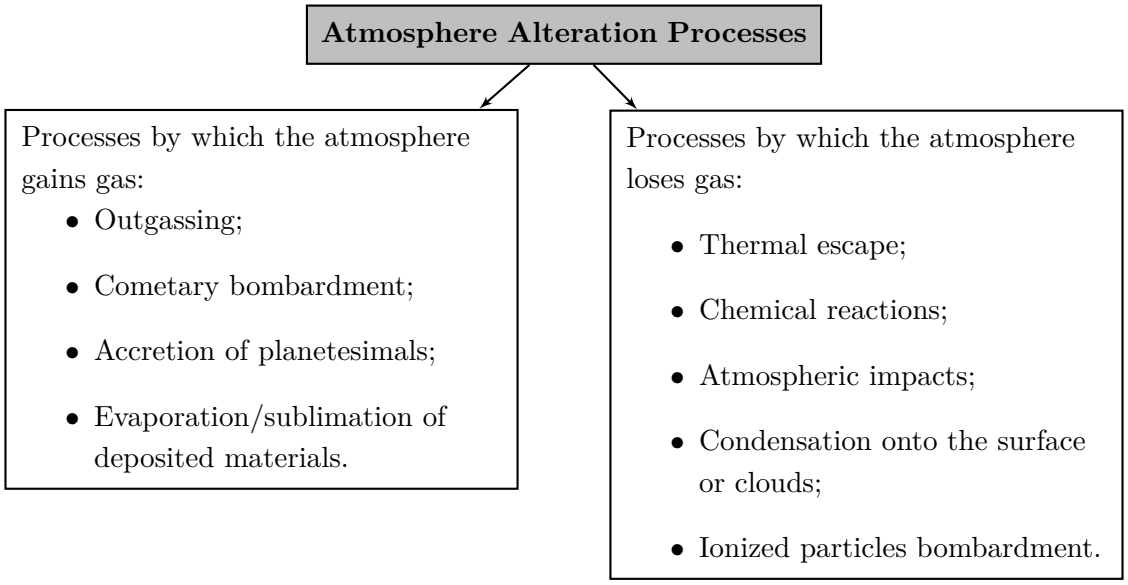

Figure 1.5: Processes of atmospheric gain and loss of gases.

Composition

The telluric planets Venus, Earth and Mars had possibly similar atmospheres regarding primordial composition and relative abundances of its constituents. It was the evolutionary path that each planet followed that lead to extreme environments such as Mars and Venus or, in Earth's case, a state where the existence of liquid water and life is possible. For example, although Earth's and Venus' atmospheres had roughly the same amount of carbon dioxide (CO_2), on Earth the major part of it is located in the crust (in the form of carbonated rocks) or dissolved in the vast oceans' water. As for Venus, most of the carbon dioxide is present in the atmosphere leading to a massive greenhouse effect (Section 1.2.3). This makes Venus an interesting case to study the possible consequences of anthropogenic emissions of greenhouse gases and consequent climate changes on Earth.

The components of Venus' atmosphere are in equilibrium with the rocks that cover the planet's surface. Examples of these surface-atmosphere interactions include outgassing of volcanic sulphur into the Venusian atmosphere and/or CO_2 absorption by the oceans on Earth. The analysis of the chemical reactions that affect atmospheric gases reveals that the chemical composition of Venus' atmosphere is determined by surface properties. On Earth this is not the case. The reason for this different behaviour lies in two factors: On the one hand, destabilising processes such as photosynthesis perturbs CO_2 levels affecting its concentration in the atmosphere. In the other hand, Venus' surface temperatures lead to fast chemical reactions and consequently chemical equilibrium is reached quickly. (Machado, 2013)

Venus' atmosphere is dominated by CO_2 (Fig. 1.6) at the present stage of atmospheric evolution. However, it is the sulphur dioxide (SO_2) concentration along other minor components

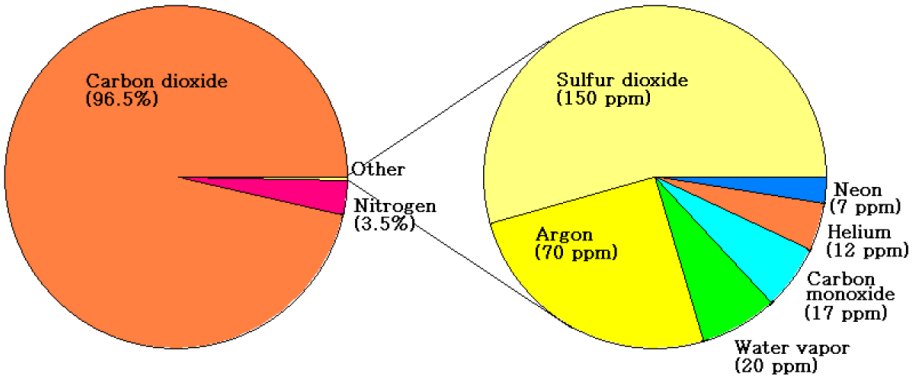

Figure 1.6: Schematic of Venus atmosphere relative composition. Minor species relative abundances are given in the magnified portion of the left graph at the right side.. Credit: NASA website

that fine tunes its atmospheric balance. (Bullock and Grinspoon, 2001) This is one of the minor components of most importance regarding surface coupling. Also worth noting as a minor component is the carbon monoxide (CO) which is produced in the upper atmosphere due to the photolysis of CO_2. In addition, it was also found evidence of the existence of H_2O in the upper atmosphere, but only at trace level. (Beatty et al., 1999)

Venus loses its atmospheric CO_2 by photolysis in the upper part of the atmosphere, H_2O is also lost by photolysis and by chemically reacting with SO_2 by forming sulphuric acid. Due to these losses, and to keep the dynamic atmospheric balance, it is necessary to have a source of replenishment.(Bullock and Grinspoon, 2001) Volcanic activity is the candidate for the replenishment process and abundance variability through time by injecting large amounts of these molecules during episodes of large-scale vulcanism.

Species	**Venus**	**Earth**	**Climate Significance**
Carbon dioxide	0.96	0.0003	Major greenhouse gas
Nitrogen	0.035	0.770	Similar total amounts
Argon	0.00007	0.0093	Evolutionary clues
Neon	0.000005	0.000018	Evolutionary clues
Water Vapour	0.000030	~0.01	Volcanic, cloud, greenhouse
Sulphur Dioxide	0.00015	0.2 ppb	Volcanic, cloud, greenhouse
Carbonyl Sulphide	0.000004		Volcanic, cloud, greenhouse
Carbon Monoxide	0.00004	0.00000012	Deep circulation
Atomic Oxygen	trace	trace	High circulation, escape processes
Hydroxyl	trace	trace	High circulation, escape processes
Atomic Hydrogen	trace	trace	Escape processes

Table 1.2: Composition of the atmospheres of Venus and Earth as fractional abundances (percentages) except where parts per billion is stated (all except the noble gases argon and neon are observed by Venus Express instruments). (Credit: Taylor and Grinspoon, 2009)

Structure

The vertical stratification of the atmosphere is dictated by how gravity and pressure balance each other, represented in the hydrostatic equilibrium equation (Eq. 1.2)

$$\frac{dP}{dz} = -g(z)\rho(z) \tag{1.2}$$

Here **P** represents the air pressure, **z** represents the altitude relative to the planet's surface, **g(z)** the gravitational acceleration and $\boldsymbol{\rho(z)}$ the density. (de Pater and Lissauer, 2007)

Since Venus is a planet which atmosphere is in equilibrium, its equation of state can be approximated by the ideal gas law (alternatively referred to as the perfect gas law):

$$P = NkT = \frac{\rho R_{gas} T}{\mu_a} = \frac{\rho k T}{\mu_a m_{au}} \tag{1.3}$$

Where **N** is the particle number density, $\boldsymbol{\mu_a}$ the mean molecular weight(in atomic mass units), $\boldsymbol{R_{gas}}$ is the universal gas constant and $\boldsymbol{m_{au}} \approx 1.67 \times 10^{-24}$ is the mass of an atomic weight unit (slightly less than the mass of an hydrogen atom). (de Pater and Lissauer, 2007)

Using both of the previous equations (1.2 and 1.3) one can find the equation to express pressure as function of altitude. Being **H(r)** the scale height:

$$P(z) = P_0 e^{-\int_0^z dr/H(r)} \tag{1.4}$$

The variation of temperature with altitude divides Venus' atmosphere into three distinct layers:

- **Troposphere (0-65km):** the densest part of Venus' atmosphere which extends from the surface to the top of the clouds and where the temperature decreases with altitude with the thermal gradient ratio of about $9K \cdot km^{-1}$ which is close to the adiabatic lapse rate ($\Gamma_d = \frac{g}{C_p} = 7.39\, K \cdot km^{-1}$). This shows that convection is not significant in this region;

- **Mesosphere (65-100km):** characterised by a less pronounced vertical thermal gradient ($\Gamma = \frac{\partial T}{\partial Z}$) (Ahrens, 2003), being noticeable the relevant horizontal variability with latitude, increasing from the equator to the poles, which is consistent with the existence of a Hadley circulation cell (Taylor et al., 1980);

- **Termosphere (100-200km):** where the balance between the incident UV radiation and the thermal conductivity of the present molecules prevails. Here exists an asymmetry between the day and night hemispheres, as the daytime temperature tends to increase with altitude between 100 and 140 km, while at night it tends to decrease along the same altitude range, above 140 km the temperatures, at both hemispheres, becomes isothermal (Fig. 1.7).

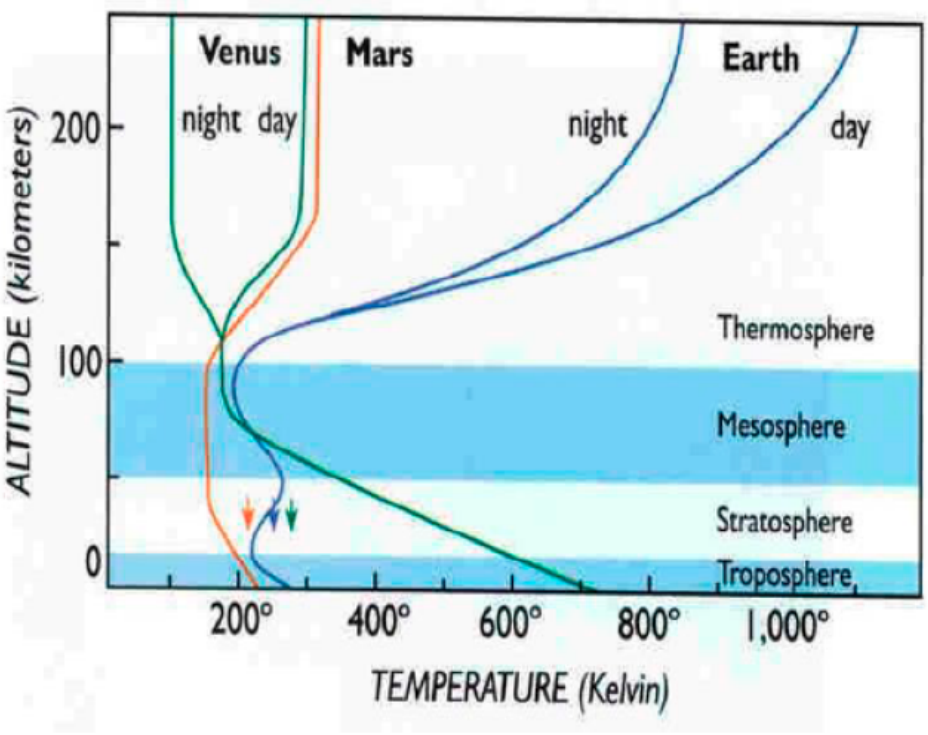

Figure 1.7: Vertical temperature profiles of Venus' atmosphere (green) compared with Mars's (red) and Earth's (blue) thermal profiles. Venus' and Earth's profiles are represented for both day and night.(Credit: B.Jakovsky).

The cloud deck on Venus has a determining influence on the planet's albedo, thermal structure and energy balance since most of the unidentified UV absorber abundance is at cloud layer. (Gonçalves, 2016) It is responsible for half of the total absorbed energy coming from solar irradiation which efficiency is increased by scattering (radiation travels longer paths). This way, the cloud medium, extending from 40 mbar (cloud top) until 1 bar (cloud base), see Fig. 1.8, absorbs roughly 92% of the incident solar flux (that is not reflected back to space due to the highly reflective albedo) and only the remaining 8% will actually reach the surface.

The cloud layer that covers the planet consists mainly of H_2SO_4 droplets and a few other aerosols of unknown composition. It ranges from 48 km to 70 km of altitude (with about 22km of thickness) with hazes starting from the 30 km bellow the cloud deck and reaching up to 90 km above it. (Esposito et al., 1983) It can be divided into three layers (Fig. 1.9) when considering the average size of their aerosol particles: (Knollenberg and Hunten, 1980)

- **Upper Layer (57-68 km):** with an averaged particle radius of 0.3 μm, and a total optical depth of 7 at 0.63 μm;

- **Middle Layer (51-56 km):** with a predominance of 1 to 1.4 μm particle sizes, with an optical depth of about 9, at the same 0.63 μm wavelength;

- **Lower Layer (48-50 km):** with an optical depth of nearly 10 (at 0.63 μm wavelength), majorly due to 3.65 μm sized particles.

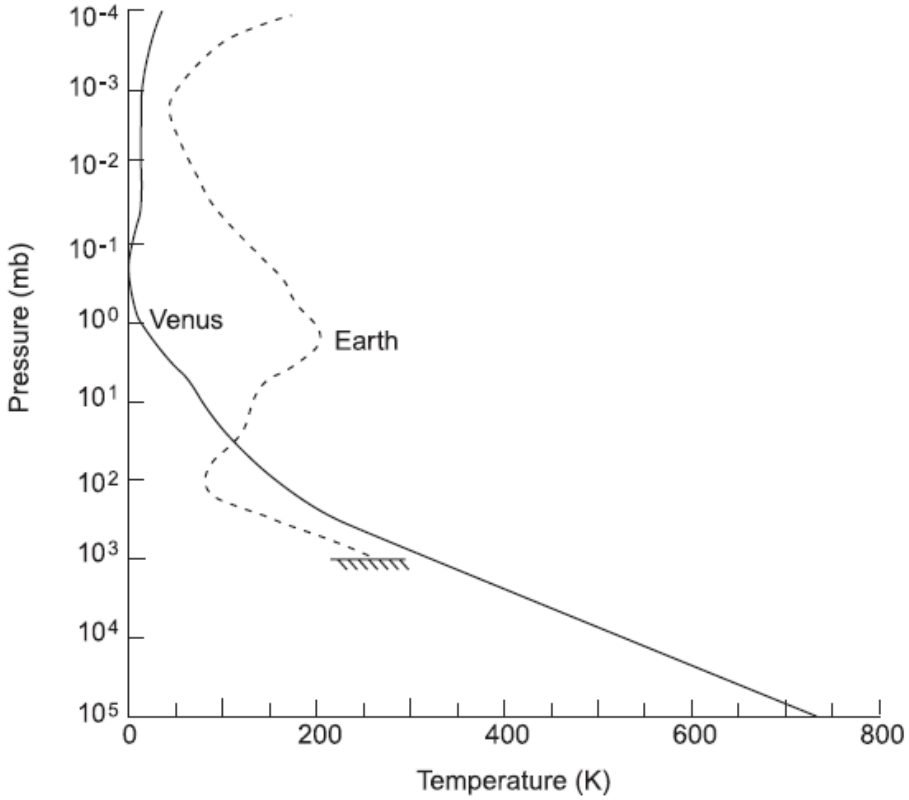

Figure 1.8: Pressure versus temperature profiles for Venus and Earth (Credit: Taylor and Grinspoon, 2009).

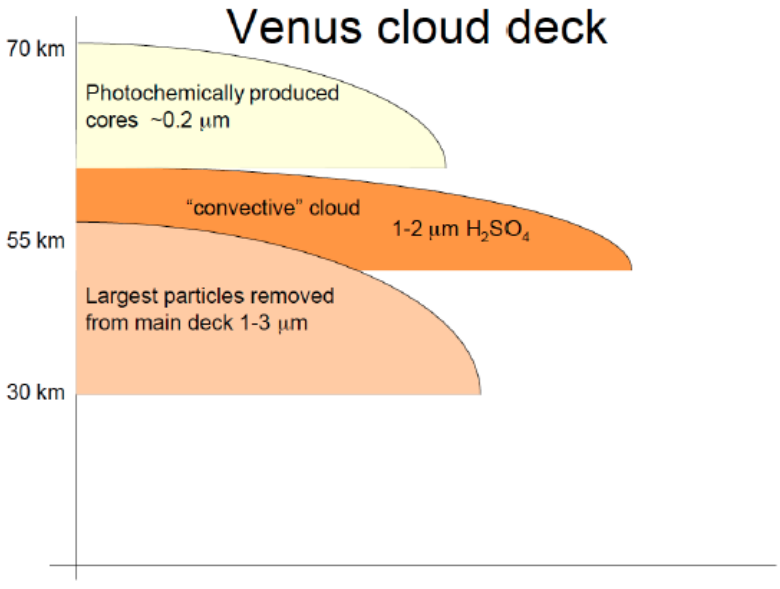

Figure 1.9: Venus' sulphuric acid cloud deck and hazes extension in altitude. Regarding the averaged aerosol particles size, the cloud deck can be divided in the three layers shown in this scheme. (Figure: Titov,D.,private communication).

Several polarimetric and spectroscopic observations point to a general composition ratio of 25% H_2O and 75% H_2SO_4 in terms of cloud particles. The sulphuric acid in the cloud tops is synthesised from photolysis and recombination process of H_2O and SO_2 that reacts with CO_2

according to the following chain reaction:

$$CO_2 + SO_2 + h\nu \rightarrow CO + SO_3 \tag{1.5}$$

$$SO_3 + H_2O \rightarrow H_2SO_4 \tag{1.6}$$

Dynamics

Venus' many fascinating characteristics and peculiarities are the root of its interesting atmosphere dynamics, which differ from those observed on Earth, even though the two planets share a few similarities. As already stated (Section 1.2), the solid globe of Venus completes a full rotation once every 243 Earth days (de Pater and Lissauer, 2007) whereas its cloud system rotates much faster. The upper cloud layer has a rotation period of 4.4 days and the lower cloud layer of about 6 days. The atmosphere dynamics in Venus are mainly driven by its low rotation rate and thermal heating.

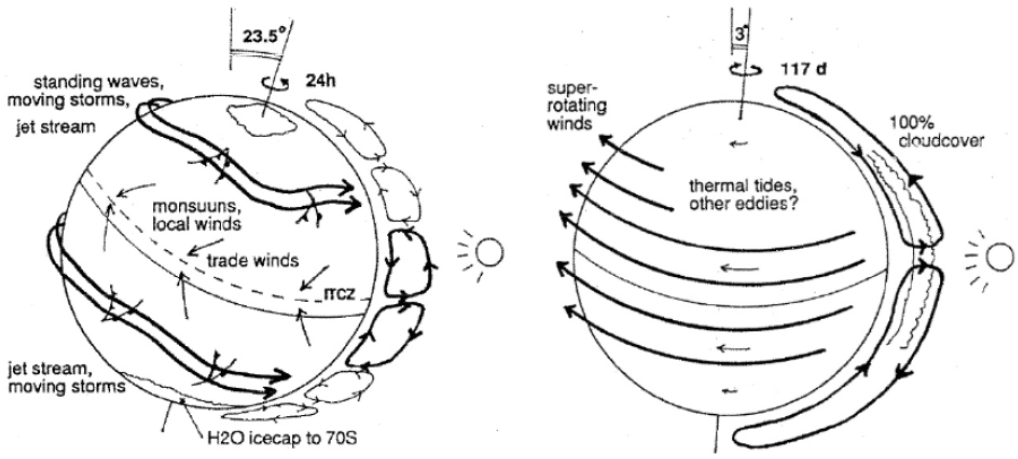

Figure 1.10: Large-scale motion of planetary atmospheres are dominated by various types of circulation patterns according to latitude, altitude and local time (left side: Earth and right side: Venus).

Three wind velocity components can be defined, being them:

- Zonal Wind (**u**) the component measured along the latitudinal lines;
- Meridional Wind (**v**) the component measured along the meridians;
- Vertical Wind (**w**) the upwards component of the winds.

We can also distinguish three main circulations processes that define Venus' atmosphere dynamics:

1. **Super-rotational retrograde zonal wind (RZW):** where wind flows at great speed in quasi laminar bands parallel to the equator. This is the most relevant atmospheric motion in the mesospheric circulation (between the altitudes of 60-100 km and stretching between mid-latitudes). The RZW is also accompanied by a Hadley-type meridional circulation from the equator to poles and both converge into a unique polar vortex circulation. On the superrotating zonal retrograde circulation, two main non-asymmetric large scale features are super-imposed: the four-day planetary wave at low and mid-latitudes and a polar vortex in both the polar regions.

2. **Subsolar to anti-solar circulation (SS-AS):** which transports the overheated air from highly isolated regions towards the night side radiation deficit area above the 120 km of altitude. The greater exposure to solar radiation and lower density are the ones which drive this characteristic motion that highlights the contrast between the night and day sides of Venus when considering temperature and density.

3. **Meridional Circulation (Hadley Cell):** Characterised by one Hadley cell in each hemisphere which is responsible for the transport of heat excess from low latitudes, poleward to cooler latitude regions. The Hadley circulation cell consists of rising air near the equator and submersion at the poles (two equator-pole cells), converging in a polar vortex circulation. The net upward transport of angular momentum by the Hadley cell is able to maintain an excess of angular momentum in the upper part of the atmosphere, balanced by planetary waves equatorward transport. However this Hadley cell circulation is yet to be clearly characterised observationally and remains as more of a theoretical construct needing quantitative support. (Gonçalves, 2016)

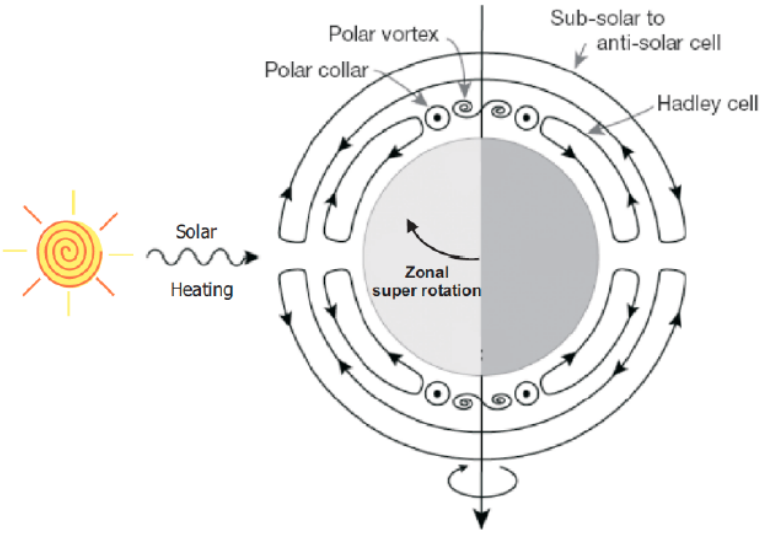

Figure 1.11: Venus global atmospheric circulation.(Credit: Taylor and Grinspoon, 2009)

Still regarding the dynamical aspects of the atmosphere of Venus, polar vortex motions, superrotation and atmospheric gravity waves (Section 1.3) will also be addressed for the purposes of this work.

Polar Vortex

The polar vortex (Fig 1.12), observed on both poles, is a three dimensional feature that is highly variable interchanging between a monopole, a dipole and a triple pole shape that has also been observed to change rather quickly (Luz et al., 2011). The vortex eye rotates around the polar axis faster than the RZW of the mid latitudinal range already discussed above in this section. The south pole vortex, observed recently, shows a period of about 2.7 terrestrial days and an exceptional variability in terms of shape (Luz et al. (2011); Garate-Lopez et al. (2013)). This means that the vortex eye rotates even faster than the super-rotating zonal winds of the mid latitudes range. It still remains to establish a relationship between the superrotation of the atmosphere and this phenomena which is a question regarded as a major theme in current scientific research.

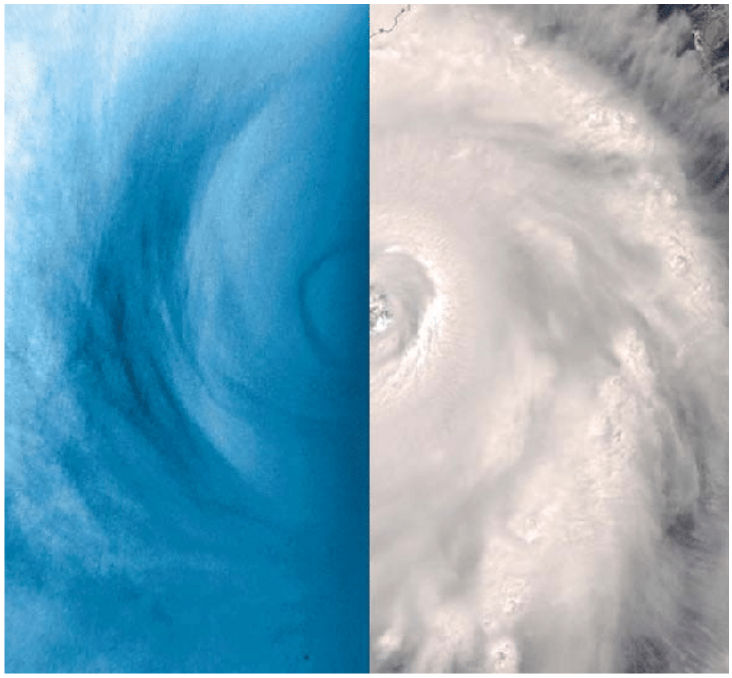

Figure 1.12: (VMC images of Venus south polar vortex (left); Hurricane Frances on Earth (right). (Limaye et al., 2009)

Superrotation of Venus Atmosphere

There are still many open questions concerning the understanding of Venus' atmospheric dynamics. One of them is how the superrotation process on Venus' atmosphere is driven and how is it maintained over time.

This rotation of Venus' atmosphere is not uniform, but depends on the latitude, a fact that can be seen by the relative motion of the cloud top layer, filleting the planet (Machado, 2013). The superrotation extends from the surface up to the cloud top ($\approx$ 70 km altitude) with wind speeds of only few meters per second near the surface and reaching a maximum value of $\approx 100 ms^{-1}$ at the cloud top, corresponding to a rotation period of 4 Earth days ($\approx$ 60 times faster than Venus itself) (Piccialli, 2010). It is indeed curious how an atmosphere of such a slow-rotating planet can be accelerated to such high speeds. Previous studies (Baker and Leovy (1987), Newman and Leovy (1992)) suggest that the superrotation is maintained by the transport of retrograde zonal momentum upward through thermal tides

at the equator and then poleward by a meridional cell. However, the attempts to model the zonal superrotation have only been partially successful so far which indicates that the mechanisms of this phenomenon are still unclear (Piccialli, 2010).

1.2.5 Venus Exploration

Many missions have departed from Earth, hoping to reach our neighbouring planet no more than a shining beacon in the sky with the name of a Goddess. Not all of them succeeded, but those which did have certainly returned a profound knowledge that still shapes our perception and understanding of space and the cosmos every single day. From the beginning of the space age, more than 30 different spacecrafts have been launched towards Venus making it the first successful planetary target for human space exploration with Mariner 2 in 1962.

The first attempts to reach Venus through robotic probes were made by the USSR. On February 1961, Tyazhely Sputnik and Venera 1 were launched, but both resulted in failures. It was only on the last month of the following year that Mariner 2 (NASA) made the first successful flyby to planet revealing that it was completely shrouded in an opaque atmosphere hiding the planet's surface and deepening the mysteries it offered.

Venera Missions (1961-1984)

The Venera program collected the first images from the surface (Fig. 1.13) and gathered information about surface chemical and physical conditions. The mission had its beginning in 1961 but suffered some initial failures and its success only became apparent later with Venera 4 that collected and sent back to Earth the first atmospheric data in 1967. A few of the Venera probes successfully landed and survived long enough on the surface in order to transmit back to Earth the data they collected. Among many scientific contributions, the Venera missions produced high resolution radar surface mapping and confirmed the existence of the superrotation phenomenon on Venus' atmosphere (Dollfus, 1975).

Mariner Program (1962-1973)

The Mariner program consisted of ten exploration probes designed by NASA which main aim was to investigate the planets. Mariner 1, 2, 5 and 10 were sent to Venus and Mariner 2 (Fig. 1.14) was the first probe to reach close contact (due to launch issues Mariner 1 ended up failing). The measurements made with its magnetometer confirmed the high surface temperatures of $460^{\circ}C$ (Sonett, 1963).

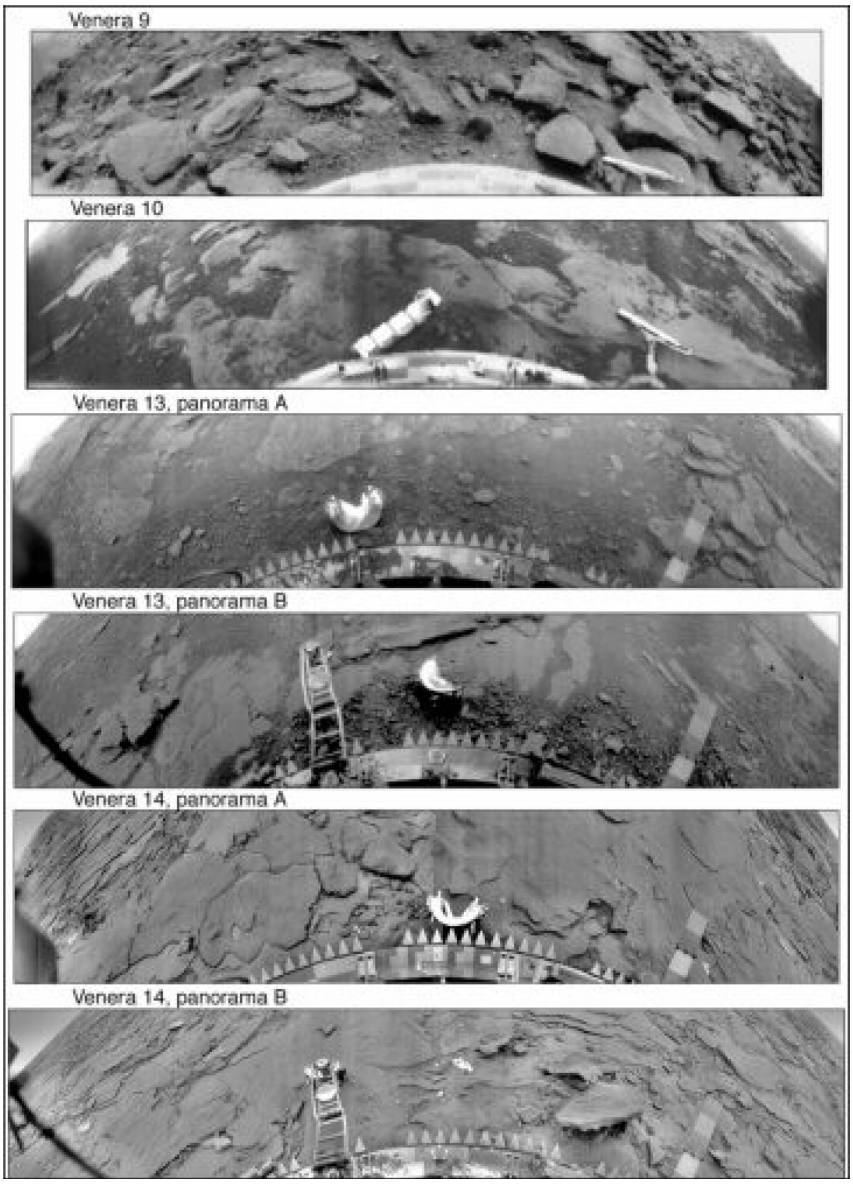

Figure 1.13: Surface images of Venus, taken from the Venera landers which were among the first images taken by mankind inside another planet. Credit:Hamilton (2005)

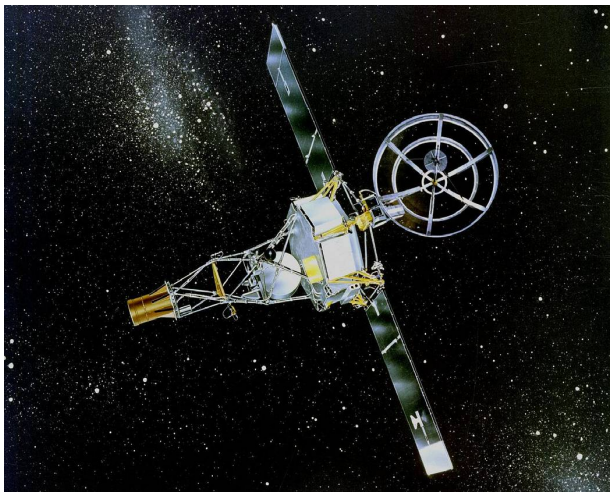

Figure 1.14: Mariner 2. Credit: NASA/JPL

Pioneer Mission (1978-1992)

The Pioneer Venus mission (NASA) consisted of two components launched separately: a Multiprobe and an Orbiter both launched in 1978. Due to its high elliptical orbit, the Pioneer allowed a global mapping of the cloud deck, ionosphere, upper atmosphere, surface mapping by radar, among many other experiments and contributions. The performed measurements of cloud and atmospheric properties were essential in the development of Venus atmospheric models (Collin and Hunten, 1977).

The mission was also the one responsible for the first measurements of Venus' weak magnetic field by means of an on-board magnetometer which was later confirmed by ESA's Venus Express. Another achievement was the discovery of the vast double vortex at the northern polar region of Venus.

On 1992, after running out of fuel, the Pioneer Mission came to its conclusion.

Vega (1984-1985)

As a continuation of the previous Venera program, this spacecraft mission combined a Comet Halley flyby and a Venus swingby and two identical spacecrafts, Vega 1 and Vega 2, were launched on December 1984 only a few days apart. The mission now included atmospheric balloons, besides the same basic probes and landers designs, as these could survive longer and measure the temperature, pressure and wind velocity (Blamont, 2008). The Vega and Pioneer missions were essential for the structured study of the atmospheric physical description and chemical behaviour since their measurements uncovered evidence of an active atmosphere, containing corrosive gases and also a thick cloud layer.

Magellan (1989-1994)

Named after the sixteenth-century Portuguese explorer Fernão de Magalhães, the Magellan spacecraft from NASA was launched on May 1989 and arrived at its destiny on August 1990. Magellan collected radar images of Venus' surface with resolution ten times better than the earlier Soviet Venera 15 and 16 missions (around 200 meters). The surface topography and electrical characteristics were also measured using radiometry and altimetry data. Upon reaching

the end of its already extended mission, the probe was crashed into the planet in a controlled manner with the last aim of obtaining some atmospheric data along its descent (Saunders et al., 1992).

Figure 1.15: Venus's surface obtained through radar data from the Magellan Orbiter in 1992. Credit: NASA/JPL. Magellan Project

Galileo (1989-2003)

On its way to Jupiter, the Galileo spacecraft made a Venus fly-by gravity assisted maneuver and made a few observations during its closest approach, taking advantage of Galileo's high resolution infrared camera. The images taken contributed to deepen the knowledge about cloud properties and their variability (Carlson et al., 1993). Galileo ceased operations on September 2003 after observing Venus, the Moon, Jupiter, two asteroids (Gaspa and Ida) and the comet Shoemaker-Levy 9 fragments from the impact with Jupiter.

Venus Express (2005-2015)

Venus Express (VEx) (Fig. 1.16) wass a spacecraft lauched by the European Space Agency (ESA) on the 9^{th} of November of 2005. Its main objective was to perform a global investigation of the venusian atmosphere breaking the long period without any space missions sent to this planet. Vex arrived at Venus on April 2006 and conducted studies under the general atmospheric circulation, cloud chemistry and escape processes for several distinct volatiles as well as interactions/connections between the surface and the atmosphere.

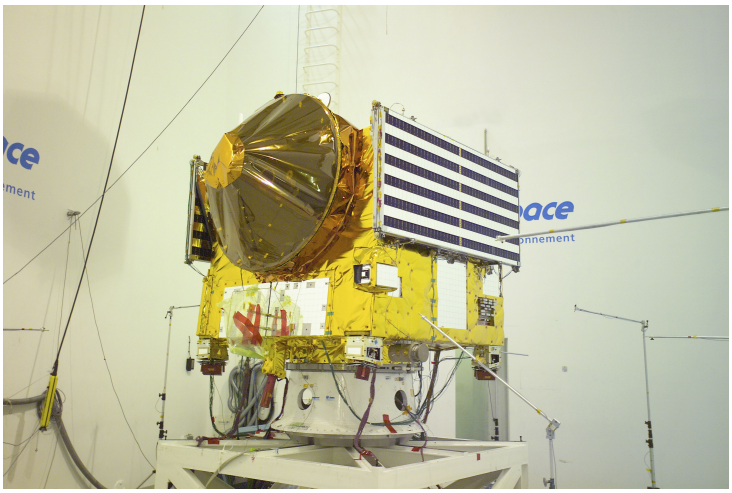

Figure 1.16: ESA's Venus Express, being packed ready to leave INTESPACE, Toulouse, for its launch site in Baikonur, Kazakhstan. It is shown with high-gain antenna wrapped and solar arrays folded. Credit: ESA

The orbital design was elliptical and highly eccentric (250 km at pericenter and 66 000 km at apocenter), with a period of 24 hours. This allowed global large scale investigations and high spatial resolution detailed studies of localised phenomena. After years of gathering knowledge and providing amazing discoveries, VEx's remaing fuel was exhausted and the contact with the spacecraft was lost. The mission reached its official end upon a declaration by ESA on the 16^{th} of December of 2014.

Venus Express most relevant scientific discoveries included the possibility of recent vulcanism, the atmosphere's superrotation speeding up, Venus' spinning slowing down, confirmation of the existence of a magnetosphere, the shape-shifting polar vortices and that Venus is loosing water through escape processes.

ESA's spacecraft carried on board some of the cutting-edge technology instruments at the time which included (Fig. 1.21):

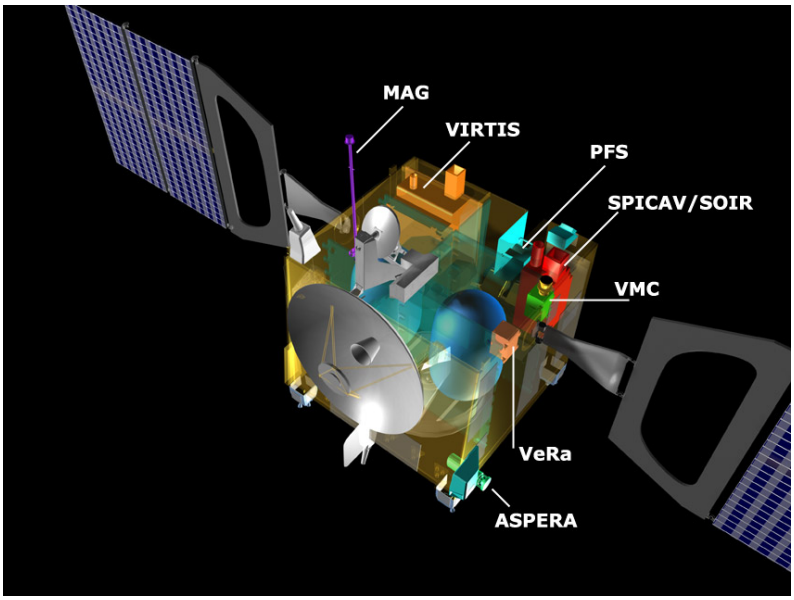

Figure 1.17: A cutaway diagram showing size and locations of Venus Express instruments: MAG, VIRTIS, PFS, SPICAM/SOIR, VMC, VeRa and ASPERA. Credit: ESA

- **ASPERA (Analyser of Space Plasma and Energetic Atoms):** designed to study the interaction between the venusian atmosphere and the solar wind, measuring outflowing particles from Venus' atmosphere and the ones that make up the solar wind and investigating how ions and molecules escape the planet;
- **PFS (Planetary Fourier Spectometer):** a high resolution instrument that measured the atmosphere's temperature from 55 km to 100 km of altitude as well as the surface's temperature, looked for vulcanic activity and made some composition measurements of the atmosphere;
- **VeRa (Venus Radio Science Experiment):** used the radio link between itself and Earth to investigate Venus' ionosphere. In addition, it was used to study the atmosphere's pressure, temperature and density (35 km up to 100 km of altitude) as well as electrical properties of the surface.
- **MAG (Venus Express Magnetometer):** studied the magnetic field generarted by the interaction between the atmosphere and the solar wind and its contribution to atmospheric escape processes;
- **SPICAV/SOIR (Ultraviolet and Infrared Atmospheric Spectometer):** searched for water in Venus' atmosphere and helped in determining the density and tempearture between 80 km and 180 km of altitude;
- **VMC (Venus Monitoring Camera):** is a wide-angle multi-channel camera capable of taking images of the planet in near-infrared, ultraviolet and visible wavelengths. It was able to make global images and study the cloud dynamics as well as imaging the surface.

VMC filter parameters				
Filter	**Centre wavelength (µm)**	**Bandwidth (µm, FWHP)**	**Observation goals**	
			Dayside	**Nightside**
F3 (UV)	0.365	0.04	Unknown UV absorber	O_2 nightglow at 0.356 & 0.376 µm
F4 (VIS)	0.513	0.05	Visible light imaging	O_2 nightglow at 0.376 µm
F5 (NIR1)	0.965	0.07	H_2O at ~70 km	H_2O below 70 km, clouds
F6 (NIR2)	1.01	0.02	H_2O below 70 km	Surface, clouds

Figure 1.18: VMC filter parameters. Credit: ESA

- **VIRTIS (Ultraviolet/Visible/Near-Infrared Mapping Spectometer):** was an imaging spectrometer that combined three observing channels in a single but powerful instrument. Its data can be used for cloud tracking (Section 2.5) in both infrared and ultraviolet wavelengths allowing the study of atmospheric dynamics at different altitudes.

Summary of VIRTIS Characteristics			
	Mapper subsystem		High resolution subsystem
	Visible channel	Infrared channel	Infrared channel
Spectral range (μm)	0.25 - 1.0	1 - 5	2 - 5
Maximum Spectral resolution (nm)	~2	~10	~3
Spectral resolving power (λ/Δλ)	100 - 200	100 - 200	1000 - 2000
Field of view (mrad) - "pushbroom" mode	64×0.25	64×0.25	0.45×2.25
Field of view (mrad) - scan mode	64×64	64×64	-
Spatial resolution (mrad)	1.0 (default) 0.25 (high)	1.0 (default) 0.25 (high)	1.0

Figure 1.19: Summary of VIRTIS characteristics. Credit: ESA website

Akatsuki or Venus Climate Orbiter

Akatsuki, meaning Dawn or Venus Climate Orbiter (VCO) is a Japanese (JAXA) space probe launched on 20 May 2010, but failed to enter orbit around Venus on 6 December 2010. After the craft orbited the Sun for five years, engineers successfully placed it into an alternative Venusian elliptic orbit on 7 December 2015 and Akatsuki could then begin its mission and it is still operational. Akatsuki's current orbital path takes it as close as 400 km to Venus,and as far away as 44 0000 km and has aperiod of 10.8 days. The goal of the Akatsuki project is to clarify the three dimensional motion of Venusian atmosphere over time and establish a meteorology of Venus. In order to achieve the ambitious goal, Akatsuki was equipped with several instruments introduce bellow:

- **LAC (Lightning and Airglow Camera):** is a camera which can detect lightning discharge at small intervals wich can be used to solve the controversial topic of lightning occurrence in the venusian atmosphere. In addition to this, it captures airglow produced by oxygen in the higher atmosphere allowing the visualisation of atmospheric waves and circulation between nightside and dayside;
- **IR1 (1 μm Camera):** uses the bands around $1\mu m$ allowing the observation bellow the clouds and near the surface of the planet. It can also allow, by comparing different infrared bands, to investigate the cloud movement in the lower atmosphere, the distribution of water vapor, the surface's mineral composition and look for the presence of volcanoes;
- **IR2 (1 μm Camera):** is used to observe the density and size of the cloud particles since the $2\mu m$ wavelengt is emmited from bellow the bottom of Venus' clouds. This will make possible to gain insight into atmospheric circulation at lower altitudes and into the formation process of clouds.
- **LIR (Long-wave infrared camera):** uses the $10\mu m$ wavelength to measure the temperature at the cloud tops making possible to study convection within the upper cloud layer as well as wind speed distributions on the upper cloud tops of both dayside and nightside;
- **USO (Ultra-Stable Oscillator):** When Akatsuki is concealed behind Venus as seen from the Earth, the radio waves transmitted by the USO graze the venusian atmosphere,

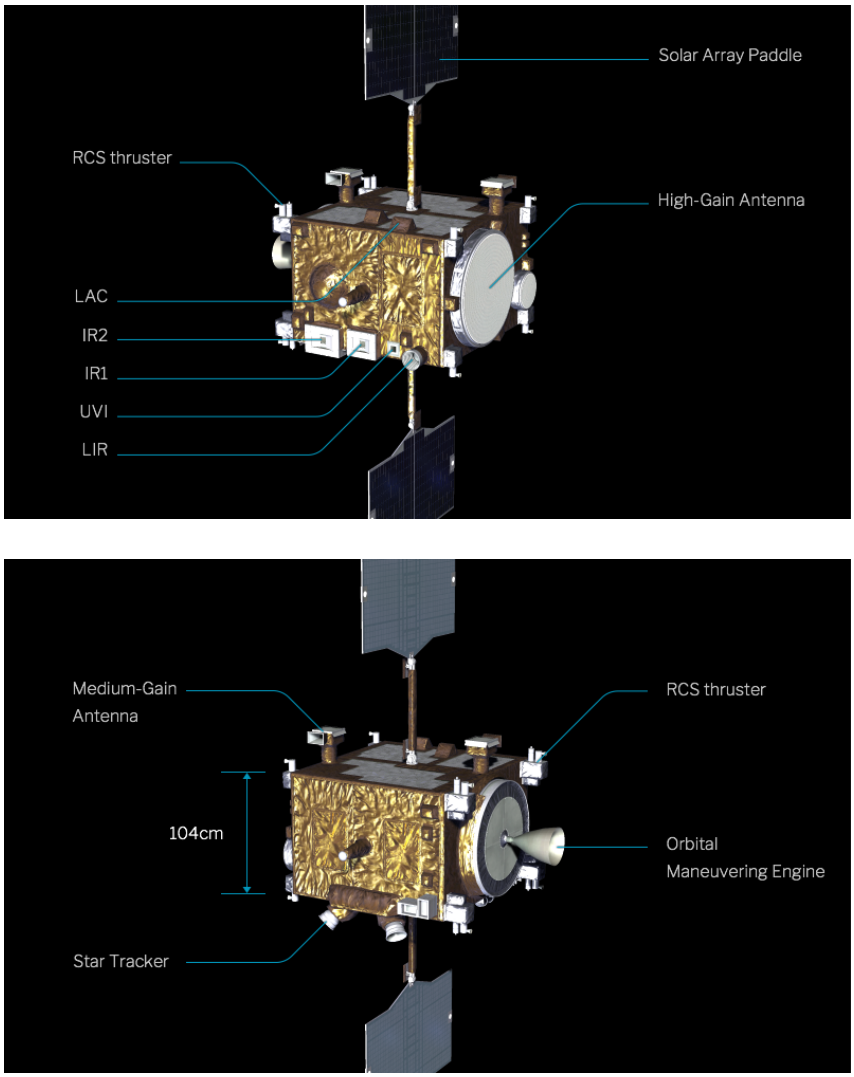

Figure 1.20: Akatsuki's components and main instruments. Credit: JAXA

changing their frequency, and reach the Earth. Analysing those changes allows scientists to measure the vertical profiles of temperature and sulphuric acid vapour;

- **UVI (Ultraviolet Imager):** acquires ultraviolet images, allowing us to obtain the distribution of sulphur dioxide, which is related to the cloud formation, and the distribution of unidentified chemical substances which absorbs the ultraviolet rays. Also, wind speeds at the cloud tops can be determined by tracing the dark-and-light pattern due to the scattering of ultraviolet rays in sunlight by Venusian clouds. This instrument operates in two different wavelengths:

  1. Ultraviolet - 283 nm (dayside of Venus and targets sulphur dioxide at cloud top);
  2. Ultraviolet - 365 nm (dayside of Venus and targets the unidentified absorbent substances).

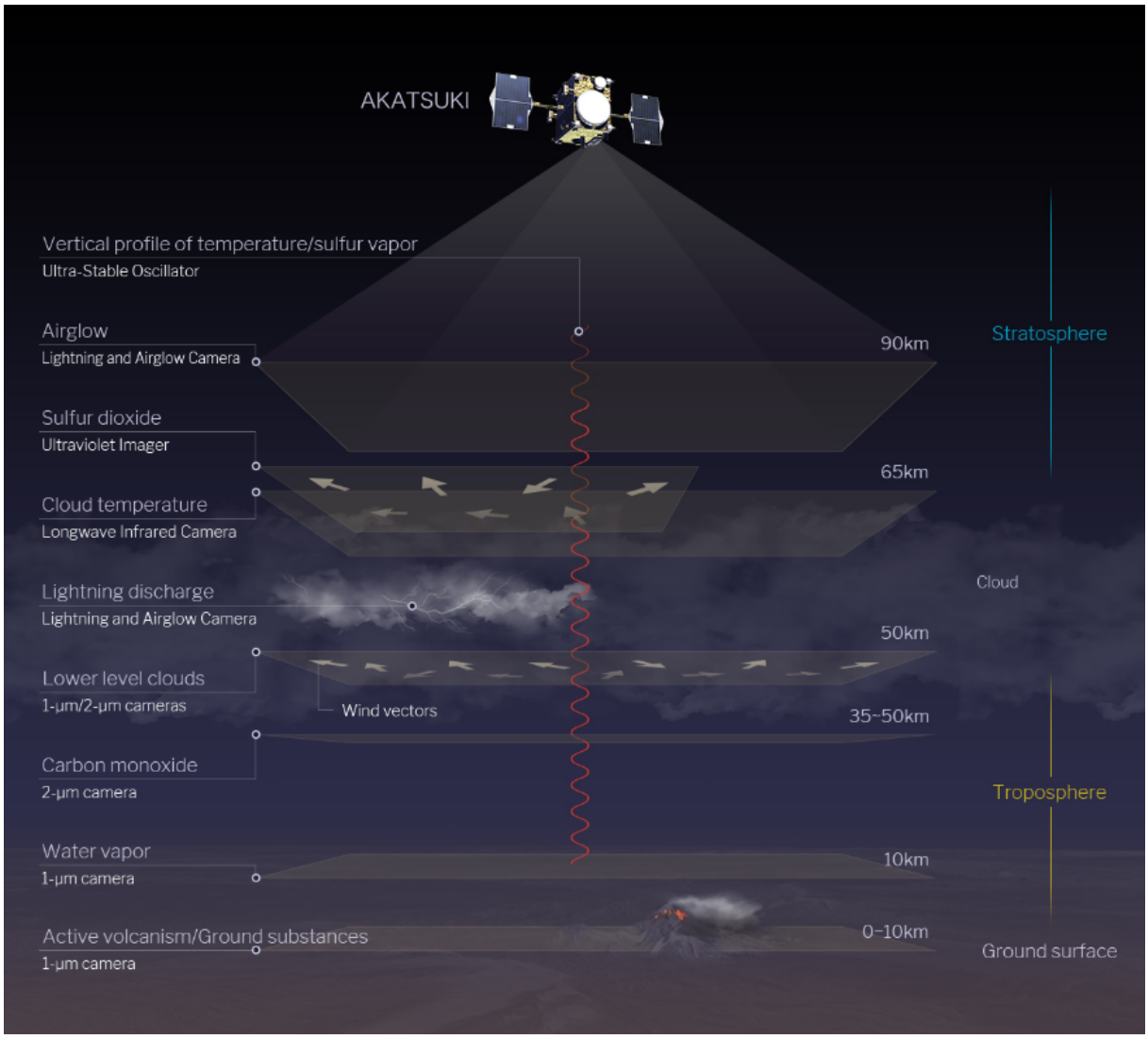

Figure 1.21: Conceptual figure of Akatsuki measurements. Credit: JAXA

1.3 Atmospheric Gravity Waves

Atmospheric gravity waves play an essential role in the global circulation of a planet's atmosphere. Generally observed in the stratosphere of most planets with atmosphere, these waves are periodic disturbances whose restoration force is buoyancy (Piccialli et al., 2014). They are responsible for very important dynamic phenomena such as, for example the vertical transfer of energy, momentum and chemical species (atmospheric gravity waves transport energy and momentum from the troposphere and deposit it in the thermosphere and mesosphere) and it is through its properties that one can draw conclusions about the static equilibrium of the atmosphere since these waves can only propagate in stably stratified regions of the atmosphere (Nappo, 2012). On Venus, gravity waves at cloud level might be due to convective motions of a lower unstable layer beneath the stable layer where these waves form. In addition, they could also be excited by Kevin-Helmholtz instabilities produced by a strongly sheared flow when close to neutral static stability (Sánchez-Lavega, 2011).

On Earth, atmospheric gravity waves are frequently generated in the troposphere by the clash of two different weather fronts or by airflow over mountains. These waves have a tendency to propagate to higher altitudes where they suffer the influence of nonlinear effects and break, transferring the energy and momentum that they carry to the mean flow of the atmosphere (Sánchez-Lavega, 2011).

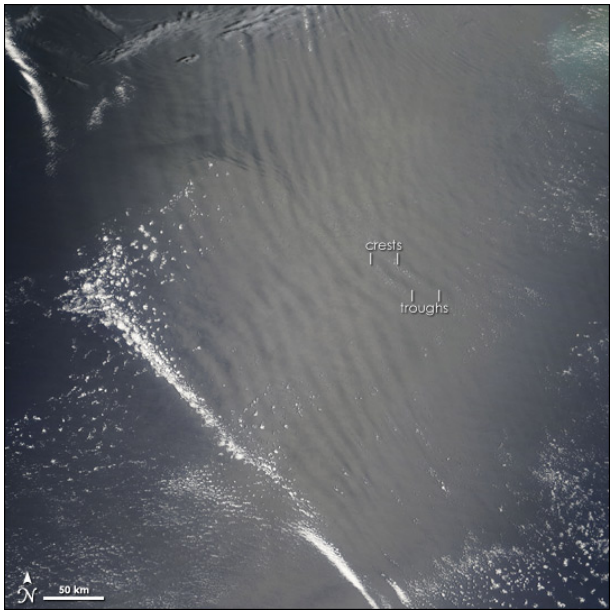

Figure 1.22: Atmospheric gravity waves on Earth's atmosphere over the Arabian Sea. Credit: NASA

A recent study (Piccialli et al., 2014) involving high resolution images acquired by Venus Monitoring Camera (VMC), at the cloud tops at high latitudes in the Northern hemisphere, observed periodic structures that have been interpreted as atmospheric gravity waves. Wave properties do not seem to vary with local time or latitude but this information is biased since VMC could not observe latitudes lower than $\approx 45^\circ S$ and neither with enough resolution (to observe these features clearly) on the nightside, considering the observations period in the published paper (Piccialli et al., 2014). The most wave activity was found between $60^\circ N$ and $80^\circ N$ (cold collar region) and was also concentrated above a continental highland in Venus (Piccialli et al., 2014).

Another systematic search for gravity waves was also carried out by (Peralta et al., 2008) but with the Visible and InfraRed Thermal Imaging Spectometer (VIRTIS) observations. Mesoscale gravity waves were detected in the upper cloud tops at about 66 km of altitude (using reflected ultraviolet light at 380 nm) on the dayside hemisphere and in the lower cloud layer at about 47 km of altitude (using $1.74\mu m$ thermal radiation) from the nightside hemisphere. The wave properties that were also measured included packet length, width, orientation and geographical position on Venus.

Chapter 2

Methods and Tools

2.1 Vex/VIRTIS-M

The VIRTIS imaging spectrometer is an instrument directly inherited from ESA's Rosetta cometary mission. It is composed by two separate telescopes that supply two different channels: VIRTIS-M, which is a mapping spectrometer working in the infrared and visible wavelengths (Fig. 1.19) and VIRTIS-H, a high resolution spectrometer that operates in the Infrared. With its unique combination of mapping capabilities at low spectral resolution (VIRTIS-M) and high spectral resolution slit spectroscopy (VIRTIS-H), the instrument is ideal for making extensive infrared and visible spectral images of planet Venus (Piccioni et al., 2007).

VIRTIS-M has also a noteworthy capability of capturing images simultaneously at different wavelengths, compressing this information into a three dimensional structure called "data cube". Using this we are provided with a vertical profile of Venus' cloud structure at different wavelengths and we are capable of studying the cloud dynamics at different altitudes. VIRTIS data is gathered and stored in the Planetary Science Archive (PSA) of ESA, where it appears divided into three types: RAW, GEOMETRY and CALIBRATED.

- **RAW:** are the non-navigated VIRTIS images. These have only been subjected to preliminary processing from telemetry data, which comes from the spacecraft, that is analysed by VEx's ground segment tasked with writing the data files. These data files are then made available in ESA's archive as Planetary Data System (PDS) files;

- **GEOMETRY:** is the data which comprises all the geometrical information of a specific image. It is basically the file that stores information on navigation measurements and geometrical calculations performed during calibration;

- **CALIBRATED:** are image files that have been processed. This means that these images are navigated and corrected in terms of instrument defects. The data in calibrated images is in physical units (radiance) and provides a description of viewing configurations (location, local time, viewing angles and season).

Regarding the contents of this work, the CALIBRATED data was the one used since it already possessed the geographical information of geometry data and is mostly corrected for defects present in RAW images. In short, the CALIBRATED images are the most suitable for both cloud tracking and gravity wave detection and characterisation.

2.2 Vex/VMC

The images captured through the VMC instrument on board Venus Express have allowed a complementary investigation of phenomena observed with VIRTIS. Despite this, VMC is better tuned for wavelengths in the visible light part of the spectrum, therefore, it was mostly used to analyse the upper clouds of Venus. In particular, UV-absorption of the top cloud layers produces noticeable features which can be tracked for wind velocity measurements. These absorptions are mainly due to the presence of sulphur dioxide and a still unidentified and unknown absorber (Markiewicz et al., 2007).

VMC images also allow search and visualisation of atmospheric mesoscale gravity waves (Section 1.3). The images with positive detections of these waves allow a certain degree of characterisation by measuring width, length, wavelength and altitude (Piccialli et al., 2014).

Unfortunately, the analysis of VMC images with PLIA (Section 2.4) was limited since the built-in navigation algorithm in PLIA was, at the time of study, not able to compute latitude-longitude coordinates for each of the image's pixels. Nevertheless , some information can still be extracted, namely the time associated with each image as well as the date. For cloud tracking purposes (explained bellow in this chapter) this can be troublesome since image navigation is required for the image correlation software to function. As such, navigated images were provided through contact with Ricardo Hueso and Javier Peralta so that this study could be performed with several different instruments and a more in depth exploration of the software could be made.

2.3 Akatsuki/UVI

The UVI instrument carried by the still operational Akatsuki takes ultraviolet (UV) images of the solar radiation reflected by the Venusian clouds, with narrow bandpass filters centered at the 283 nm and 365 nm wavelengths. These wavelengths are considerably relevant since there are absorption bands of sulphur dioxide (SO_2 which has an absorption band in the wavelengths 210–320 nm) and unknown absorber (which maximum absorption is around 400 nm) in these cloud regions (Pollack et al. (1980) and Esposito et al. (1997)). UVI takes nominal sequential images every 2 hours considering that higher observation frequencies are inhibited to maintain the thermal condition of the instrument.

The UV images are able to provide the spatial distribution of SO_2 and the unknown absorber around cloud top altitudes. In addition, these images are used to estimate the horizontal winds by tracking cloud features. The images also allow a better understanding of the cloud top morphology and haze properties. UVI data, combined with data from other onboard instruments, is also used for the investigation of the generation mechanism of superrotation in the Venus' atmosphere (Yamazaki et al., 2018).

Observation target	Solar radiation scattered at cloud top
Optics design	Camera with off-axial catadioptric optics
Observational wavelength	283 and 365 nm
Field-of-view	12°
FOV per pixel	0.20 mrads
Spatial resolution	∼200 m (periapsis)–76 km (60Rv)
Optics	
F-number	16
Focal length	63.3 mm
Aperture size	39.89 mm (hood entrance)
Bandpass widths of the filters	14 nm
Detector	
CCD	SiCCD (back-illuminated and full-frame transfer)
Pixel number	1024 × 1024 pixels
CCD control	
Exposure time	4 ms–11 s
Data depth	12 bit

Table 2.1: Characteristics of UVI from VCO where R_V is Venus' radius. Credit: Yamazaki et al. (2018)

2.4 PLIA - Planetary Laboratory Image Analysis

PLIA is an integrated set of programs written in Interactive Data Language (IDL) that possesses a fully operational and practical Graphic User Interface (GUI). PLIA was developed at the University of the Basque Country and was shared wit the research group in Lisbon by the Bilbao team in a shared study collaboration opportunity.

PLIA's software aims to aid in the study of atmosphere dynamics by allowing the processing of astronomical images. This includes, to some extent, planetary navigation which is essentially the assignment of longitude and latitude values to each one of the pixels in an image. Such navigation is imperative and crucial to most of scientific measurements in planetary sciences since it becomes possible to ascertain the position, displacement and velocity of surface and atmospheric features present on planets and moons. PLIA also incorporates a wide range of numerous image correction tools, some dedicated to certain instruments like VEx/VIRTIS, photometric scans and is also capable to compute geometric projections of images into cylindrical and polar maps, which are useful for cloud-tracking procedures. These geometrical projections show only small sections of the complete Venus' map, where the size is inherited from the original limits of the unprocessed image. This a crucial step for cloud tracking which is performed by auxiliary software to PLIA described in later sections.

One of PLIA's most important and useful features is the possibility of performing image corrections, exemplified by Figure 2.1. Even on already calibrated data, this element is helpful for extracting features for our study. Most "original" images, untouched by the software, are not appropriate for the identification of more subtle features such as cloud formation hence some treatment is required before proceeding to the analysis. Additionally, images may contain artificial features of the detector that can be diminished and removed with the software when possible.

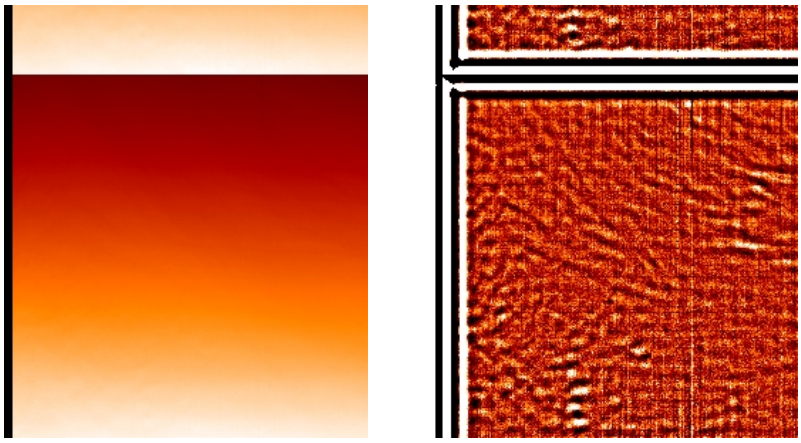

Figure 2.1: example of a selected data plane of a calibrated VIRTIS image. Left panel shows an unprocessed image loaded into PLIA while the right panel shows an image with enhanced contrast after several unsharp-mask processes.

The wavelength range of VIRTIS observations makes possible to select, inside the range of interest, optimal wavelengths where image aberrations are least present. The most common treatment performed on images is contrast enhancement which makes most features in VIRTIS images visible, often accompanied by an unsharp mask filter (several more filters are available and can be used when deemed appropriate).

This software can run on any operating system supported by IDL and was already widely used to analyse images retrieved by the Galileo Solid Stage Imaging of Jupiter and Venus (Belton et al., 1992), Cassini Image Science Subsystem of Jupiter and Saturn (Drossart et al., 2007) as well as hyperspectral cube images obtained by VIRTIS on board Venus Express (Hueso et al., 2010).

2.5 Cloud Tracking

As a focus point for this work, the image processing steps described above are required, for the most part, to allow clear observation of the movement of cloud features on planet Venus.

By analysing a pair of navigated and processed images, and knowing the time interval between both, it is possible to probe the movement of cloud features from the first image to the second image, either by matching specific areas or specific points in both images. This matching process allows us to measure displacements and velocities of cloud features and, at last, deduct the average velocity for a certain cloud layer of the atmosphere, selected in the wavelength range of the observations. The method for cloud tracking used also allows to retrieve separate wind velocity measurements for both zonal wind $\mathbf{u}$ and meridional wind $\mathbf{v}$ defined in Section 1.2.4.

Cloud tracking is performed with the aid of designated software and may be performed in a fully automatic manner by a computer algorithm, semi-automatic where there is an input of the user or even entirely manual where the user is involved in the whole process. Regarding this, it has been noticed that full automation produces many wind measurements but also may lead to some untrustworthy wind velocity results (Hueso et al., 2013). Thus, the method used in this work relied on supervised (PICV2) and manual (ACT) procedures when evaluating the wind tracers determined by the software.

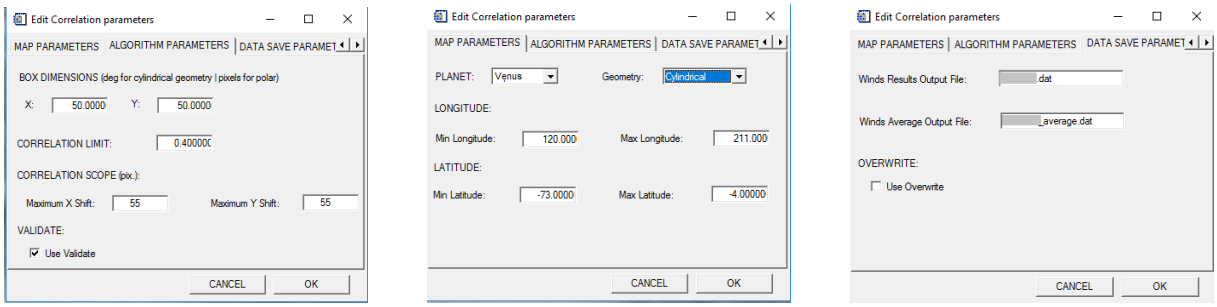

Figure 2.2: Showcase of PICV2 correlation options before performing cloud tracking. Left panel lets the user provide information regarding mapping of the image and the target planet.The middle panel allows the user to choose a correlation box size as well as a correlation limit for validation of wind vector and the maximum feature displacement (given in pixels) between the image pair that can be measured. The panel on the right manages where the results of cloud tracking will be exported to.

2.5.1 PICV2

The Planetary Image Correlation Velocimetry (PICV) (the version used was 2.2 hence PICV2) is an IDL based program such as PLIA and it works as an auxiliary tool for PLIA's software. The Venus' images must be navigated, properly named and spaced in a time interval between 30 minutes and 2 hours in order for PICV2 to determine wind vectors correctly. In addition to this, processing and contrast enhancement is imperative for PICV2 to adequately recognise and identify different atmospheric patterns in the clouds. This will allow the software's image correlation algorithm to associate the cloud patterns in an appropriate manner.

This software operates firstly by applying an image correlation algorithm between both images to recognise atmospheric cloud patterns, which are identified through image contrasting shapes. PICV2 will then measure the pixel displacement of these features from the first to the second image and, using the information provided regarding geometry and time associated with each image, it is able to compute each of the winds' components mentioned above and draw the corresponding wind vector on the second image.

To apply the image correlation algorithm, the software divides each images' area box into smaller correlation boxes, which size is previously customised by the user, until all possible available space in the are box is occupied. The size should be appropriate for the cloud features present in the area selected during cloud tracking. For example, if these features appear as elongated shapes, a rectangular (more stretched) correlation box shape is preferential to completely capture said feature. The same pair of images can also be analysed several times with different box sizes in search for an optimal one or to capture both elongated and smaller cloud features. Furthermore, it is of utmost importance to provide the latitude and longitude limits of the images in addition to the type of projection they possesses (polar or cylindrical) since this changes how the software's algorithm works.

The user can, depending on the typical wind velocity of the target, select the correlation scope for cloud tracking by applying limits to the vertical and horizontal displacement (shift) that is recognised as cloud movement. Once again, the image projections' geometry plays an important role when the software interprets the values given. If the user is working on a cylindrical projection, these values are degrees whereas for dealing with polar projections, these values are in pixels.

Finally, still before the software starts the correlation procedure, the user must manage where the results will be saved. The output file is a statistical average of the wind velocities

obtained along an horizontal line, representing the average wind velocity in a latitudinal zone. These output files are stored in data files readable by any standard text editor software.

As the software runs its correlation algorithm, another interface window will show up which allows the user to supervise each wind vector that is measured by PICV deciding whether it is a valid measurement or not. This is called a semi-automatic cloud tracking method. The new window will show the relative correlation boxes on each image accompanied by their surrounding areas so the user can evaluate which cloud features are being compared by the algorithm. Along with these sections of the images, a colour map is shown representing how the correlation values varies between the images. A good wind measurement is obtained when this s correlation map shows a sharply localised zone of high correlation values (about 0.7 or better depending on the images' quality). It is possible to "abort validation" and let PICV continue the correlation process, without the supervision and validation of the user, based on previous validation decisions made and all the criteria selected previously to the start of the cloud tracking process. This is the method often called fully automated cloud tracking.

When the area box selected for cloud tracking is exhausted, the wind results are stored in the appointed data files that can be used for plot building. As stated above, it is possible to perform cloud tracking several times in the same image pair, focusing on different zones to better cover other features or on the same area but with a different parameter selection for the whole process of cloud tracking. The equations that permit wind velocity determination are the following:

$$u = \frac{\Delta X}{\Delta t} \tag{2.1}$$

$$v = \frac{\Delta Y}{\Delta t} \tag{2.2}$$

Where ΔX and ΔY are the latitudinal and longitudinal displacements of the cloud features respectively (in meters) and Δt is the time interval between both images (in seconds).

Error Handling

This section is dedicated to describing the process of error handling with PICV. Instrumental errors, that are inherent to each image and, thus, unpredictable, are ignored in this description. However some sources of error that require careful examination still remain and must be tackled so that cloud tracking results are scientifically accurate.

The process of image navigation is performed individually on each image, and all the calculations involved, rely on previous information about planetary body shape, size, and time values. Navigation of a target planet may be inaccurate by a certain number of pixels in the image which can generate a "mapping" difference when both images in the pair are navigated and geometrically projected. This error in geographical coordinates between a pair of images will certainly induce an error when PICV2 computes displacements of atmospheric features (due to the error in the features' position) to measure wind velocity components.

Another source of error that can affect the wind velocity measurements is linked to time. The time interval between the images selected for cloud tracking is computed as the difference between the time dates registered on each of the images, which come from a calculation based

on the on-board spacecraft clock. Although most of the clocks implemented on spacecrafts are atomic clocks, which are known for their precision and regularity, the time coordinates transformation can introduce a temporal error. In short, these errors will translate in a slight deviation on the wind velocity values since PICV2 uses the date provided on the name of both images needed for cloud tracking.

As described above in this section, PICV makes use of correlation boxes to recognise cloud patterns and determine their displacement from the first to the second image. The size of the boxes is customised by the user of the software and can be adjusted to different dimensions within the image pair being analysed. As the image correlation algorithm depends on the size of this box and on the vertical and horizontal displacement in each measurement, this is also a source of errors for the wind vectors that are calculated.

In an approximation, PICV computes the wind velocity vectors. as explained, by measuring the displacement of cloud features within the given time interval between the image pair (Equations 2.1 and 2.2). Regarding this, the error of the measurements made depends on the latitude and longitude coordinates of the projected images used for cloud tracking, and on the precision of the time between both images.

When a cylindrical or polar projection is performed with PLIA, the user is able to choose the resolution, given in degree/pixel, with which the projection process will be carried out. It is then necessary to account for the conversions necessary to obtain an error in meters such as converting degrees to radian units, take into account the radius of the target observed as well as the height of the cloud layer that is being analysed (Equation 2.3).

$$\delta s = \delta\theta \cdot (R_p + h) \tag{2.3}$$

Where δs is the displacement error, $\delta\theta$ is the resolution of the projected image in radians, R_p is the radius of the planet (in the case of this work is Venus' radius) in meters and **h** is the height of the atmospheric layer.

Regarding the temporal error, it will be considered negligible since the precision of the clocks on-board the spacecrafts is of the order of the millisecond which makes the temporal error insignificant compared to the displacement error, and thus, it can be discarded. The error of the wind velocity δw_v is given by (Peralta et al., 2008):

$$\delta w_v = \frac{\delta s}{\Delta t} \tag{2.4}$$

To handle these fluctuations throughout the work, one simple but effective technique which can be used is the application of a data binning through a weighed average of the data points that are generated by the cloud tracking software within a certain latitudinal range. Given all the data points retrieved by PICV2 between a minimum and maximum latitude values, the weighed average within the selected latitudinal interval ($WA(V^{obs})$) can be given by:

$$WA(V^{obs}) = \frac{\sum_{i=1}^{n} V_i^{obs} \sigma_i^{-2}}{\sum_{i=1}^{n} \sigma_i^{-2}} \tag{2.5}$$

Where V_i^{obs} is the i^{th} data value to average and σ is the error associated with each individual

observation point. This strategy is indeed quite simple, however it becomes powerful as it negates the effects of outliers in the data used which in turn leads to better results.

2.5.2 ACT

ACT or Automatic Cloud Tracking is a software mainly developed by Javier Peralta, which allows the user to apply a manual cloud tracking method to Akatsuki's images.

Similarly to PICV, this software relies on the navigation of Venus images to accurately determine wind vectors. However, uncertainties such as the thermal distortion affecting the Akatsuki spacecraft and the on-board cameras, prevent high accuracy in the navigation of the Venus' atmosphere images at present, so additional corrections in the navigation (Figure 2.3) are still required (Peralta et al., 2018). The navigation of the images was then corrected with an algorithm able to perform an ellipse fitting from a manual determination of the planetary limb pixels, already available in the software. In order to perform this correction, the user selects four locations on the limb (limb points) and manually fits the grid using these points as reference (Figure 2.4). The software allows the interactive adjustment of the position, size, and orientation of the planet's grid. For this work, the grid was adjusted to the 1 pixel precision whenever it was deemed necessary but it was never needed to adjust the grids in size nor orientation. It was possible to save the new grids as geometry files for a second cloud tracking process if needed.

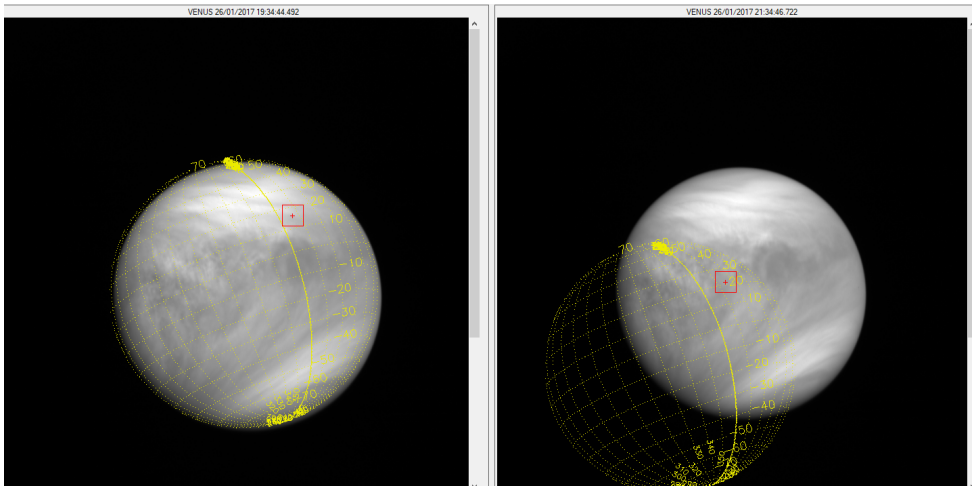

Figure 2.3: UVI image pair (day 26/01/2017 of the 365 nm filter) where the right image shows an incorrect navigation (grid in yellow).

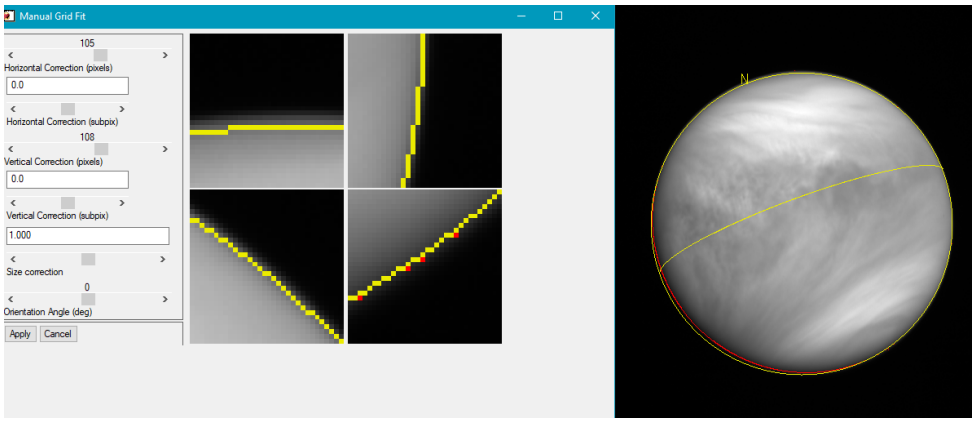

Figure 2.4: Grid fitting process (day 26/01/2017 of the 365 nm filter) by using four limb points as reference (new grid in yellow).

After verifying the navigation, correcting the image in a similar way to PLIA was necessary, this time to help the user, and not the software, to better distinguish between the cloud features presented on the image pair. In order to achieve this, both images were subjected to adjustments of brightness and contrast, followed by a sharpening of the images with an unsharp-mask filter technique. This processing was done simultaneously to both images on each cloud tracking session so that the two would have as similar as possible corrections (Figure 2.5).

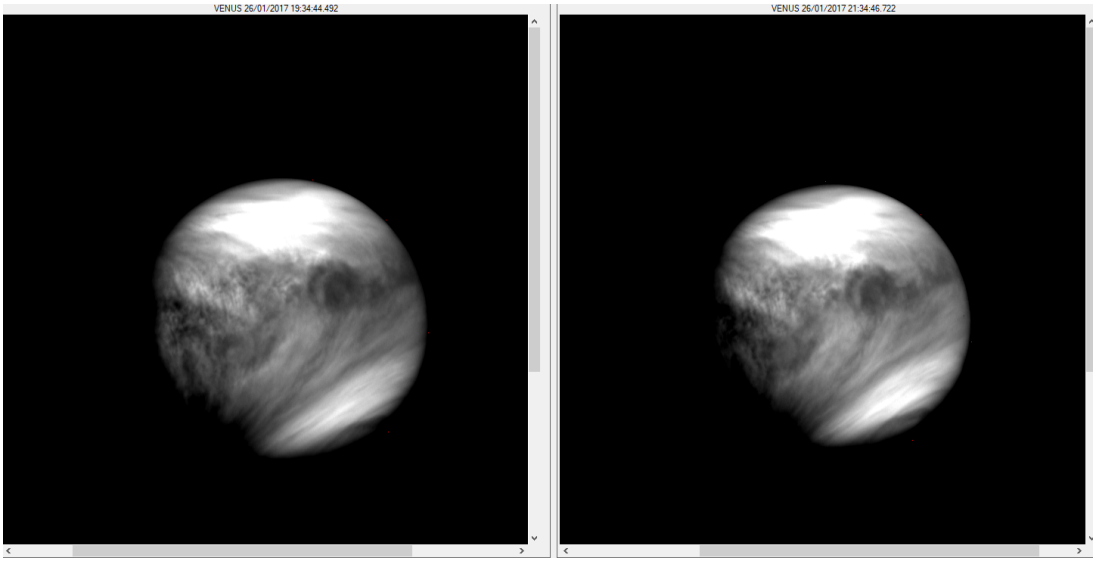

Figure 2.5: UVI processed image pair for 26/01/2017 of the 365 nm filter (before projection).

After correcting the navigation and processing the images, these were geometrically projected onto an equirectangular (cylindrical) geometry with a certain chosen by the user. The manual cloud tracking technique could then be applied. Wind tracers were marked by manually searching for a feature in both images, followed by a fine adjustment using automatic template matching, which is visually accepted or rejected by the human operator performing the study. This means that, when the tracer identification is judged as not satisfactory by the user running the analysis, the wind measurement is discarded. These manual measurements can be verified by a human operator by looking at visual reports (similar to Figure 2.7) that are saved along with tracer identifications and wind measurements. The measurements are obtained by comparing the position on the map of cloud features that can be identified in two consecutive images with

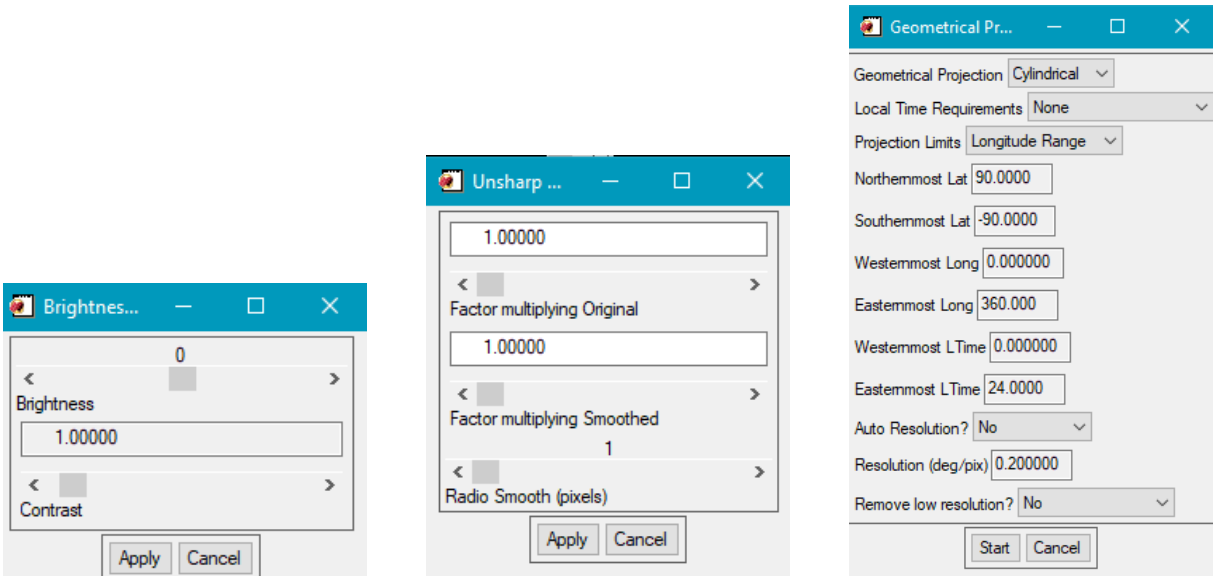

Figure 2.6: Showcase of ACT correlation options to fine tune before performing cloud tracking. Left panel lets the user manipulate image contrast and brightness, middle panel shows the specifications of the unsharp mask filter that can be changed for optimal results and the right panel allows the user to fill the projection limits and change the projection resolution.

a given time difference. The errors for the wind speeds obtained with manual tracking were calculated from the spatial resolution and the time interval between the images (Bevington and Robinson, 1992).

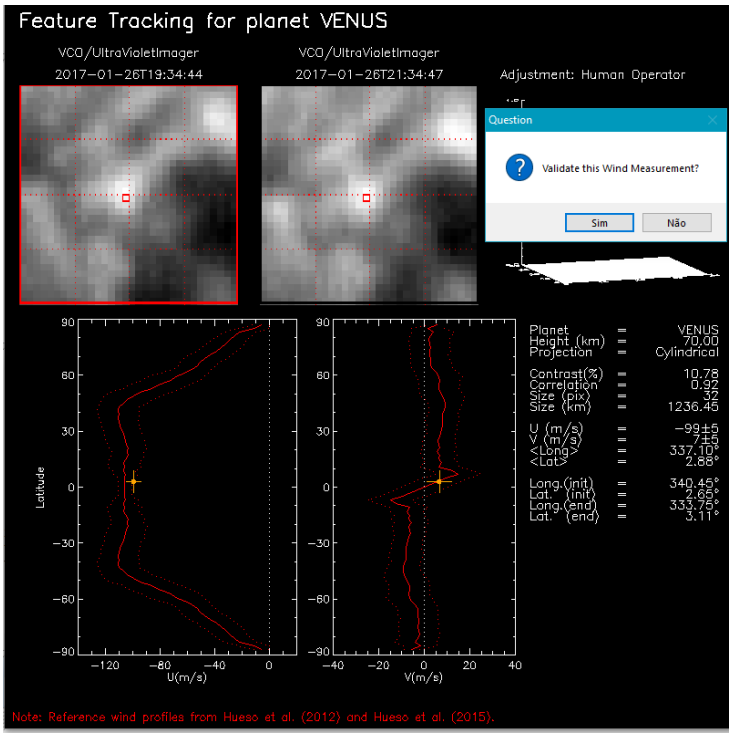

Figure 2.7: Validation process of a manually selected wind tracer.

Once the wind measurements were obtained, the same binning process, described in Section 2.5.1 for PICV2, was applied to obtain latitudinal wind profiles similar to Sánchez-Lavega et al. (2008).

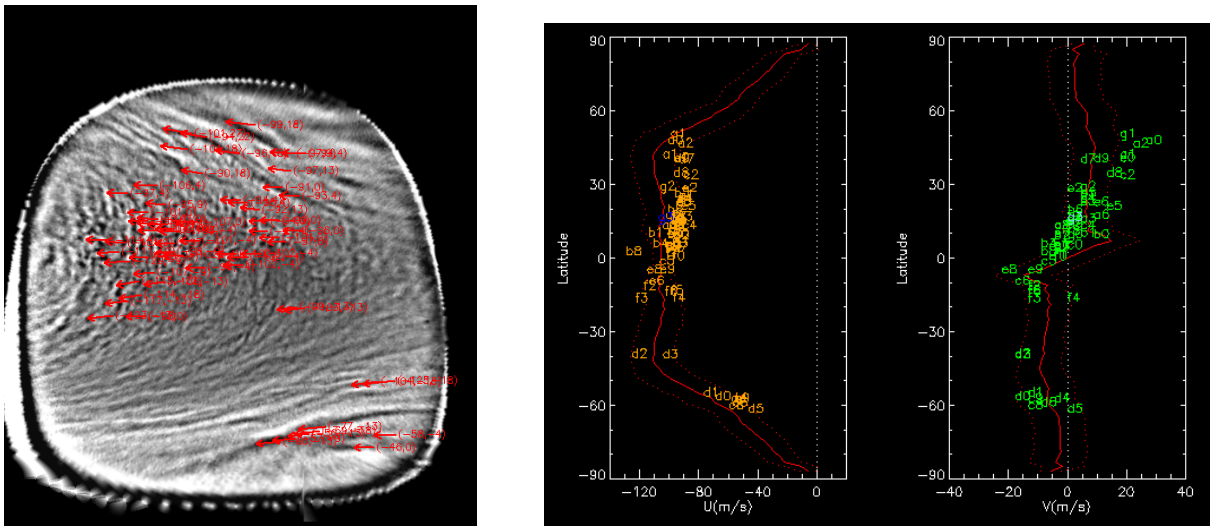

Figure 2.8: Wind tracers mapped on top of UVI image from 26/01/2017 of the 365 nm filter (left picture) and profiles showing the distribution of the same tracers as zonal (left) and meridional (right) wind measurements (right picture).

2.6 Atmospheric Gravity Waves

The detection and characterisation of atmospheric gravity waves, described on Section 1.3, is of utmost importance for the analysis and study of the Venusian atmospheric dynamics. Understanding how these waves are created and how they influence the atmosphere can supply valuable clues to solve the still vaguely known phenomena of Venus such as superrotation. In this section it will be briefly described how the detection and characterisation of atmospheric gravity waves were processed in the course of this work.

2.6.1 Detection

The detection of atmospheric gravity waves was processed solely on VMC images following the works of (Piccialli et al., 2014) and (Peralta et al., 2008). Each VMC image was manually checked and analysed with three main concerns: firstly, the existence of atmospheric gravity waves, secondly, the existence of image defects and imperfections and lastly, how severe these were. A data base was filled in Excel, similar to the work of (Silva, 2017), in order to display the information needed in an understandable and accessible way and complete it with a statistical analysis of atmospheric gravity wave detection numbers on each orbit analysed.

Atmospheric gravity waves appear in VMC images as sequences of crests above the cloud layer and can present different morphologies and lengths (at times two wave packets can be identified interacting with each other in the same image). Images that presented at least three visible crests in a row were classified as “positive” for presence of atmospheric gravity waves.

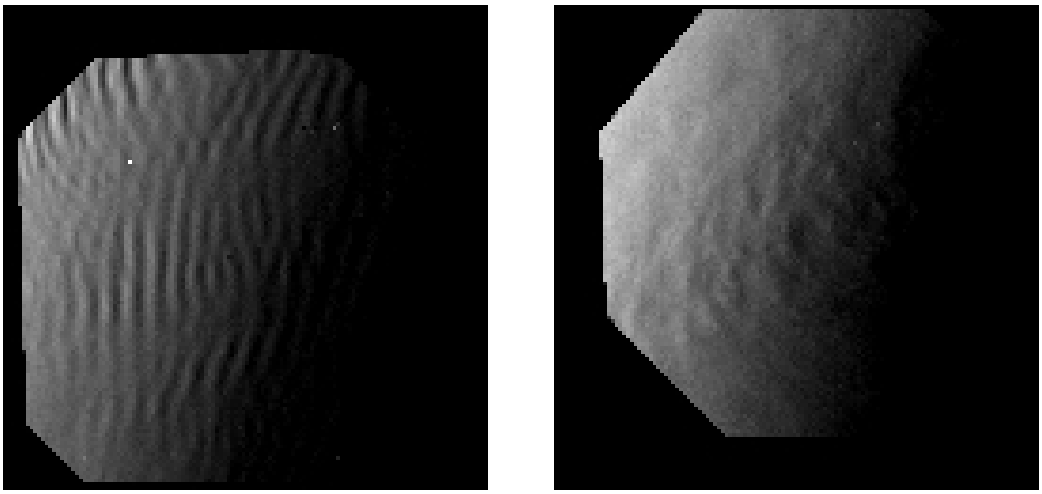

Figure 2.9: Atmospheric gravity waves on Venus as observed by the VMC instrument.The left image was taken with the NIR2 filter and the right image with the VIS filter, showing the appearance of atmospheric gravity waves at different wavelengths.

However, the quality of the images can be a hindrance wen identifying these features since the clarity can be compromised. The "doubt" classification in the Excel data base was then used for the cases where a trustworthy confirmation was not possible. The reasons for doubts are also briefly registered in a text file, allowing an easier verification as to whether or not the image actually presents waves.

To complete the data base, a column describing image imperfections and artifacts was also filled with a classification based on how much the image was affected by these aberrations. The terms used were the following (Silva, 2017):

1. **"No":** the image presented no visible imperfections and no feature stood out as an aberration (Figure 2.10);

2. **"Mild":** the image presented small artifacts or imperfections which did not overall influence the examination of the image for the detection of the atmospheric gravity waves (Figure 2.11);

3. **"Moderate":** the image showed an overall noise signature and imperfections which affected and lowered image quality and made the detection of waves harder (Figure 2.12);

4. **"Strong":** the image was completely or almost completely covered in artifacts and noise that significantly degraded the image's quality (Figure 2.13). Detection was impossible in this images since it was impossible to distinguish any kind of feature on the atmosphere of Venus.

2.6.2 Characterisation

Once gravity waves were identified, they needed a proper characterisation. Wavelength and phase velocity measurements were performed solely on VIRTIS images, provided by Pedro Machado (Instituto de Astrofísica e Ciências do Espaço), since at the time of this work it was not possible to perform wave characterisation on VMC images as they lacked image navigation.

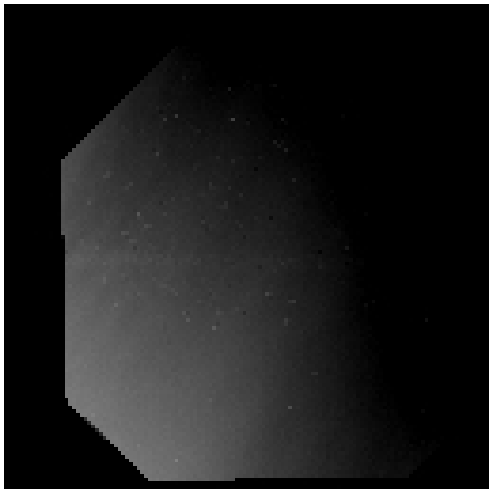

Figure 2.10: VMC image with no noticeable defections or aberrations.

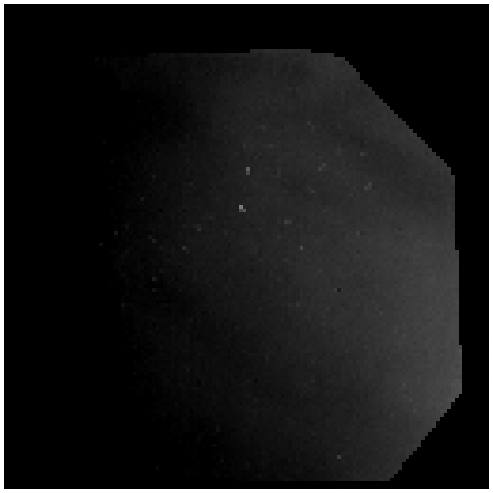

Figure 2.11: VMC image with Mild defections or aberrations.

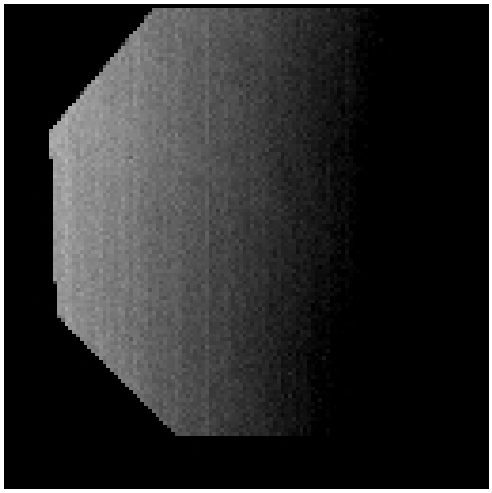

Figure 2.12: VMC image with Moderate defections or aberrations.

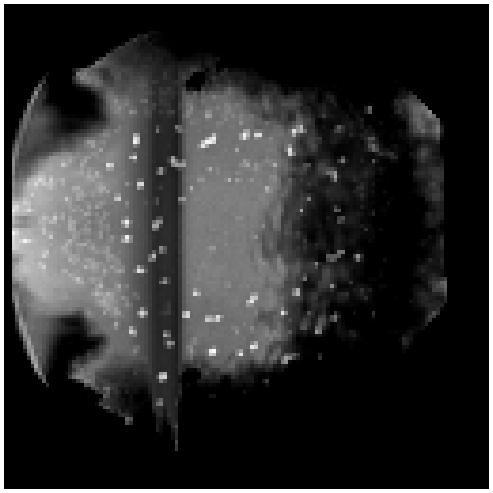

Figure 2.13: VMC image with Strong defections or aberrations.

The VIRTIS images already had attached a geometry file, which provided a proper navigation required in order to measure the distance between two points on the observable cloud layer.

Wavelengths of atmospheric gravity waves are measured by selecting two consecutive crests of a train of waves, determine their latitude-longitude coordinates and finally performing the following calculation:

$$\lambda = R_V \times \frac{\pi}{180} \sqrt{(Lat_2 - Lat_1)^2 + (Long_2 - Long_1)^2} \tag{2.6}$$

Where R_V represents Venus' radius which value is 6 051 km (Table 1.1), Lat the latitude and $Long$ the longitude, both in degrees, of points 1 and 2 marked on the crests of the waves as shown in Figure 2.14. For a correct measurement of the wavelength, it is needed to take into account not only the radius of Venus but also the height at which the instrument is probing, which can range from 48 km for lower clouds and 66-70 km for the upper clouds. Equation 2.6 is a general formula to measure the distance between two points on the surface of a planetary body and can also be used to compute a preliminary result for phase velocity of the trains of waves observed with VIRTIS instrument.

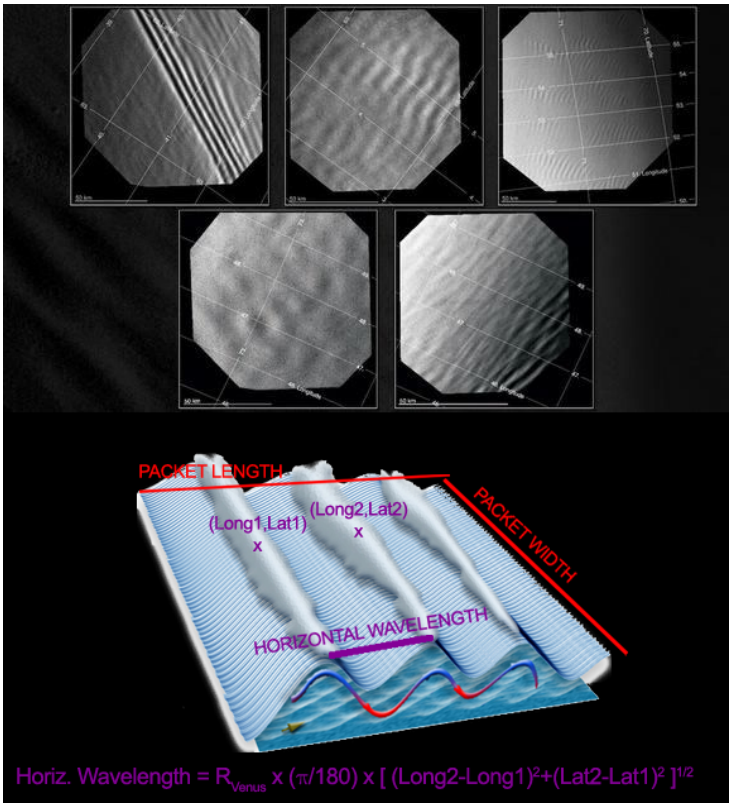

Figure 2.14: Schematic that illustrates how wavelengths of atmospheric gravity waves can be measured, provided the image is navigated. It also shows some examples of wave features (top) on which these calculations can be performed. Credits:Private communication,Javier Peralta (JAXA-Japanese Aerospace Exploration Agency).

To obtain an accurate measure, the line that separates both points on the wave crests must be perpendicular to the crests (parallel to the direction of propagation of the wave train). This guarantees that the distance measured is the shortest possible. Since the measurements were performed solely manually and by eye, special care was taken to ensure that the measurements were performed as thoroughly as possible.

Chapter 3

Observations

3.1 Venus Express

3.1.1 VMC

A complete collection of VMC data is available in PSA, however, these images are not navigated and PLIA is unable to perform navigation on these images, since its algorithm does not perform this step on VMC data. Fortunately, two pairs of navigated VMC images (Table 3.1), covering the entire southern hemisphere of Venus, were provided by Ricardo Hueso and then cloud tracked using PICV2.

Vex Orbit	**Image Pairs**	**Date (dd/mm/yyyy)**	**Time Interval (min)**	**Latitude Range (°)**
V0030	V0030_0099_UV2	20/05/2006	47	90° S - 0° S
	V0030_0117_UV2			
V0031	V0031_0000_UV2	21/05/2006	58	90° S - 0 S°
	V0031_0040_UV2			

Table 3.1: VEx/VMC observations in the UV (365nm) where cloud tracking was performed. Image navigation and cylindrical projections performed by Ricardo Hueso.

Since it was possible to access a large number of VMC images, detection of gravity waves was done on over 50 orbits starting on orbit 1604 and finishing on orbit 1654 where each image was analysed using the criteria explained above (Section 2.6.1). These include observations in all VMC filters at the designated wavelengths (Figure 1.18).

3.1.2 VIRTIS

For Venus, specific wavelengths of interest in the infrared range were analysed in each cube image, mainly 1.74μm, 2.3μm and 5μm for polar regions, and the entire VIRTIS-M channel with a wavelength range illustrated in Figure 1.19.

Due to Venus Express highly elliptical orbit, and the long integration time of the hyperspectral images from VIRTIS (10 to 15 minutes), only the south hemisphere could be observed by this instrument (Peralta et al., 2008).

The following table shows the image pairs considered to show optimal features for cloud tracking from all the data analysed in this work:

Vex Orbit	Image Pairs	Date (dd/mm/yyyy)	Time Interval (min)
471	VI0471_04 and VI0471_05	05/08/2007	60
473	VI0473_01 and VI0473_04	06/08/2007	90
2936	VV2936_04 and VV2936_07	04/05/2014	60
2936	VV2936_05 and VV2936_07	04/05/2014	30
2939	VV2929_05 and VV2939_07	07/05/2014	60
2944	VV2944_01 and VV2944_03	12/05/2014	60
2944	VV2944_04 and VV2944_06	12/05/2014	60

Table 3.2: VEx/VIRTIS observations which image pairs contained suitable features for wind vector measurements with PICV2. Listed in this table are the number associated with the VEx orbit, the name of the data cube for each image in the pair, date, and time interval between images.

3.2 Akatsuki

3.2.1 UVI

Akatsuki's UVI images were also cloud tracked using the software mentioned previously on Section 2.5.2. A total of six days of observations, each one with three images for each one of the two filters of the UVI instrument, was processed and cloud tracked using combinations of 2-hour spaced images. For example, for 26/01/2017 cloud tracking was done on pair 17:34:46-19:34:44 and pair 19:34:46-21:34:46. All the dates and times used for each filter are resumed in Table 3.3 bellow.

Filter (nm)	Date (dd/mm/yyyy)	Time (hh:mm:ss)
365	26/01/2017	17:34:46
		19:34:44
		21:34:46
	27/01/2017	17:04:44
		19:04:45
		21:04:43
	28/01/2017	18:04:44
		20:04:46
		22:04:44
	29/01/2017	18:54:44
		20:54:45
		22:54:43
	30/01/2017	18:04:45
		20:04:44
		22:04:44
	31/01/2017	17:24:43
		19:24:45
		21:24:42
283	26/01/2017	17:31:11
		19:31:11
		21:31:12
	27/01/2017	17:01:11
		19:01:11
		21:01:10
	28/01/2017	18:01:11
		20:01:11
		22:01:11
	29/01/2017	18:51:10
		20:51:10
		22:51:10
	30/01/2017	18:01:11
		20:01:10
		22:01:11
	31/01/2017	17:21:10
		19:21:09
		21:21:09

Table 3.3: Akatsuki's images analysed and cloud tracked organised by filter, day and time.

Chapter 4

Results

In this section, the results and progress done in the course of this work are presented. They are divided according to the image source instruments and subdivided in atmospheric gravity waves studies and cloud tracking results.

4.1 VEX - VMC

4.1.1 Atmospheric Gravity Waves Detection

On the subject of atmospheric gravity waves, the built database contains all the information like in Figure 4.1 for future use and to easily pinpoint images with atmospheric gravity waves for a more in-depth analysis of wave packet properties or other pertinent studies. In this data base, a single orbit was assigned for each Excel sheet, which could contain between 50 and 300 images each.

File Name	Image Number	VMC Channel	Waves Present?	Image Defective
V1604_0000_UV2.jpg	0	UV	No	No
V1604_0001_N22.jpg	1	NIR2	No	No
V1604_0002_UV2.jpg	2	UV	No	No
V1604_0003_N22.jpg	3	NIR2	No	No
V1604_0004_UV2.jpg	4	UV	No	No
V1604_0005_N22.jpg	5	NIR2	No	No
V1604_0006_UV2.jpg	6	UV	No	No
V1604_0007_N22.jpg	7	NIR2	No	No
V1604_0008_UV2.jpg	8	UV	No	No
V1604_0009_N22.jpg	9	NIR2	No	No
V1604_0010_UV2.jpg	10	UV	No	No
V1604_0011_N22.jpg	11	NIR2	No	No
V1604_0012_UV2.jpg	12	UV	No	No
V1604_0013_N22.jpg	13	NIR2	No	No
V1604_0014_UV2.jpg	14	UV	No	No
V1604_0015_N22.jpg	15	NIR2	No	No
V1604_0016_UV2.jpg	16	UV	No	No
V1604_0017_N22.jpg	17	NIR2	No	No
V1604_0018_UV2.jpg	18	UV	No	No
V1604_0019_N22.jpg	19	NIR2	No	No
V1604_0020_UV2.jpg	20	UV	No	No
V1604_0021_N22.jpg	21	NIR2	No	No
V1604_0022_UV2.jpg	22	UV	???	No
V1604_0023_N22.jpg	23	NIR2	No	No
V1604_0024_UV2.jpg	24	UV	No	No
V1604_0025_N22.jpg	25	NIR2	No	No
V1604_0026_UV2.jpg	26	UV	No	Mild
V1604_0027_N22.jpg	27	NIR2	No	Mild
V1604_0028_UV2.jpg	28	UV	No	Mild
V1604_0029_N22.jpg	29	NIR2	No	Mild
V1604_0030_UV2.jpg	30	UV	No	Mild
V1604_0031_UV2.jpg	31	UV	Yes	Mild
V1604_0032_UV2.jpg	32	UV	Yes	Mild
V1604_0033_N22.jpg	33	NIR2	No	Mild
V1604_0034_UV2.jpg	34	UV	Yes	Mild
V1604_0035_UV2.jpg	35	UV	???	Mild
V1604_0036_N22.jpg	36	NIR2	No	Mild
V1604_0037_N22.jpg	37	NIR2	No	Mild
V1604_0038_UV2.jpg	38	UV	???	Mild
V1604_0039_UV2.jpg	39	UV	???	Mild
V1604_0040_N22.jpg	40	NIR2	Yes	Mild
V1604_0041_N22.jpg	41	NIR2	Yes	Mild

Number of Images with Gravity Waves in Orbit	Number of Images with GW doubts in orbit	Number of Gravity Waves (Doubts included)
11	7	18

Figure 4.1: A single partial sheet of the VMC atmospheric gravity waves database with information on orbit 1604.

Each orbit of the atmospheric gravity waves database for Vex/VMC images (Figure 4.1) shows the heading and its organisation. A small section which illustrates the number of images that have confirmations of waves (green shading) and doubts in the presence of waves (yellow shading). For each image it is registered the name of the image file, and a number associated with it (starting in 0 for each orbit), the filter used for the image, the classification regarding the presence of atmospheric gravity waves and the information based on defects and artifacts showed by the image.

4.1.2 Wind Profiles

By cloud tracking on the available image pairs and applying the binning method (Section 2.5.1, the following plot was built (Figure 4.4), showing the mean zonal wind flow on a latitude profile of the southern hemisphere. PICV2 was the software used to obtain the wind measurements for this plot. The meridional winds measured by the software do not have much significance (and so I chose not to present them) as the zonal velocity component, since there is not enough resolution on the images to properly track vertical winds, which are weaker and of similar magnitude as the error bars.

In Figure 4.4, the scale for the velocities is presented negative since the winds move following the retrograde movement of the planet Venus.

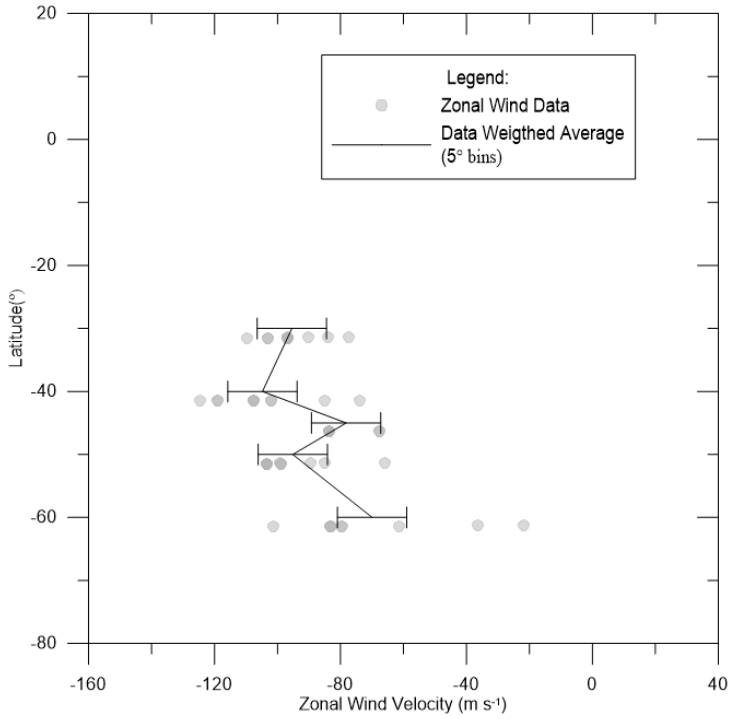

Figure 4.2: Zonal wind weighed average cloud tracked at 365 nm (Ultraviolet) using VMC images and bins of 5 degrees.

4.2 VEx - VIRTIS

4.2.1 Atmospheric Gravity Waves Characterisation

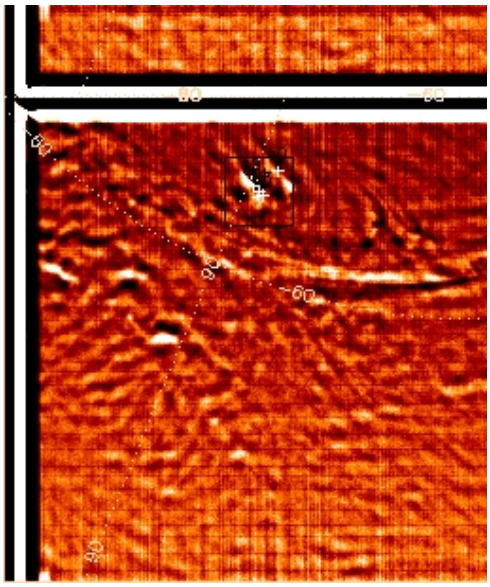

Figure 4.3: Atmospheric gravity waves presence in orbit 472 of August 5, 2007, wavelength 1.74 μm wave (Near Infrared).

For atmopheric gravity waves wavelength measuremets, the best image candidate, which was in image `VI0472_05` (Figure 4.3), was selected and a preliminary characterisation was done using PLIA software. Preliminary results for wavelength are presented in Table 4.1.

Image	Lat1	Long1	Lat2	Long2	Wavelength
VI0472_05	-63,8744	91,5856	-64,9584	93,2337	208,364
VI0472_05	-64,3356	89,6702	-65,5192	91,1822	202,822
VI0472_05	-64,3356	89,6702	-65,1292	91,8319	243,235
VI0472_05	-63,7887	91,667	-64,8704	93,3146	208,186
VI0472_05	-63,7887	91,667	-64,7825	93,3948	210,538
VI0472_05	-64,6361	89,1012	-65,5192	91,1822	238,783
VI0472_05	-64,6361	89,1012	-65,6542	90,7861	207,938
VI0472_05	-64,6361	89,1012	-65,6618	90,2646	163,827
VI0472_05	-64,144	90,842	-64,9717	92,7284	217,592
VI0472_05	-64,1440	90,8420	-64,9890	92,2174	170,507

Table 4.1: Preliminary results for the wavelength on the atmospheric gravity waves present on the provided VIRTIS image. The latitudes and longitudes above are not precise since atmospheric gravity waves are extended features.

4.2.2 Wind Profiles

During observations with VIRTIS instrument, it was noticed that some images provided better wind tracers but also that some images covered similar latitudinal regions. Because of this I will only present here some of the results, targeting the south hemisphere. Both zonal wind profile in the visible and some polar data for higher latitudes will be shown in this section. All the wind tracer measurements were obtained with PICV2 software.

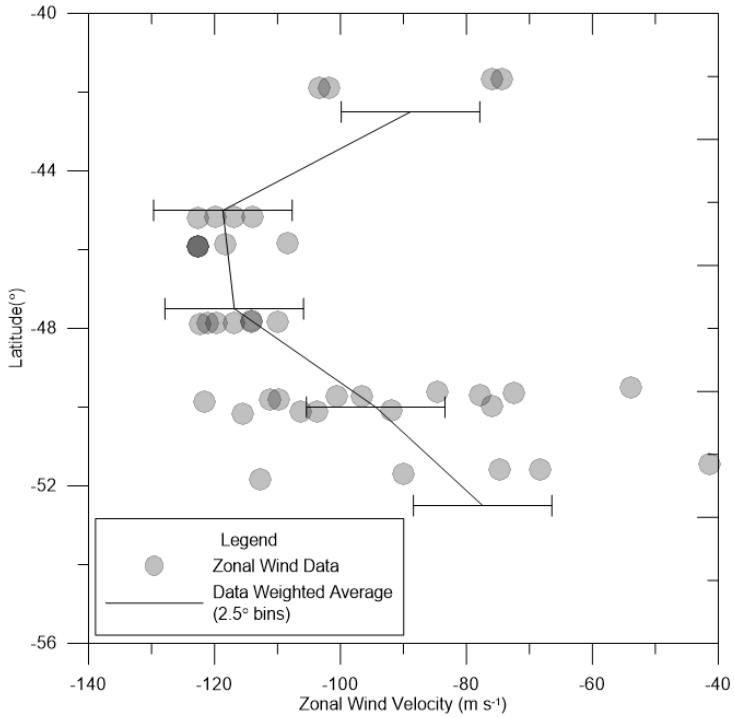

Figure 4.4: Zonal wind weighed average cloud tracked in the 365-400 nm band (Ultraviolet) using VIRTIS images and bins of 2.5 degrees.

Once again, similarly to the VMC image study, the meridional winds obtained are limited by resolution and these winds are much weaker than the zonal velocity component.

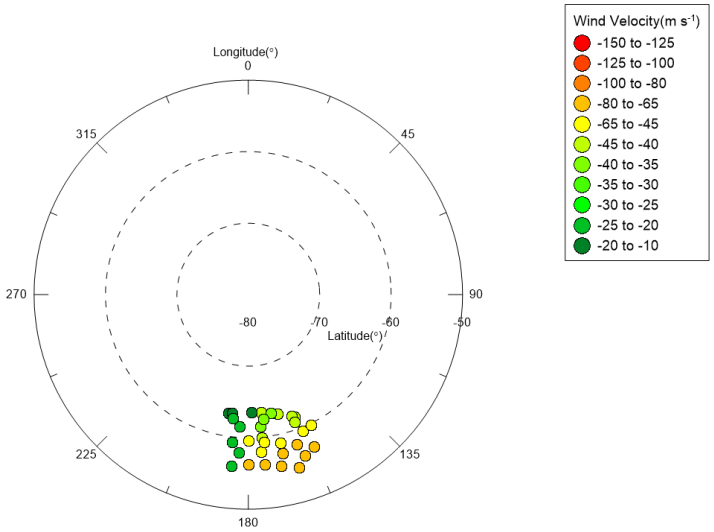

Figure 4.5: Zonal wind velocity profile as a function of longitude in the Visible band (it was not possible to display error bars but the error bars have a value of 11 m/s.

Even though only a small section of the south hemisphere of Venus was covered, the polar plot allow us to to see the drop in zonal wind velocity as we approach the south pole, starting close to $60° S$.

4.3 Ground Based Observations

Acquiring ground based observations is commonly more viable, regarding availability and monetary budget, than relying on space based observations. However, there is a critical question that involves whether these observations can reproduce accurately the space based observations collected by spacecrafts. In order to answer this question, cloud tracking was performed on ground based observations provided by Pedro Machado. The software used was ACT and these observations dated from August of 2012 and where acquired in the $2.3\,\mu m$ wavelength by the Galileo National Telescope (located at the Roque de los Muchachos Observatory on the island of La Palma in the Canary Islands, Spain). The wind tracers measured are shown in Figure 4.6 and the correspondent latitudinal profile on Figure 4.7. The plot shows a steady zonal wind profile between $50° N$ and $55° S$ centred approximately on the $65\,ms^{-1}$.

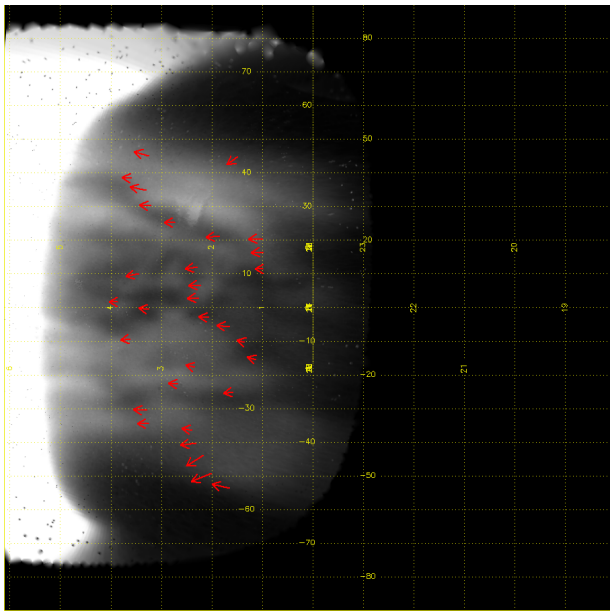

Figure 4.6: Wind vectors tracked using ACT for ground based observations from August 2012 in the Near-Infrared.

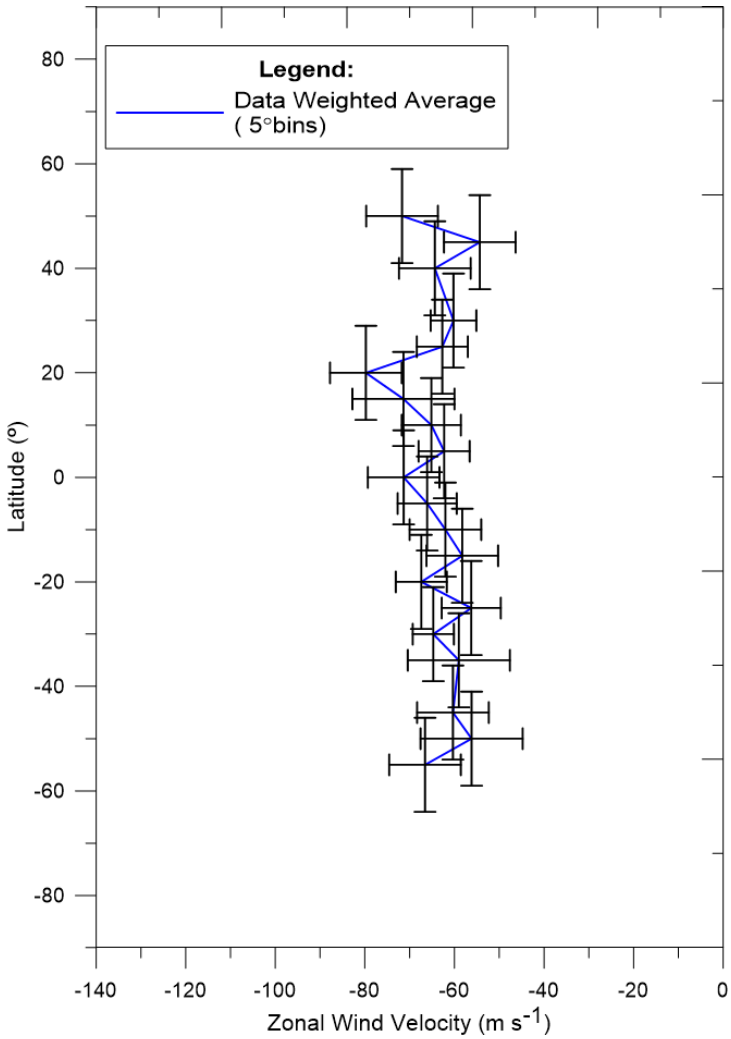

Figure 4.7: Zonal wind profiles for cloud tracked ground based data from August 2012 on the 2.3 μm filter (Near-Infrared). Data provided by Pedro Machado. The profile represents the weighed average with 5° bins.

4.4 Akatsuki - UVI

Analysing and studying Akatsuki's observations was a key element of my Master's development and work. The aim was to, given the case study, show the overall results and performance at both filter wavelengths (365 nm and 283 nm). The following section will focus on mean latitudinal wind profiles as well as the similarities and differences of winds obtained at the two wavelengths, all based on the six day data available.

The filters in question sound the atmosphere at about 70km of altitude. Zonal wind profiles were retrieved for each of the days in each of the filters. A total of 12 zonal wind profiles and 12 meridional wind profiles were produced, which are represented in Figures 4.8 and 4.9 and divided by day in Appendix A. For this study, I limited the scope of the results, as best as I could, between $60° N$ and $70° S$ with a focus on lower latitudes. Cloud tracking with UVI is far more difficult for high latitudes because of Akatsuki's equatorial orbit and because UV cloud features at mid to high latitudes are exhibited as mostly featureless streaks (Titov et al., 2012).

It is observed that each day shows a steady zonal wind velocity profile (between $45° N$ and between $45° S$) with a quick drop in velocity when reaching the poles. In Figure 4.10, it is evident the zonal wind velocity differences between the two filters even at error bar level, which does not happen with meridional wind since the two profiles fall into each others error bars. The results suggest that the westward winds obtained from the 283 nm filter images are faster than those from 365 nm images, on average, the mean difference is 8–15 m/s. The profiles also indicate that that poleward flow becomes slower at 283 nm when compared to the 365 nm filter. The results also suggest an asymmetry between the northern and southern hemispheres in zonal wind, evident in the 365 nm filter which does not carry on to 283 nm filter.

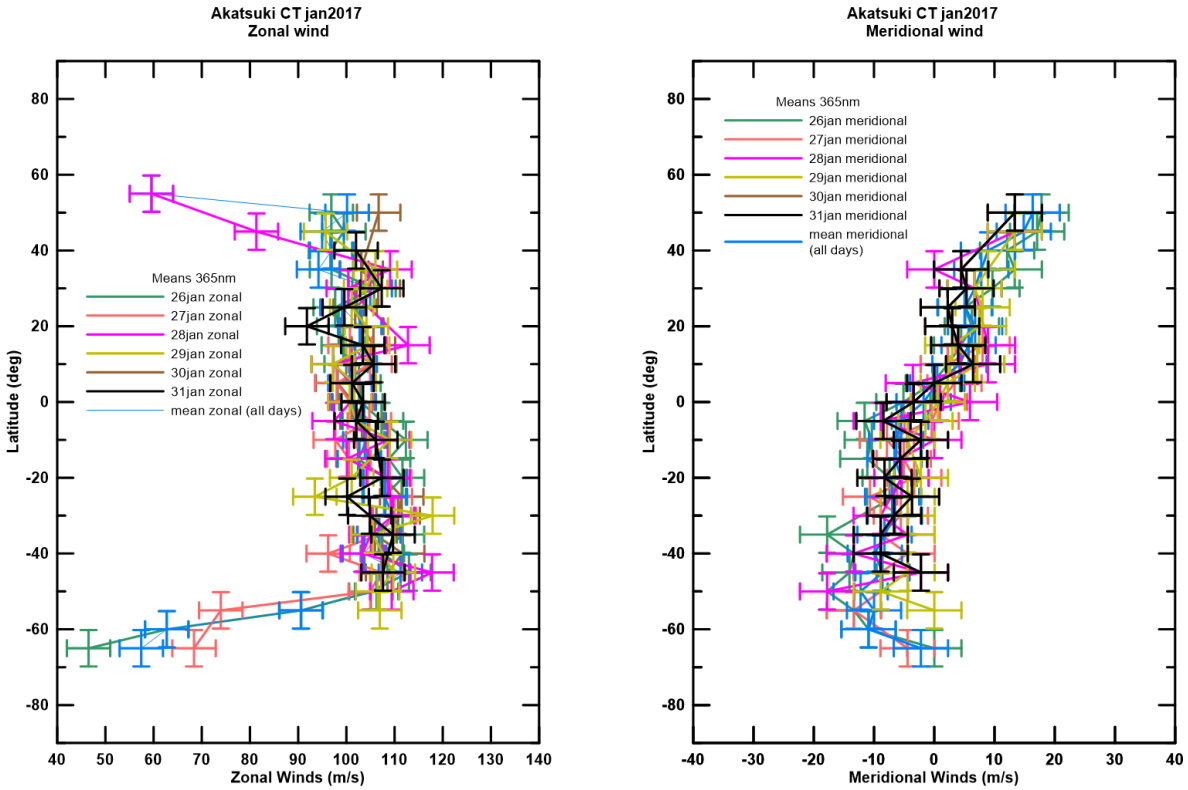

Figure 4.8: Zonal (left) and meridional (right) wind profiles for cloud tracked Akatsuki's data. Each plot shows all individual latitudinal zonal wind profiles for each day for the 365 nm filter.

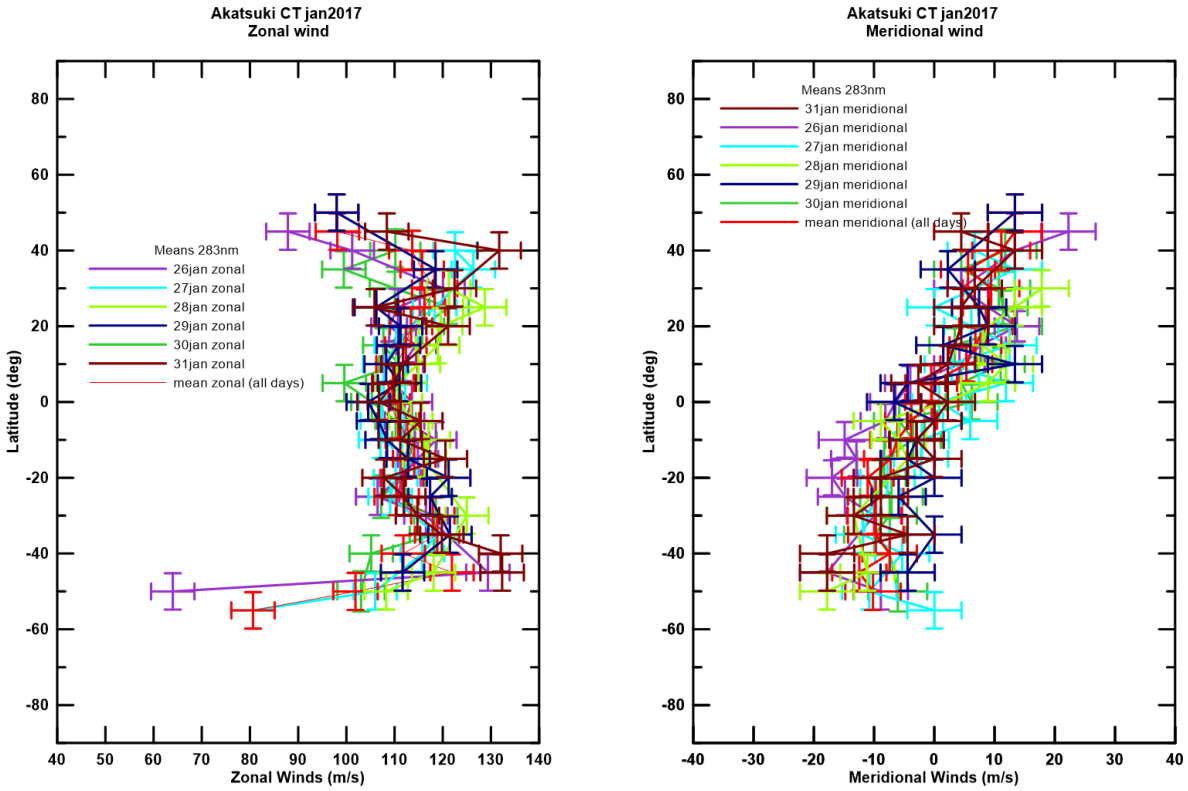

Figure 4.9: Zonal (left) and meridional (right) wind profiles for cloud tracked Akatsuki's data. Each plot shows all individual latitudinal zonal wind profiles for each day for the 283 nm filter

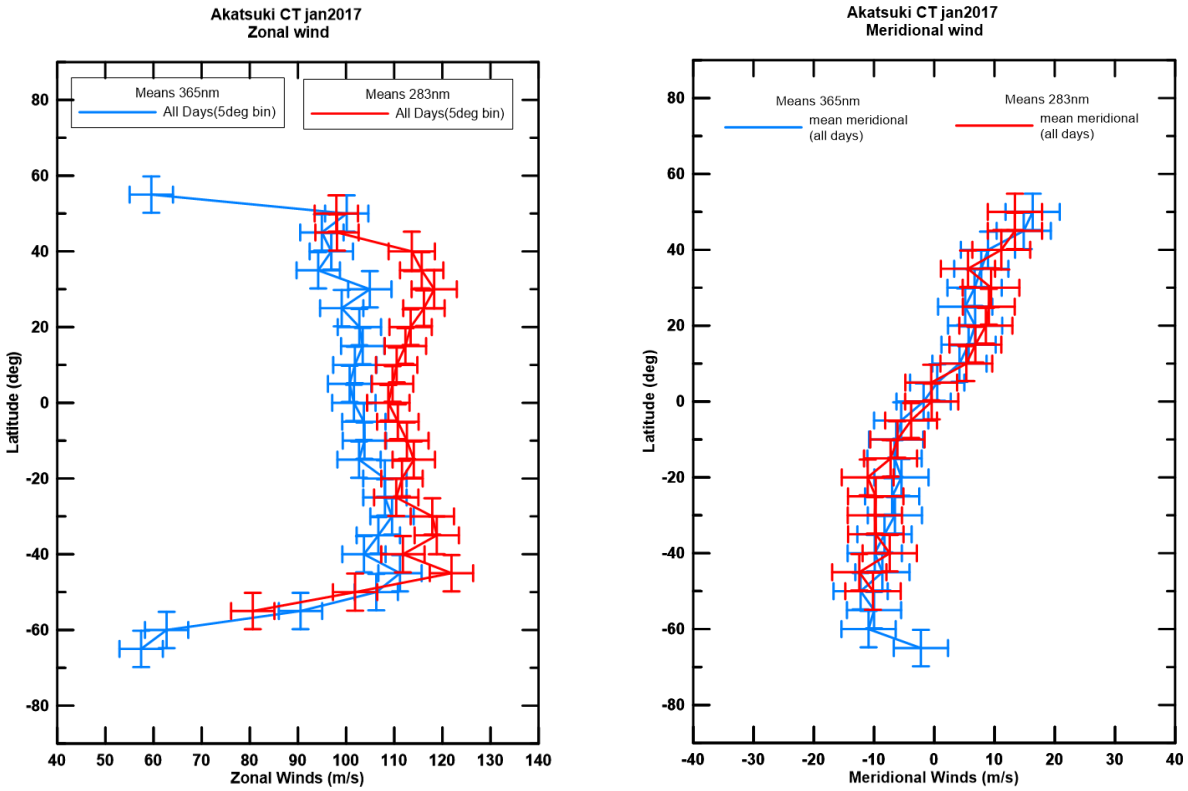

Figure 4.10: Zonal (left) and meridional (right) wind profiles for cloud tracked Akatsuki's data. Each plot shows a mean latitudinal wind profile for each filter, which resulted from a weighted average with 5° bins.

Chapter 5

Discussion

5.1 VEx

Figure 5.1 shows a satisfactory agreement between both Sánchez-Lavega et al. (2008) and this work's results, even if cloud tracking could only be performed in a limited latitudinal range.

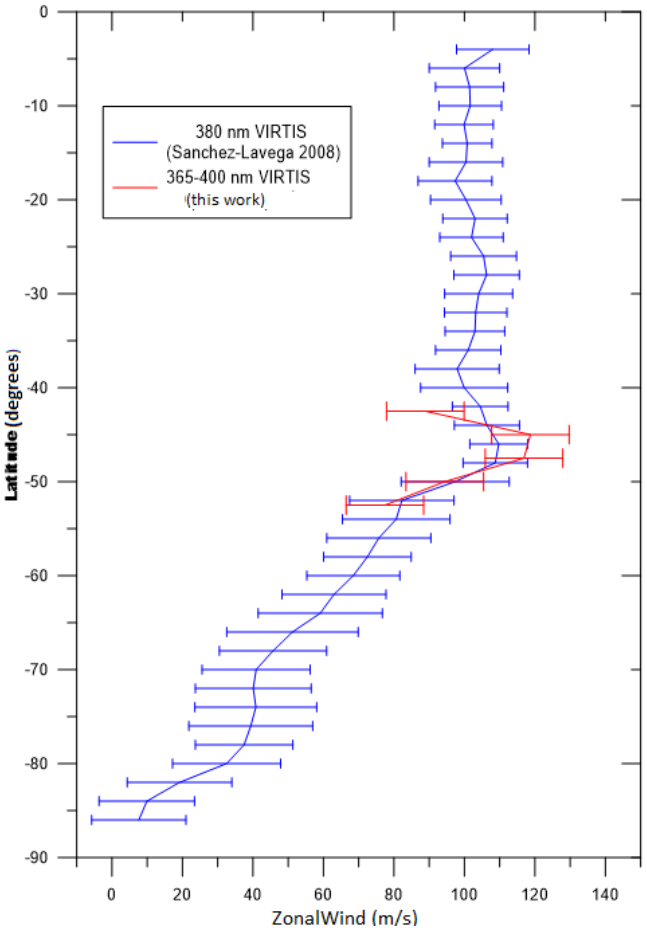

Figure 5.1: Zonal wind profiles from Sánchez-Lavega et al. (2008) and the one from this work obtained from the tracked tracers. The blue line represents Sanchez-Lavega data with 380 nm and in red this work's data from a 365-400 nm band.

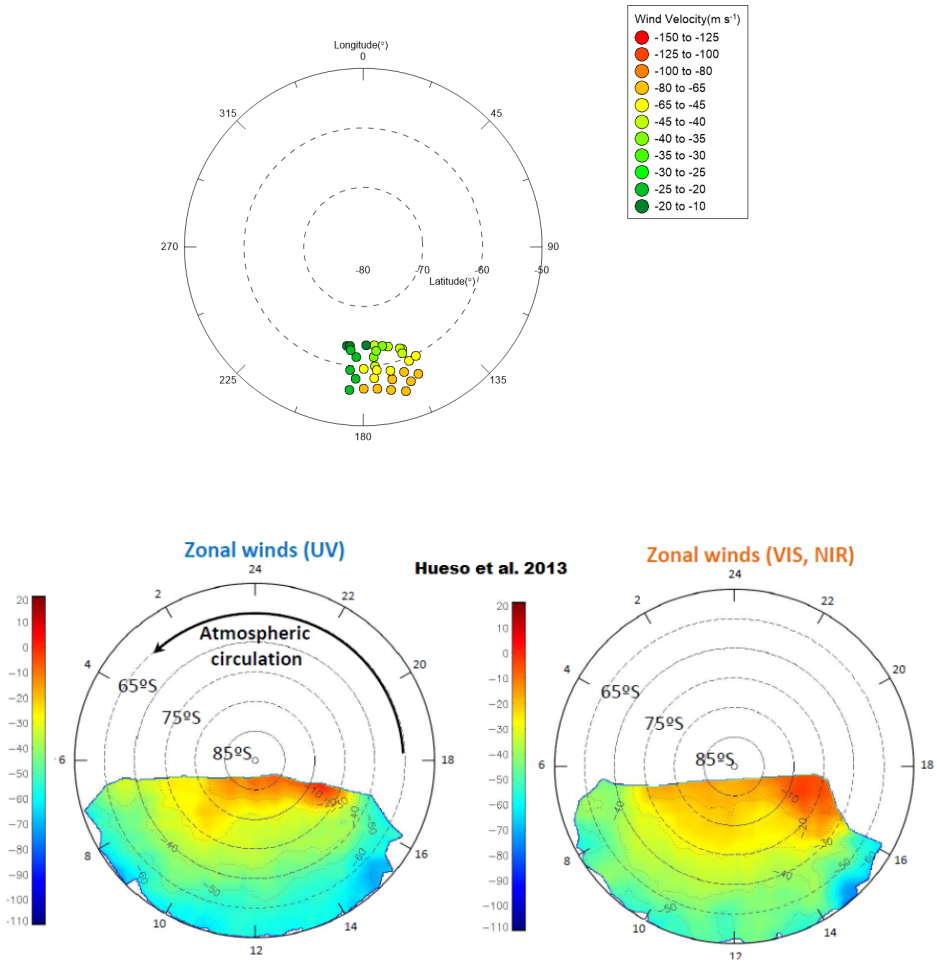

Figure 5.2: Colour mapped cloud tracked winds at high latitudes on Venus with VIRTIS at Ultraviolet, Visible and Near-Infrared wavelengths from Hueso et al. (2013) (bottom panel) and the results from this work at Visible wavelengths (top panel).

Closely analysing Figure 5.2 results from Hueso et al. (2013) have the zonal winds plotted against local time which can be related with longitude on the day side of planet Venus. Though I was not able to average the zonal winds over an extended area , we can see that the decreasing retrograde wind motion towards the pole is present in the results,which is consistent with results from Hueso et al. (2013).

5.2 Ground Based Observations

By comparing the results obtained by (Sánchez-Lavega et al., 2008) in the 1.74 μm filter and the results obtained by this work on the 2.3 μm (Figure 5.3) using the same range of latitudes we can see that the levels of precision of both ground and space based observations are quite similar.

With ground based observations was also possible to capture and represent wind variability as can be seen in Figure 5.4. The zonal wind points calculated from the tracers follow, to some extent, the previous spacecraft results, which models are represented by the full lines. It is important to refer that ground-based observations can be much easier and cheaper to obtain than any space mission, which is a key factor in space research.

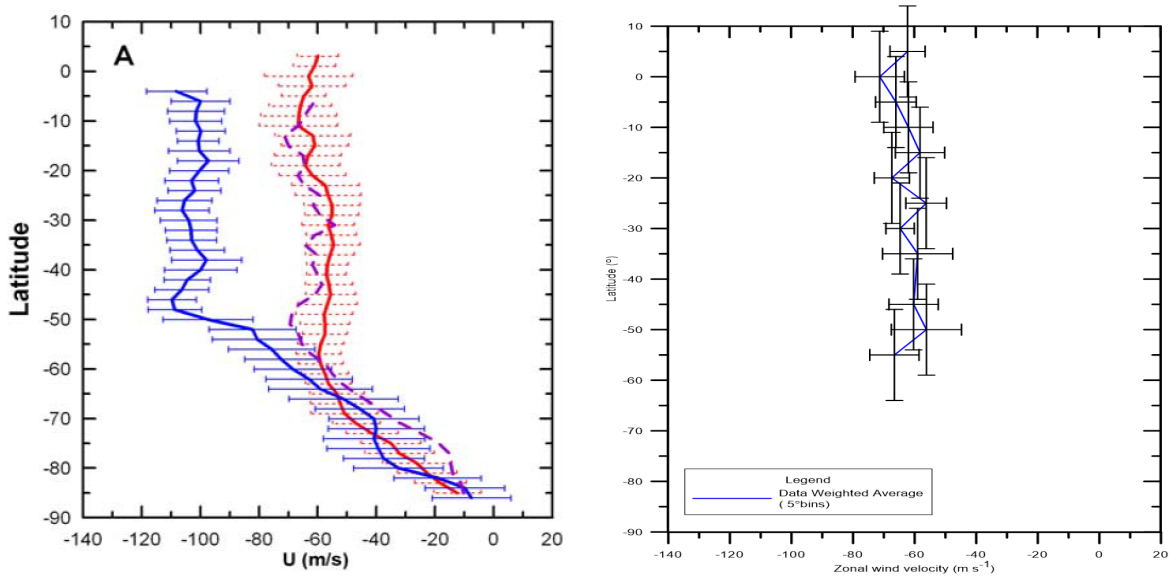

Figure 5.3: Left panel: Averaged wind profiles from (Sánchez-Lavega et al., 2008) in Venus southern hemisphere at cloud level. The zonal velocity is drawn as a function of latitude as measured using cloud tracers at three wavelengths: Ultraviolet (blue, 380 nm, upper cloud), Near-Infrared (violet, 980 nm, upper cloud), and Infrared (red, 1.74 μm, lower cloud). Right panel: Latitudinal cut of Figure 4.7 to match (Sánchez-Lavega et al., 2008) results. Cloud tracked ground based data from August 2012 on the 2.3 μm filter(Near-Infrared)

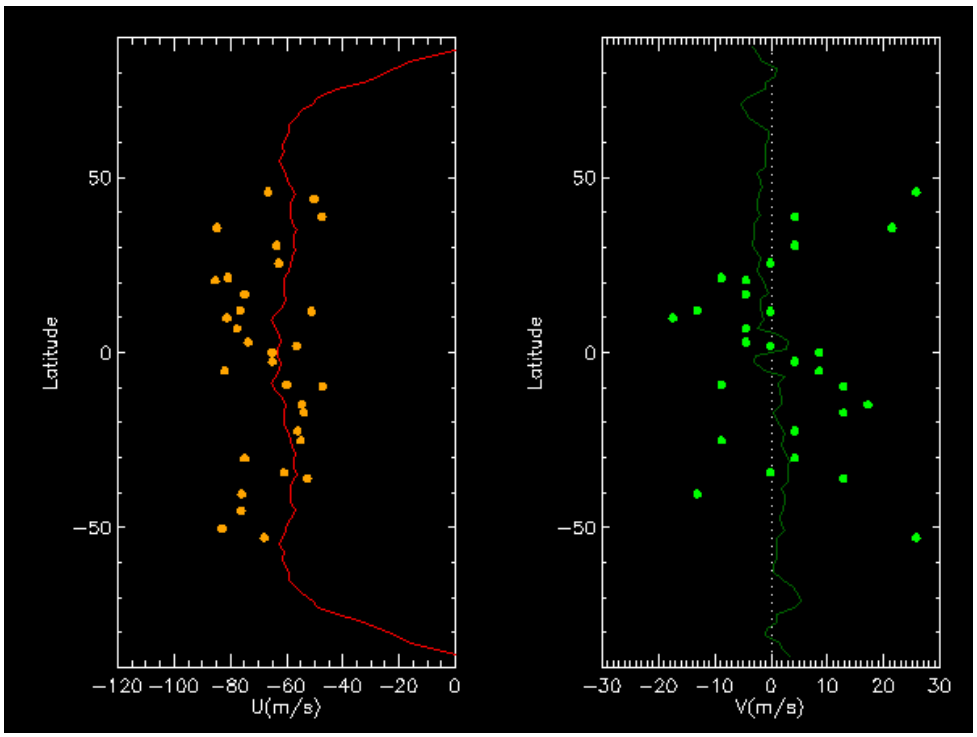

Figure 5.4: Zonal and meridional wind values obtained from the manually tracked tracers. The continuous line on both graphics represents a model of the average wind velocity for each component which result from spacecraft data.

5.3 Akatsuki/UVI

Results for both Akatsuki's filters have been published by (Horinouchi et al., 2018), which are exemplified by Figures 5.5 and 5.6 . The analysis done in this recent study involved the use of an automatic cloud tracking method as opposed to my work which used a manual cloud tracking method. In addition, (Horinouchi et al., 2018) studied the long-term wind variability by using all Akatsuki's data from December 2015 (first Akatsuki's observations) to December 2017. Figure 5.7 shows the differences between the winds obtained at the two wavelengths (283-nm results minus 365 nm results) averaged over the observation period in Horinouchi et al. (2018).

The results suggest that the winds obtained from 283 nm images were faster than those from 365 nm images, on average; the mean difference was 2–4 m/s (Figure 5.7). A higher difference for these two filters was found in the course of my study with UVI data, however this could be due to the difference in observation periods used since the larger sample of wind vectors by Horinouchi et al. (2018) could impact this difference. As seen in Fig. 5.9 the 283 nm velocity results obtained are indeed faster than the 365 nm images, however with a difference, on average, of 8-15 m/s. It also shows that winds in higher latitudes become slower on the 283 nm filter when compared to the 365 nm filter since the only negative results are registered for latitudes with modules equal or above 50°. This could be derived to the difficulty of studying higher latitudinal zones in Akatsuki's images since the spacecraft has an equatorial orbit. Figure 5.8 show a comparison between Hueso et al. (2015) VIRTIS data used to complement Sánchez-Lavega et al. (2008) studies and Horinouchi et al. (2018) Akatsuki data on the 365 nm filter. We can see the that the results show a good agreement with the ones obtained from these two previous works especially regarding meridional wind. Once again, the larger sample for Horinouchi et al. (2018) work could explain the slight difference in zonal wind velocities between the 2018 work and this dissertation's work.

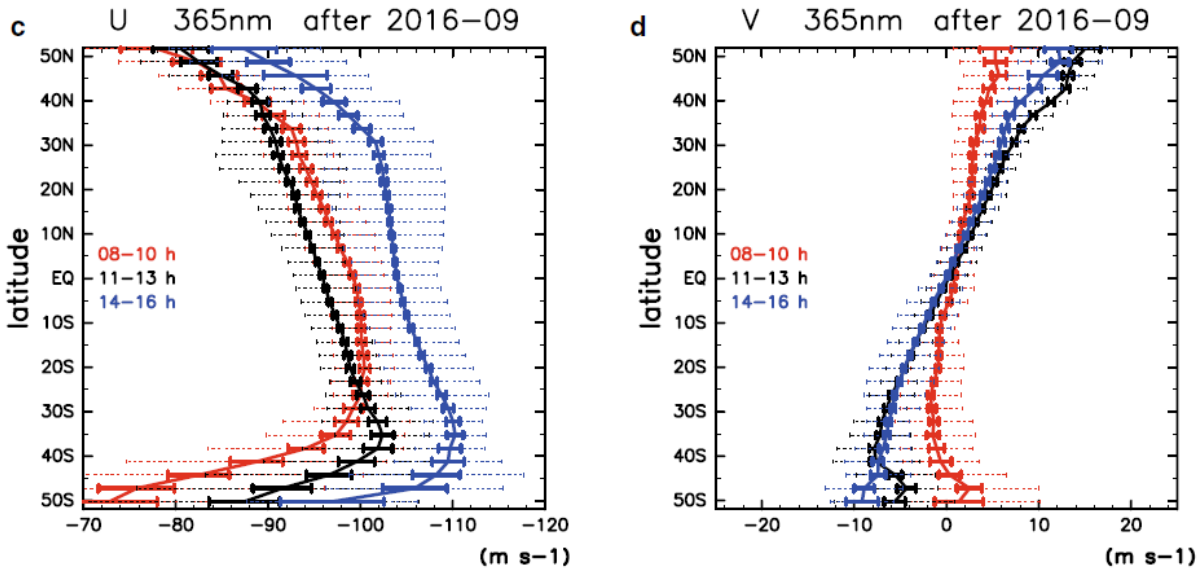

Figure 5.5: Meridional profiles of mean winds depending on local time (LT) and observation period for the 365 nm filter. Zonal (left) and meridional (right) winds over October 2016–March 2017. The winds are averaged over LTs: 8–10 h (red), 11–13 h (black), and 14–16 h (blue). Credit: Horinouchi et al. (2018)

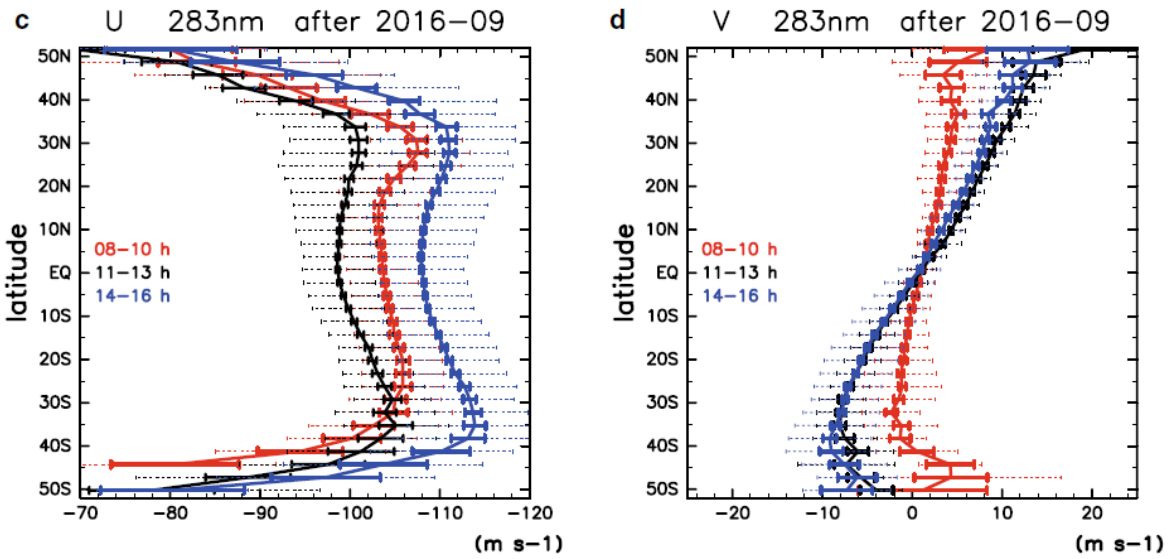

Figure 5.6: Latitudial profiles of mean winds depending on local time (LT) and observation period for the 283 nm filter. Zonal (left) and meridional (right) winds over October 2016–March 2017. The winds are averaged over LTs: 8–10 h (red), 11–13 h (black), and 14–16 h (blue). Credit: Horinouchi et al. (2018)

Regarding the asymmetry observed in the 365 nm filter, Lee et al. (2019) presents a study on the variability of the cloud albedo at 365 nm and its impact on Venus solar heating rates based on an analysis of Venus Express and Akatsuki's UV images, and Hubble Space Telescope and MESSENGER's UV spectral data. Results indicate that the 365-nm albedo varied by a factor of 2 from 2006 to 2017 over the entire planet, which produced a change in the low latitude solar heating rate according to Lee et al. (2019) radiative transfer calculations. This could explain the variation in zonal wind in the 365 nm filter and the wind velocity asymmetry observed.

What causes the difference in zonal winds obtained from the 283 nm and 365 nm images is a question still unanswered. A possible explanation, provided by (Horinouchi et al., 2018) is that that while the velocity captured at one wavelength represents the flow velocity, the velocity captured at the other wavelength represents the phase velocity of atmospheric waves. A close inspection suggests it is unlikely since the kind of atmospheric waves that should be considered is gravity waves (small scale Rossby waves are too slow to distinguish from flows) and, in most cases, clear wave features were not found. Another explanation proposed for the velocities disagreement is that small-scale features at the two wavelengths reflect clouds at different heights. This means that the 283 nm filter is sounding the atmosphere 2 km above the 365 nm filter and we are dealing with two different atmospheric layers and that the difference therefore is from vertical shear. In fact, (Lee et al., 2017) found that the phase-angle dependency in Akatsuki UVI 365-nm data can be explained if the unknown absorber is distributed slightly below the cloud top rather than above. In contrast, the SO_2 mixing ratio increases upward from the cloud-top level and therefore, 283 nm images reflect flows at higher altitude. Finally, we could speculate that, on average, it is likely that the superrotation of the Venusian atmosphere is increased with height, even at the cloud top level (Horinouchi et al., 2018).

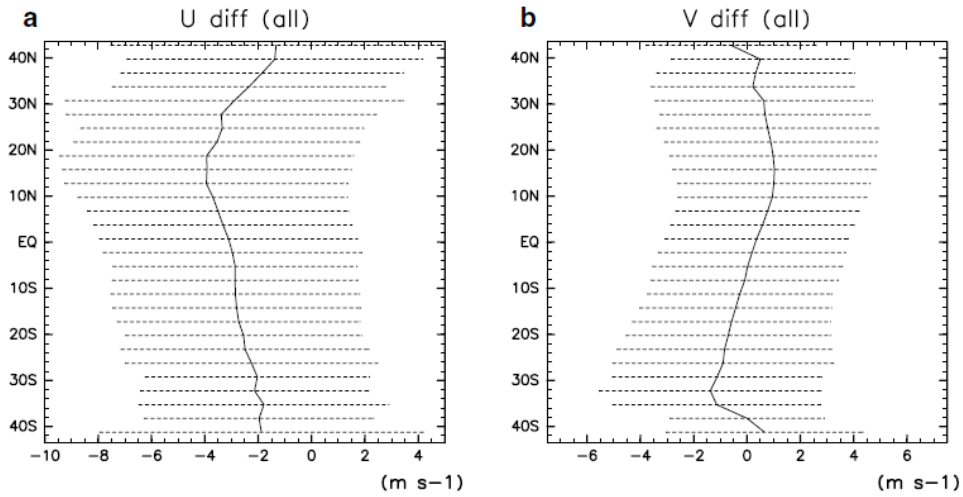

Figure 5.7: Mean differences in zonal (a) and meridional (b) winds (m/s) between the two UV filters (283-nm results minus 365-nm results) averaged over the observational period (December 2015–March 2017). The dashed lines in a, b show the standard deviation at each latitude. Credit: Horinouchi et al. (2018)

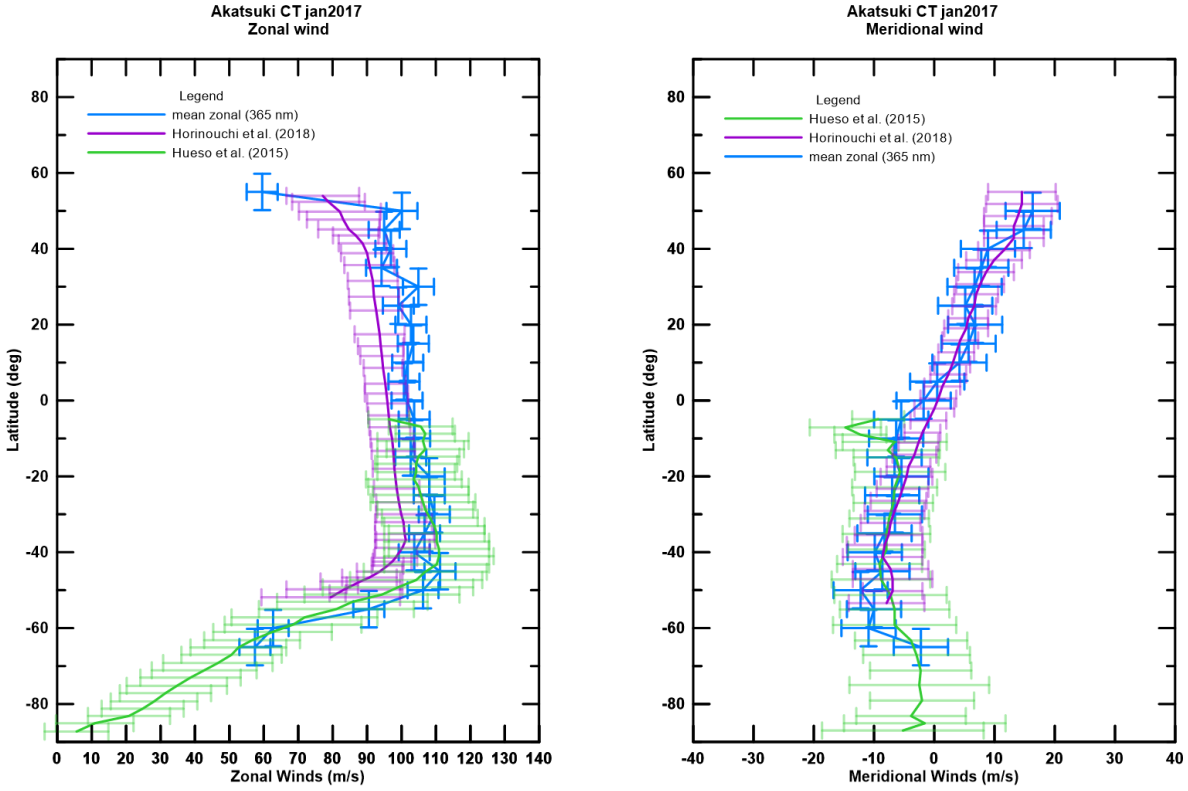

Figure 5.8: Comparative results between this work Akatsuki's results (blue) at 365 nm, VIRTIS observations (green) at 380 nm by (Hueso et al., 2015), and Akatsuki's observations at 365 nm by Horinouchi et al. (2018). Results for the zonal wind are on the left panel and meridional wind on the right panel.

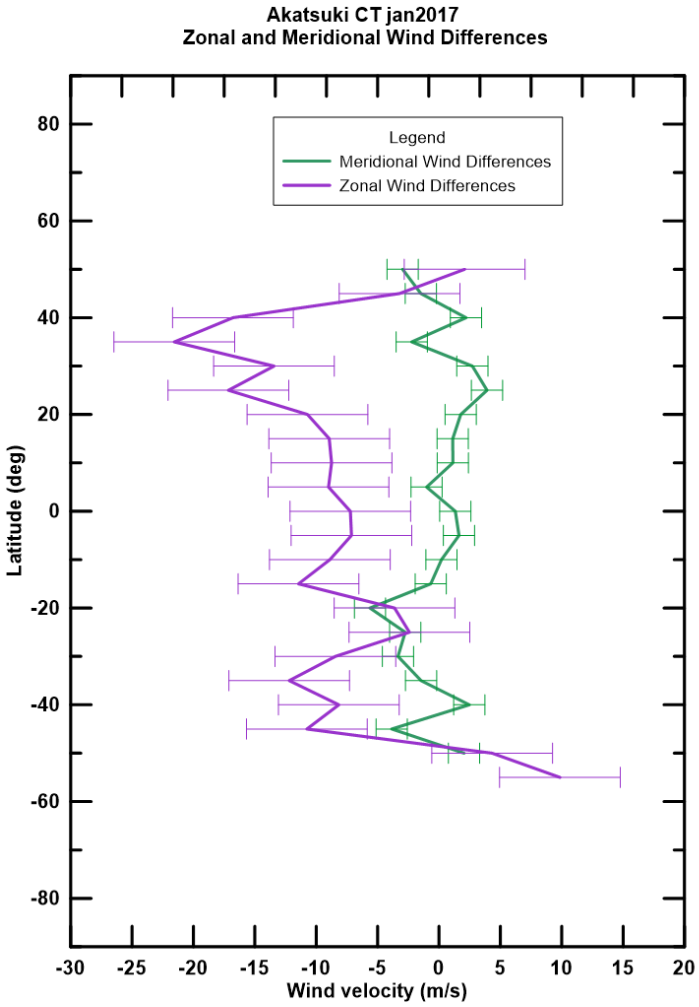

Figure 5.9: Mean differences in zonal (purple) and meridional (green) winds (m/s) between the two UV filters (283-nm results minus 365-nm results) averaged over the observational period (December 2015–March 2017). The error bars show the standard deviation at each latitude.

Chapter 6

Conclusions

By using a manual cloud tracking method with ACT, it was possible to achieve results with a certain degree of consistency when compared with previous studies and observations by Hueso et al. (2015) and Horinouchi et al. (2018). With this tool, two different ultraviolet filters were studied revealing velocity profiles with different zonal wind velocities (the two profiles differ by 8 to 15m/s in zonal wind velocity). It was found that these two filters sound Venus atmosphere at different altitude levels with a separation of approximately 2 km of altitude. With ACT, it was also possible to study ground based data from Galileo National Telescope achieving the same levels of precision for wind velocities as space based reference results from Sánchez-Lavega et al. (2008) . This is extremely important when considering the economical and time constraints for obtaining necessary data to study. The ACT software along with its tools is presently one of the best in the science world sharing the spotlight with PLIA and PICV2, which allow a semi-automatic approach to cloud tracking. The VIRTIS and VMC results in this work were also consistent with works from Sánchez-Lavega et al. (2008) and Hueso et al. (2013) both using cylindrical and polar projections.

Akatsuki's and Venus Express mission data proved to be most useful in applying cloud tracking to several different atmospheric layers of Venus as well as in the study of atmospheric gravity waves. Characterisation and detection of these waves is a recent goal since high resolution images are necessary to fully observe these waves.

This thesis was a first step into the world of Venus' atmospheric dynamics and a large amount of data still remains unexplored and in need of careful analysis, which could open the doors to interesting results especially since the role of atmospheric gravity waves and Venus' superrotation regime are yet to be fully understood.

6.1 Achievements

The major achievements of the present work encompass all the knowledge earned in planetary atmospheres, specifically Venus atmosphere dynamics and evolution. It was an extremely fruitful experience to be able to work and explore different software, such as PLIA, PICV2 and ACT as well as learning more about their complementary tools which included Grapher and IDL programing language.

Working with data from two crucial missions in the history of Venus exploration was also a valuable experience. To be able to work with several different instruments and complement the work done with ground based observations certainly provided me with new insights on the

vast gaseous layer that covers the planet that is so much alike ours, and at the same time so peculiarly distinct.

Bibliography

C. D. Ahrens. *Meteorology Today: An Introduction to Weather, Climate, and the Environment.* Brooks/Cole - Thomson Learning, 2003.

N. L. Baker and C. B. Leovy. Zonal winds near venus' cloud top level: A model study of the interaction between the zonal mean circulation and the semidiurnal tide. *Icarus*, 69(2):202 – 220, 1987. ISSN 0019-1035.

J. K. Beatty, C. C. Petersen, and A. Chaikin. *The New Solar System.* Cambridge University Press, 4th edition, 1999.

M. J. S. Belton, K. P. Klaasen, M. C. Clary, J. L. Anderson, C. D. Anger, M. H. Carr, C. R. Chapman, M. E. Davies, R. Greeley, D. Anderson, L. K. Bolef, T. E. Townsend, R. Greenberg, I. Head, James W., G. Neukum, C. B. Pilcher, J. Veverka, P. J. Gierasch, F. P. Fanale, A. P. Ingersoll, H. Masursky, D. Morrison, and J. B. Pollack. The Galileo Solid-State Imaging experiment. , 60(1-4):413–455, May 1992. doi: 10.1007/BF00216864.

P. R. Bevington and D. K. Robinson. *Data Reduction and Error Analysis for the Physical Sciences.* McGraw-Hill, 1992.

J. Blamont. Planetary balloons. *Experimental Astronomy*, 22:1–39, 10 2008.

S. W. Bougher, M. J. Alexander, and H. G. Mayr. Upper Atmosphere Dynamics: Global Circulation and Gravity Waves. In S. W. Bougher, D. M. Hunten, and R. J. Phillips, editors, *Venus II: Geology, Geophysics, Atmosphere, and Solar Wind Environment*, page 259, 1997.

M. A. Bullock and D. H. Grinspoon. The recent evolution of climate on venus. *Icarus*, 150(1): 19 – 37, 2001. ISSN 0019-1035.

L. B. K. Carlson, R.W.and Kamp, D. Pollack, J.B.and Grinspoon, P. Encrenaz, T.and Drossart, and F. Taylor. Variations in venus cloud particle properties: a new view of venus's cloud morphology as observed by the galileo near-infrared mapping spectrometer. *Planetary and Space Science*, 41(7):477 – 485, 1993. ISSN 0032-0633.

E. Chassefière, R. Wieler, B. Marty, and F. Leblance. The evolution of venus: Present state of knowledge and future exploration. *Planetary and Space Science*, 63-64:15 – 23, 2012. ISSN 0032-0633. Advances in Planetary Atmospheres and Exploration.

L. Collin and D. M. Hunten. Pioneer Venus experiment descriptions. , 20:451–525, Jun 1977.

I. de Pater and J. J. Lissauer. *Planetary Sciences.* Cambridge University Press, 2007.

A. Dollfus. Venus: Evolution of the upper atmospheric clouds. *Journal of the Atmospheric Sciences*, 32(6):1060–1070, 1975.

P. Drossart, G. Piccioni, A. Adriani, F. Angrilli, G. Arnold, K. H. Baines, G. Bellucci, J. Benkhoff, B. Bézard, J.-P. Bibring, A. Blanco, M. I. Blecka, R. W. Carlson, A. Coradini, A. Di Lellis, T. Encrenaz, S. Erard, S. Fonti, V. Formisano, T. Fouchet, R. Garcia, R. Haus, J. Helbert, N. I. Ignatiev, P. G. J. Irwin, Y. Langevin, S. Lebonnois, M. A. Lopez-Valverde, D. Luz, L. Marinangeli, V. Orofino, A. V. Rodin, M. C. Roos-Serote, B. Saggin, A. Sanchez-Lavega, D. M. Stam, F. W. Taylor, D. Titov, G. Visconti, M. Zambelli, R. Hueso, C. C. C. Tsang, C. F. Wilson, and T. Z. Afanasenko. Scientific goals for the observation of Venus by VIRTIS on ESA/Venus express mission. , 55:1653–1672, Oct. 2007.

L. W. Esposito, R. G. Knollenberg, M. I. Marov, O. B. Toon, and R. P. Turco. *The clouds are hazes of Venus*, pages 484–564. 1983.

L. W. Esposito, J. F. Bertaux, V. A. Krasnopolsky, V. I. Moroz, and L. V. Zasova. Chemistry of lower atmosphere and clouds. 1997.

I. Garate-Lopez, R. Hueso, A. Sánchez-Lavega, J. Peralta, G. Piccioni, and P. Drossart. A Chaotic Long-Lived Vortex at the Southern Pole of Venus. *Nature Geoscience*, 6:254–257, Apr. 2013.

R. H. M. Gonçalves. Dynamics of venus' atmosphere: wind characterization with doppler velocimetry. Master's thesis, Faculdade de Ciências - Universidade de Lisboa, 2016.

R. M. Goody and J. C. C. G. Walker. *Atmosferas planetarias*. Edgard, 1975.

D. H. Grinspoon. *Venus Revealed: A New Look Below The Clouds Of Our Mysterious Twin Planet*. Helix Books, 1997.

D. H. Grinspoon and M. A. Bullock. Astrobiology and venus exploration. In L. Esposito, E. R. Stofan, and T. E. Cravens, editors, *Exploring Venus as a Terrestrial Planet*. American Geophysical Union, Washington DC, 2007.

W. Hamilton. Plumeless venus preserves an ancient impact-accretionary surface. *Special Paper of the Geological Society of America*, 388, 01 2005.

T. Horinouchi, T. Kouyama, Y. J. Lee, S.-y. Murakami, K. Ogohara, M. Takagi, T. Imamura, K. Nakajima, J. Peralta, A. Yamazaki, M. Yamada, and S. Watanabe. Mean winds at the cloud top of venus obtained from two-wavelength uv imaging by akatsuki. *Earth, Planets and Space*, 70:10, 12 2018.

R. Hueso, J. Legarreta, J. F. Rojas, J. Peralta, S. Pérez-Hoyos, T. del Río-Gaztelurrutia, and A. Sánchez-Lavega. The Planetary Laboratory for Image Analysis (PLIA). *Advances in Space Research*, 46(9):1120–1138, Nov 2010. doi: 10.1016/j.asr.2010.05.016.

R. Hueso, I. Garate-Lopez, J. Peralta, T. Bandos, and A. Sánchez-Lavega. Venus winds from ultraviolet, visible and near infrared images from the virtis instrument on venus express. 10 2013.

R. Hueso, J. Peralta, I. Garate-Lopez, T. Bandos, and A. Sánchez-Lavega. Six years of venus winds at the upper cloud level from uv, visible and near infrared observations from virtis on venus express. *Planetary and Space Science*, 113-114:78 – 99, 2015. ISSN 0032-0633. URL http://www.sciencedirect.com/science/article/pii/S0032063314004024. SI:Exploration of Venus.

R. G. Knollenberg and D. M. Hunten. The microphysics of the clouds of venus: Results of the pioneer venus particle size spectrometer experiment. *Journal of Geophysical Research: Space Physics*, 85(A13):8039–8058, 1980.

Y. J. Lee, A. Yamazaki, T. Imamura, M. Yamada, S. Watanabe, T. M. Sato, K. Ogohara, G. L. Hashimoto, and S. Murakami. Scattering Properties of the Venusian Clouds Observed by the UV Imager on board Akatsuki. , 154:44, Aug. 2017.

Y. J. Lee, K.-L. Jessup, S. Perez-Hoyos, D. V. Titov, S. Lebonnois, J. Peralta, T. Horinouchi, T. Imamura, S. Limaye, E. Marcq, M. Takagi, A. Yamazaki, M. Yamada, S. Watanabe, S. ya Murakami, K. Ogohara, W. M. McClintock, G. Holsclaw, and A. Roman. Long-term variations of venus's 365 nm albedo observed by venus express, akatsuki, MESSENGER, and the hubble space telescope. *The Astronomical Journal*, 158(3):126, aug 2019.

J. Lewis. *Physics and Chemistry of the Solar System*. International geophysics series. Elsevier Academic Press, 2004. ISBN 9780124467446.

S. S. Limaye, J. P. Kossin, C. Rozoff, G. Piccioni, D. V. Titov, and J. W. Markiewicz. Vortex circulation on venus: Dynamical similarities with terrestrial hurricanes. *Geophysical Research Letters, v.36 (2009)*, 36, 02 2009.

D. Luz, D. L. Berry, G. Piccioni, P. Drossart, R. Politi, C. F. Wilson, S. Erard, and F. Nuccilli. Venus's southern polar vortex reveals precessing circulation. *Science*, 332(6029):577–580, 2011.

P. M. Machado. *Dynamics of Venus' Atmosphere - Characterization of its Global Circulation with Doppler velocimetry*. Scholar's Press, 2013.

W. Markiewicz, D. Titiov, N. Ignatiev, H. Keller, D. Crisp, S. Limaye, R. Jaumann, R. Moissl, N. Thomas, L. Esposito, S. Watanabe, B. Fiethe, T. Behnke, I. Szemerey, H. Michalik, H. Perplis, M. Wedemeier, I. Sebastian, W. Boogaerts, and K. Matz. Venus monitoring camera for venus express. *Planetary and Space Science*, 55:1701–1711, 10 2007.

C. J. Nappo. *An Introduction to Atmospheric Gravity Waves*. International Geophysics, Volume 102. Academic Press, 2nd edition, 2012. ISBN 978-0-12-385223-6.

M. Newman and C. Leovy. Maintenance of strong rotational winds in venus' middle atmosphere by thermal tides. *Science*, 257(5070):647–650, 1992. ISSN 00368075, 10959203.

J. Peralta, R. Hueso, A. Sánchez-Lavega, G. Piccioni, O. Lanciano, and P. Drossart. Characterization of mesoscale gravity waves in the upper and lower clouds of venus from vex-virtis images. *Journal of Geophysical Research: Planets*, 113(E5), 2008.

J. Peralta, K. Muto, R. Hueso, T. Horinouchi, A. Sánchez-Lavega, S.-y. Murakami, P. Machado, E. Young, Y. J. Lee, T. Kouyama, H. Sagawa, K. McGouldrick, T. Satoh, T. Imamura, S. Limaye, T. Sato, K. Ogohara, M. Nakamura, and D. Luz. Nightside winds at the lower clouds

of venus with akatsuki/ir2: Longitudinal, local time and decadal variations from comparison with previous measurements. 10 2018.

R. J. Phillips and M. C. Malin. *The interior of Venus and Tectonic implications*, pages 159–214. 1983.

A. Piccialli. *Cyclotrophic wind in the mesosphere of Venus from Venus Express observations*. PhD thesis, 06 2010.

A. Piccialli, D. Titov, A. Sanchez-Lavega, J. Peralta, O. Shalygina, W. Markiewicz, and H. Svedhem. High latitude gravity waves at the venus cloud tops as observed by the venus monitoring camera on board venus express. *Icarus*, 227:94 – 111, 01 2014.

Piccioni, Drossart, Barbis, Bonello, Cherubini, Dami, Dupuis, Henry, Hofer, Huntzinger, and et al. Virtis: The visible and infrared thermal imaging spectrometer, Dec 2007. URL `http://adsabs.harvard.edu/abs/2007ESASP1295.....P`.

J. B. Pollack, O. B. Toon, R. C. Whitten, R. Boese, B. Ragent, M. Tomasko, L. Esposito, L. Travis, and D. Wiedman. Distribution and source of the uv absorption in venus' atmosphere. *Journal of Geophysical Research: Space Physics*, 85(A13):8141–8150, 1980.

C. Porco, R. West, S. Squyres, A. Mcewen, P. Thomas, C. Murray, A. Delgenio, A. Ingersoll, T. Johnson, G. Neukum, J. Veverka, L. Dones, A. Brahic, J. Burns, V. Haemmerle, B. Knowles, D. Dawson, T. Roatsch, K. Beurle, and W. Owen. Cassini imaging science: Instrument characteristics and anticipated scientific investigations at saturn. *Space Science Reviews*, 115:363–497, 01 2004. doi: 10.1007/1-4020-3874-7_6.

A. Ringwood and D. L. Anderson. Earth and venus: A comparative study. *Icarus*, 30(2):243 – 253, 1977. ISSN 0019-1035. URL `http://www.sciencedirect.com/science/article/pii/0019103577901567`.

C. Russell. The dynamics of planetary magnetospheres. *Planetary and Space Science*, 49(10-11): 1005–1030, 2001.

R. S. Saunders, A. J. Spear, P. C. Allin, R. S. Austin, A. L. Berman, R. C. Chandlee, J. Clark, A. V. Decharon, E. M. De Jong, D. G. Griffith, J. M. Gunn, S. Hensley, W. T. K. Johnson, C. E. Kirby, K. S. Leung, D. T. Lyons, G. A. Michaels, J. Miller, R. B. Morris, A. D. Morrison, R. G. Piereson, J. F. Scott, S. J. Shaffer, J. P. Slonski, E. R. Stofan, T. W. Thompson, and S. D. Wall. Magellan mission summary. *Journal of Geophysical Research: Planets*, 97(E8): 13067–13090, 1992.

G. G. Schaber, R. G. Strom, H. J. Moore, L. A. Soderblom, R. L. Kirk, D. J. Chadwick, D. D. Dawson, L. R. Gaddis, J. M. Boyce, and J. Russell. Geology and distribution of impact craters on venus: What are they telling us? *Journal of Geophysical Research: Planets*, 97 (E8):13257–13301, 1992.

J. E. O. Silva. Characterising solar system planets' atmosphere using cloud tracking wind velocities retrieval method. Master's thesis, Faculdade de Ciências - Universidade de Lisboa, 2017.

S. Smrekar, E. Stofan, N. Mueller, A. Treiman, L. Elkins-Tanton, J. Helbert, G. Piccioni, and P. Drossart. Recent hotspot volcanism on venus from virtis emissivity data. *Science*, 328 (5978):605–608, 4 2010. ISSN 0036-8075.

C. P. Sonett. A Summary Review of the Scientific Findings of the Mariner Venus Mission. , 2 (6):751–777, Dec 1963.

H. Svedhem, D. V Titov, F. Taylor, and O. Witasse. Venus as a more earth-like planet. *Nature*, 450:629–32, 12 2007.

A. Sánchez-Lavega. *An Introduction to Planetary Atmospheres*. CRC Press, 2011.

A. Sánchez-Lavega, R. Hueso, G. Piccioni, P. Drossart, J. Peralta, S. Pérez-Hoyos, C. F. Wilson, F. W. Taylor, K. H. Baines, D. Luz, S. Erard, and S. Lebonnois. Variable winds on venus mapped in three dimensions. *Geophysical Research Letters*, 35(13), 2008.

F. W. Taylor, D. J. McCleese, L. S. Elson, J. V. Martonchik, D. J. Diner, J. T. Houghton, J. Delderfield, J. T. Schofield, and S. P. Bradley. Infrared remote sensing of the atmosphere of Venus from the Pioneer 12 Orbiter. In M. J. Rycroft, editor, *Space Research XX*, pages 227–230, 1980.

D. V. Titov, W. J. Markiewicz, N. I. Ignatiev, L. Song, S. S. Limaye, A. Sanchez-Lavega, J. Hesemann, M. Almeida, T. Roatsch, K.-D. Matz, F. Scholten, D. Crisp, L. W. Esposito, S. F. Hviid, R. Jaumann, H. U. Keller, and R. Moissl. Morphology of the cloud tops as observed by the venus express monitoring camera. *Icarus*, 217(2):682 – 701, 2012. ISSN 0019-1035. Advances in Venus Science.

D. L. Turcotte. How does venus lose heat? *Journal of Geophysical Research: Planets*, 100(E8): 16931–16940, 1995.

A. Yamazaki, M. Yamada, Y. J. Lee, S. Watanabe, T. Horinouchi, S.-y. Murakami, T. Kouyama, K. Ogohara, T. Imamura, T. M. Sato, Y. Yamamoto, T. Fukuhara, H. Ando, K.-i. Sugiyama, S. Takagi, H. Kashimura, S. Ohtsuki, N. Hirata, G. L. Hashimoto, M. Suzuki, C. Hirose, M. Ueno, T. Satoh, T. Abe, N. Ishii, and M. Nakamura. Ultraviolet imager on venus orbiter akatsuki and its initial results. *Earth, Planets and Space*, 70(1):23, Feb 2018. ISSN 1880-5981.

Appendix A

Akatsuki's Daily Wind Profiles

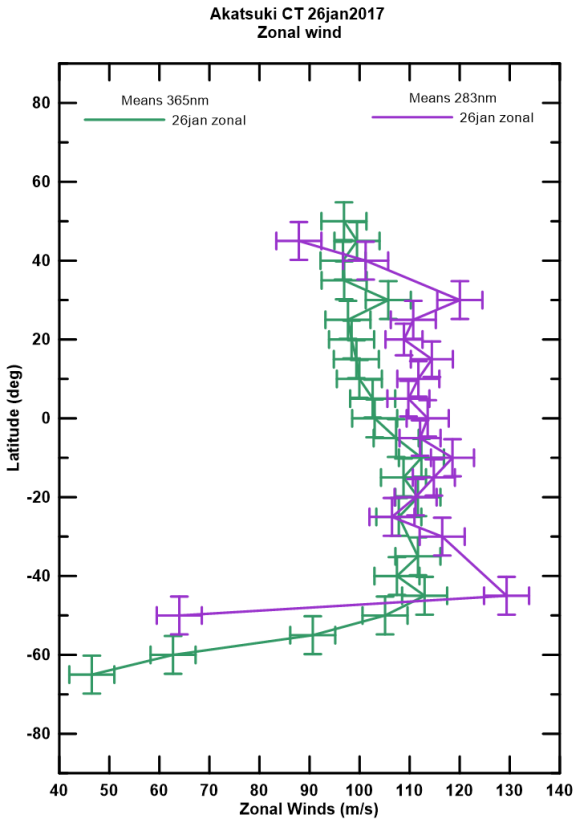
Akatsuki CT 26jan2017
Zonal wind
Means 365nm
26jan zonal
Means 283nm
26jan zonal
Latitude (deg)
Zonal Winds (m/s)

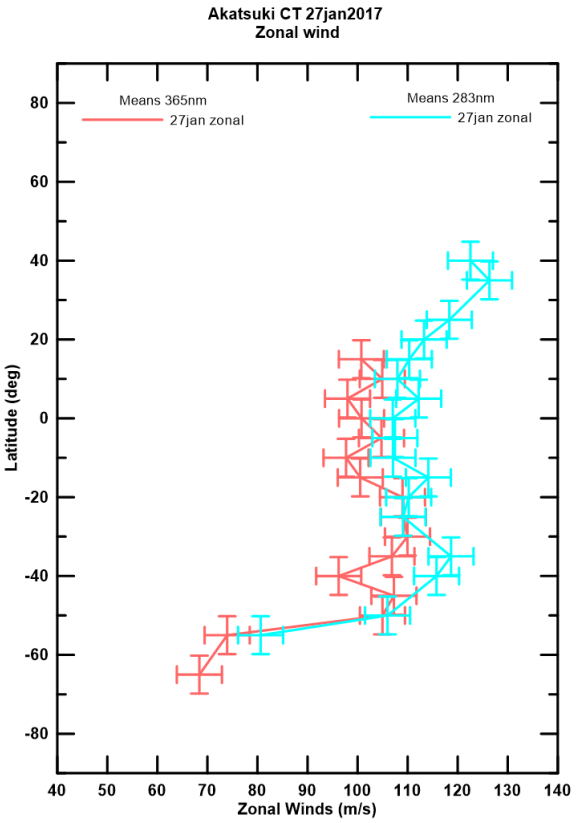
Akatsuki CT 27jan2017
Zonal wind
Means 365nm
27jan zonal
Means 283nm
27jan zonal
Latitude (deg)
Zonal Winds (m/s)

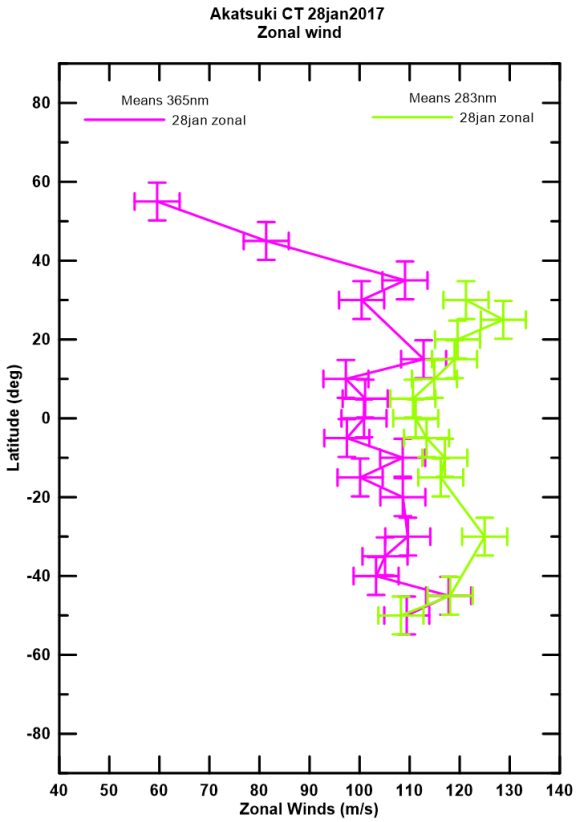
Akatsuki CT 28jan2017
Zonal wind
Means 365nm
28jan zonal
Means 283nm
28jan zonal
Latitude (deg)
Zonal Winds (m/s)

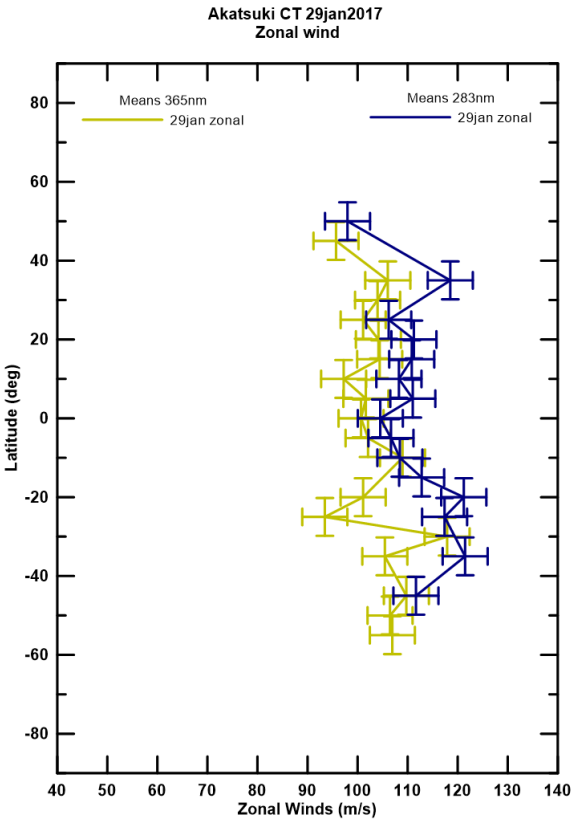
Akatsuki CT 29jan2017
Zonal wind
Means 365nm
29jan zonal
Means 283nm
29jan zonal
Latitude (deg)
Zonal Winds (m/s)

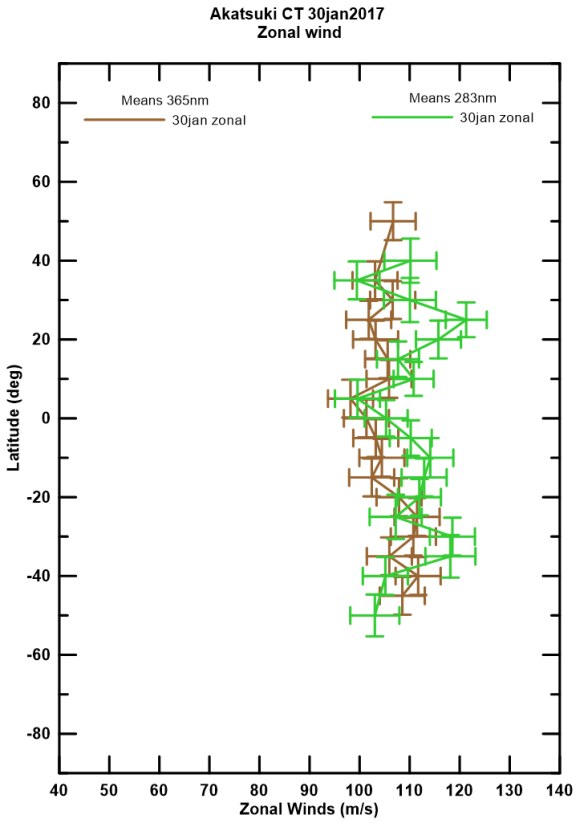
Akatsuki CT 30jan2017
Zonal wind
Means 365nm
30jan zonal
Means 283nm
30jan zonal
Latitude (deg)
Zonal Winds (m/s)

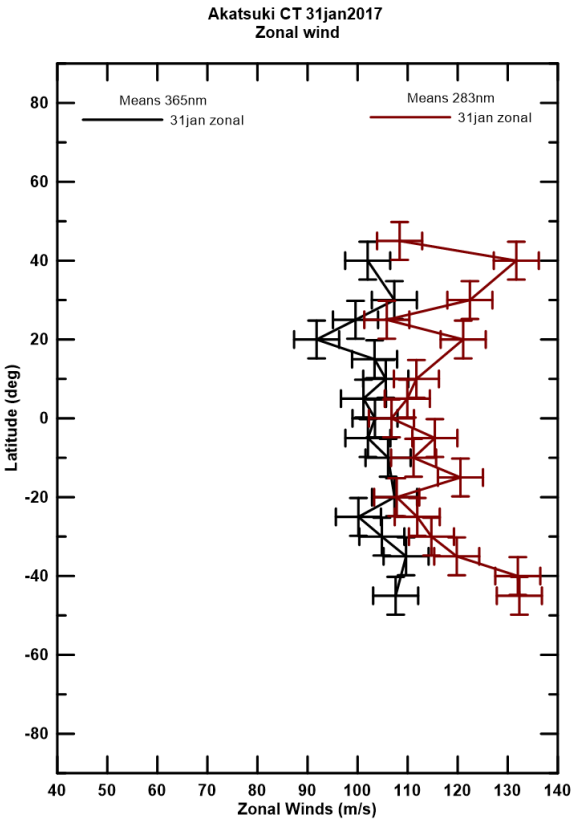
Akatsuki CT 31jan2017
Zonal wind
Means 365nm
31jan zonal
Means 283nm
31jan zonal
Latitude (deg)
Zonal Winds (m/s)

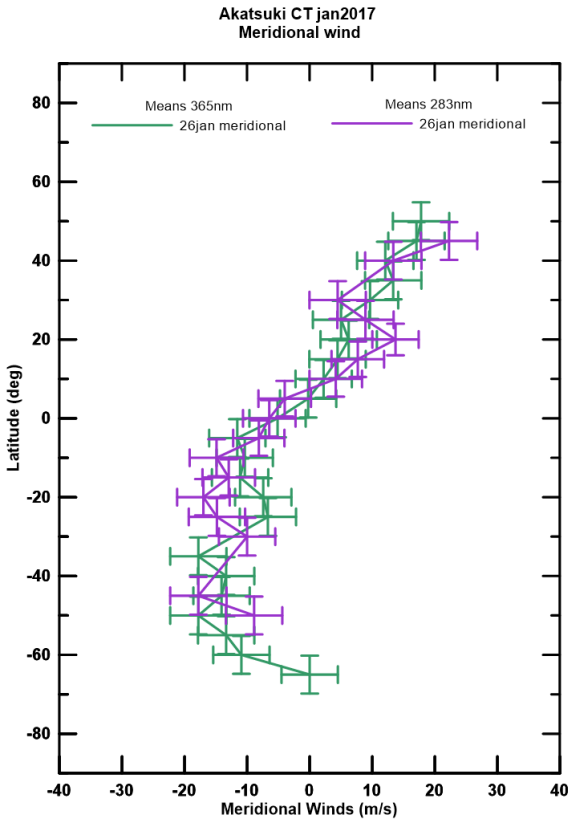
Akatsuki CT jan2017
Meridional wind
Means 365nm
26jan meridional
Means 283nm
26jan meridional
Latitude (deg)
Meridional Winds (m/s)

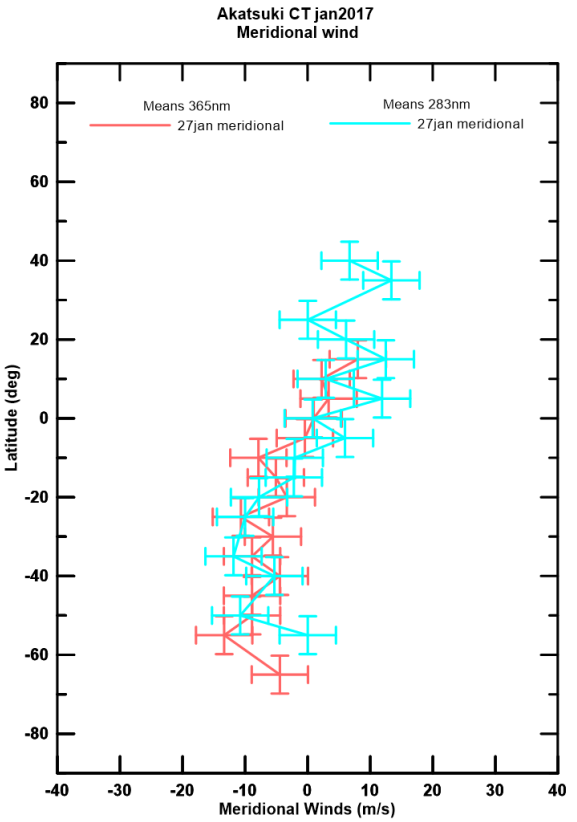
Akatsuki CT jan2017
Meridional wind
Means 365nm
27jan meridional
Means 283nm
27jan meridional
Latitude (deg)
Meridional Winds (m/s)

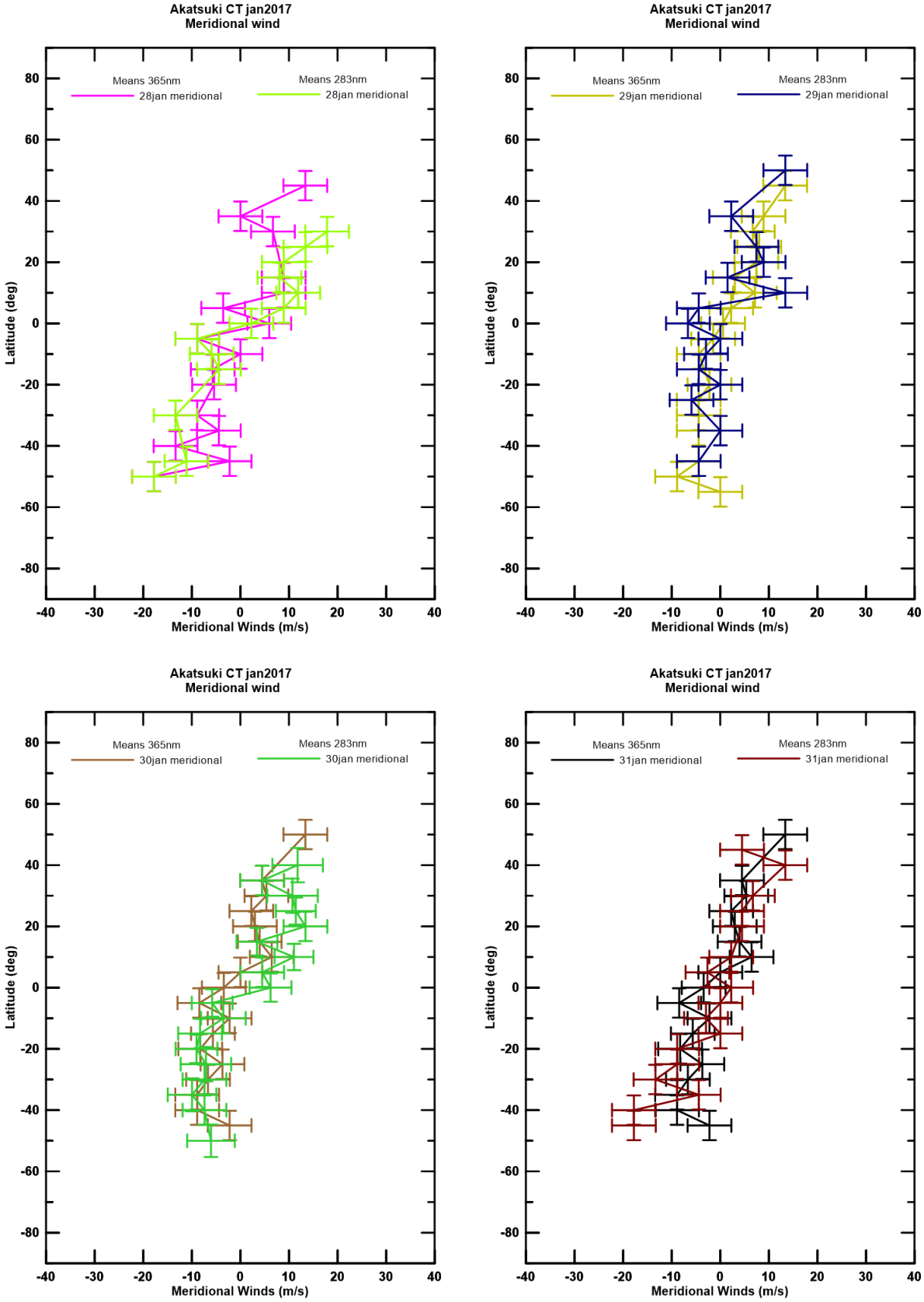

Figure A.1: Akatsuki's latitudinal wind profiles divided by day. Each plot shows a latitudinal profile for each on of the two filters (refer to each plot legends for days and colour matching).